ENEA Ricerca Sistema Elettrico	Sigla di identificazione	Distrib.	Pag.	di
	ADPFISS-LP1-032	L	1	83

Titolo

Lessons Learned from the Result Comparison of Calculations of a Reference Severe Accident Sequence on a TMI-2 Like PWR Reactor of 900 MWe with the Integral Codes ASTEC and MELCOR

Descrittori

Tipologia del documento: **Rapporto Tecnico**

Collocazione contrattuale: Accordo di programma ENEA-MSE: Piano Annuale di Realizzazione 2013, Linea Progettuale 1, Obiettivo A: Acquisizione, Sviluppo e Validazione di Codici e Metodi per Studi ed Analisi di Sicurezza e Sostenibilità, Task A3.3

Argomenti trattati: Sicurezza Nucleare

Sommario

This report presents the activity performed in the frame of LP1, Objective A (Acquisition, development and validation of methods and codes for sustainable and safety studies and analyses), Task A3.3 of PAR2013, ADP ENEA-MSE. In this study the integral codes ASTEC and MELCOR have been applied for the calculation of a reference severe accident sequence (SBLOCA) on the TMI-2 plant (PWR of 900 MWe). Several insights on the reliability and consistency of code response have been gained from a detailed comparison of the main code results. The reasons of the differences in code results have been thoroughly investigated and tentatively explained. Recommendations have been made for sensitivity studies on important and uncertain core degradation parameters and model options, in order to better understand the different code behavior and make proposals for further code model improvements.

Note:

This document has been prepared by the following main contributors:
- G. Bandini (ENEA)
- M. Di Giuli, M. Sumini (CIRTEN - Università di Bologna) ([1])
- A. Manfredini, W. Ambrosini (CIRTEN - Università di Pisa) ([2])

([1]) Ref. doc. CERSE-UNIBO RL 1556/2014; ([2]) Ref. doc. CERSE-UNIPI RL 1533/2014

REV.	DESCRIZIONE	DATA		REDAZIONE	CONVALIDA	APPROVAZIONE
2			NOME			
			FIRMA			
1			NOME			
			FIRMA			
0	EMISSIONE	17/09/14	NOME	G. Bandini	F. De Rosa	F. De Rosa
			FIRMA			

List of Contents

1. Introduction

Since the Three Mile Island Unit 2 (TMI-2) reactor accident in 1979, there have been extensive research activities to try to understand the phenomena involved, and to develop accident management strategies to mitigate the consequences of core melt accidents. Given that a severe accident cannot be simulated at or near full scale, since all the experimental database on core heat up, melt progression and fission product release is limited to the results of small-scale experiments, which are only partially representative of what could occur in a real reactor. Therefore, integral codes are used to describe core degradation transients in nuclear reactors without a clear idea of their predictive capabilities. This is the reason why TMI-2 provides a unique opportunity to assess the capability of integral codes to simulate a severe accident in a full scale Pressurizer Water Reactor (PWR).

The TMI-2 reactor modeling used in computer codes for severe accidents as MELCOR, ASTEC, MAAP 4 and ATHLET-CD has improved significantly over the years due to better understanding, and the simulation results confirm these continuous improvements. In the frame of Task 3.3 of PAR2013 - LP1, the CIRTEN activity, in collaboration with ENEA, is devoted to verify the progress and reliability of ASTEC and MELCOR codes through the result comparison for a representative severe accident sequence in a pressurized nuclear power plant of 900 MWe.

Starting from the same reactor model realized to simulate the real TMI-2 accident, it was decided to analyze an alternative severe accident scenario such as a Small Break Loss-Of-Coolant Accident (SBLOCA) with simultaneous loss of main feedwater to the steam generators, and without safety injection. The evolution of the accident has been studied until molten core slumping into the lower plenum and possible lower head vessel failure. The entire transient was analyzed by means of the integral ASTEC and MELCOR codes widely used worldwide for severe accident analysis in light water reactors. In the present study, the results of the two calculations have been compared and the differences pointed out and deeply investigated, in order to understand and try to explain the reason for the main discrepancies, and thus identify eventual code weaknesses and areas where further code model improvements is deemed necessary.

In Section 2 of this report, the reference specifications for both code calculations are defined regarding: the SBLOCA accident scenario, the boundary conditions, the TMI-2 plant data and the steady-state conditions of the TMI-2 plant at transient initiation, with the aim to best harmonize the two code input decks. In Section 3, the results of the MELCOR calculation performed by the University of Pisa are presented in details, along with a short description of the code models used in the analysis to best represent the in-vessel core degradation phase. Similarly, in Section 4, the results of the ASTEC calculations performed by the University of Bologna and the code models used are presented in detail using two different modeling options for the core late degradation phase. In Section 5, the main code results are compared and the main differences tentatively explained. Finally, main conclusions are drawn and recommendations for further activity in this area are made in Sec. 6.

2. Accident scenario and plant data

2.1 Accident scenario

The initial event is a small break (size = 0.0015 m2) in the hot leg A at t = 0 s, with simultaneous loss of main feedwater on the secondary side of steam generators (SGs). The primary pressure begins to reduce along with the pressurizer level as soon as the break opens. After few seconds, the fast SG dryout with consequent loss of heat removal from the primary side results in sudden primary pressure increase. The opening of the pressurizer PORV is not enough to limit the pressure rise and, therefore, reactor scram occurs when the pressurizer pressure set-point of 16.3 MPa is reached. The further primary pressure increase after reactor scram might be attenuated by the pressurizer safety valve operation (valve pressure set-point at 17.0 MPa).

The auxiliary feedwater starts at t = 100 s trying to restore 1 m water level in the SG secondary side. The primary pump stop occurs when the whole primary water mass (liquid + steam) inventory reduces below 85000 kg.

Then the accidental transient is let free to evolve towards core uncovery and heatup, core melting and corium relocation in the lower plenum, until possible lower head vessel failure. No HPI or LPI injections are actuated during the transient phase. The transient calculation should be pursued until vessel failure using code model options and parameter values recommended by code Best Practice Guidelines.

2.2 Boundary conditions

The SBLOCA scenario is specified with very simple and well defined boundary conditions, in order to minimize the influence of uncertainty of these conditions on the variability of code results.

2.2.1 Power

- Initial core power = 2772 MW.
- Thermal heat losses from primary system to containment atmosphere are not taken into account.
- Core residual power after reactor scram is given in Table 2.1 below.

Table 2.1: Core power evolution

Time (s)	Power (W)
0	2772.00e6
ts (scram time)	2772.00e6
ts + 1	167.94e6
ts + 4	147.96e6
ts + 10	130.14e6
ts + 40	103.14e6
ts + 100	86.13e6
ts + 400	65.34e6
ts + 800	52.92e6
ts + 1000	49.95e6
ts + 2000	42.39e6
ts + 4000	34.56e6
ts + 8000	28.35e6
ts + 10000	26.05e6
ts + 20000	21.46e6

- Radial core power profile (6 rings) is given in Table 2.2 below (according to the radial discretization and number of fuel rods defined in the ASTEC simulation by ENEA in ATMI Benchmark [1]).

Table 2.2: Radial profile of core power

Ring	Factor	Number of fuel rods	External radius (m)
1	1.2572	1040	0.27
2	1.2127	3120	0.54
3	1.1469	5200	0.81
4	1.0596	7072	1.08
5	0.951	9152	1.35
6	0.8198	11232	1.665

- Axial profile of core power is given in Table 2.3 below (same axial power profile in different rings).

Table 2.3: Axial profile of core power

Z (m)	Factor
0	0
0.15	0
0.302	0.675
0.607	0.857
0.912	1.037
1.217	1.153
1.522	1.202
1.826	1.231
2.131	1.241
2.436	1.209
2.893	1.102
3.503	0.595
3.81	0
4	0

The radial and axial profiles in Table 2.2 and Table 2.3 are valid for intact core geometry. The change in power distribution following core degradation and fuel relocation must be taken into account by the respective code models.

2.2.2 Steam generator pressure and level control

Boundary conditions for the SG secondary side are given by controlling the steam generator pressure and water level (in the riser) as follows:

- SG pressure at steady-state value in the first 100 s (P = 6.41 MPa), then pressure rise up to 7.0 MPa in 100 s and constant value until the end of the transient, as shown in Figure 2.1.
- SG level reduces quickly down to 0 due to heat transfer from primary side (timing of SG dryout is calculated by the code), then linear increase from t = 100 s, by startup of auxiliary feedwater, reaching the 1 m value at 200 s, and then constant until the end of the transient, as shown in Figure 2.2, by auxiliary feedwater flow rate control.

Regarding the feedwater control, we assume:

- Maximum feedwater flow rate = 50 kg/s per SG.
- Feedwater temperature = 295.15 K.

The linear increase of SG level up to 1 m, starting at 100 s by auxiliary feedwater injection, might be delayed because of strong evaporation inside the SG and due to the limit on maximum feedwater flow rate.

Also based on the experience of the ATMI Benchmark, it seems important to note that the SG pressure and level might deviate from the boundary values, when SG power removal reduces down close to 0, due to stop of natural circulation in the primary loops, after the initial boil-off phase. By this time, steam condensation in the secondary side of SG leads to slow progressive decrease of the SG pressure below 7.0 MPa and, at the same time, leads to slow progressive increase of the SG level above 1 m. In any case, and in particular in this situation, the pressure cannot be controlled by steam ingress into the SG dome, so as the level cannot be controlled by water draining from the SG bottom.

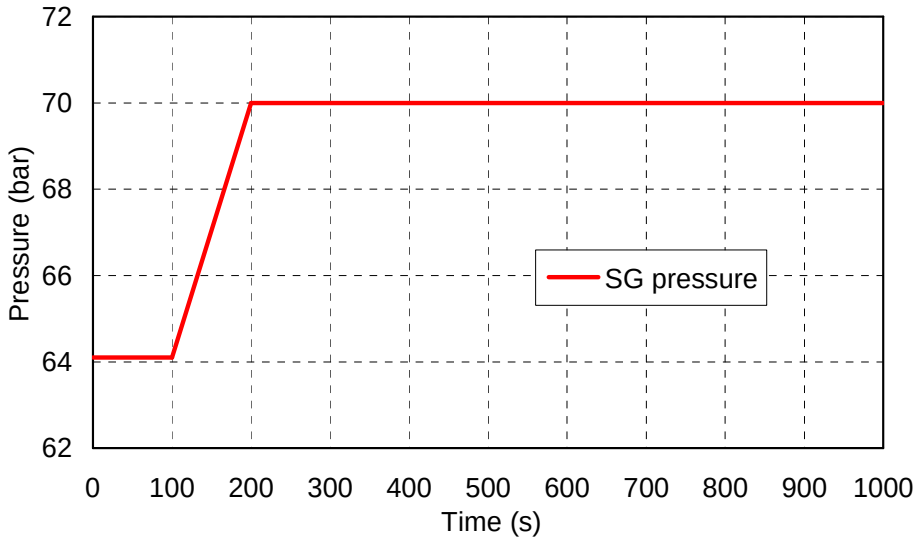

Figure 2.1: SG pressure control

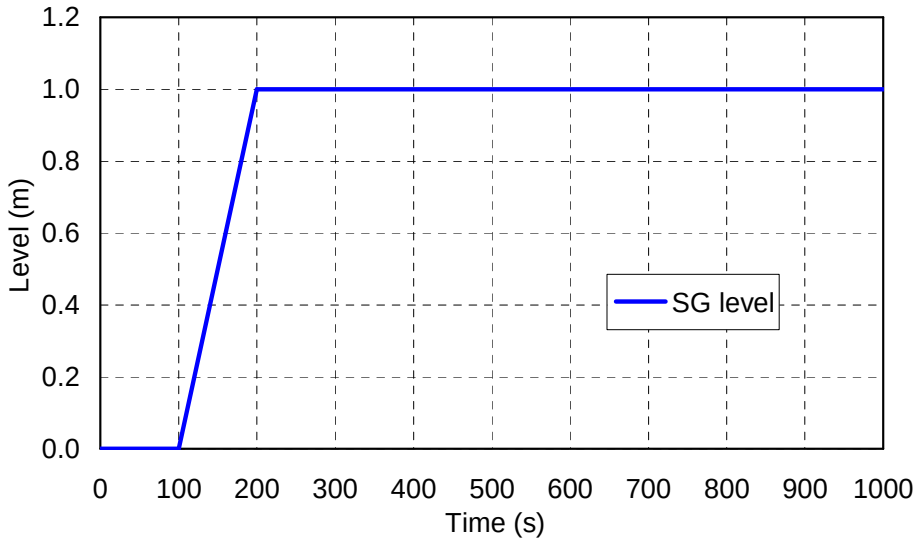

Figure 2.2: SG level control

2.2.3 Hot leg break

- Break size = 0.0015 m^2
- Break position = 4 m along the hot leg of loop A, from vessel outlet nozzle
- Containment pressure = 0.1 MPa (pressurization of the containment atmosphere is not taken into account)
- No stratification in the hot leg during the boil-off phase before primary pump stop, which may significantly affect the break mass flow rate value.

2.2.4 Letdown/make-up flow and ECCS injections

- Letdown flow rate = 0
- Make-up flow rate = constant value of 2 kg/s during the all transient in cold leg 2B (water temperature = 315.15 K)
- No HPI injection
- No LPI injection

2.2.5 Threshold set-point values

- Pressurizer PORV opening → Pressurizer pressure > 15.56 MPa
- Pressurizer PORV closure → Pressurizer pressure < 14.96 MPa
- Reactor scram → Pressurizer pressure > 16.30 MPa
- Pressurizer safety valve set-point → 17.0 MPa (valve capacity = 86.9 kg/s)
- Primary pump stop → Primary mass (liquid + steam) < 85000 kg

2.3 TMI-2 plant data

General plant geometry is defined according to the Final Report of the OECD/ATMI Benchmark [1]. Plant data concerning free volumes of the primary system have been updated according to the Final Specifications of MSLB Benchmark Report [2]. Other details on the overall TMI-2 plant layout can be found in Ref. [2] if needed.

The radial and axial core discretization is let free to the code user, but the power distribution in the core must be consistent with the radial and axial power profiles given in Section 2.2.1.

2.3.1 Free volumes

- Primary system volume without the pressurizer = 288.29 m^3
- Pressurizer volume = 42.5 m^3
- Reactor pressure volume = 113.6 m^3
- Secondary side free volume of one SG (up to the SG exit) = 34.4 m^3

2.3.2 Heat transfer with secondary side

- SG tubes surface per SG (secondary side) = 12302.5 m^2
- Number of tubes per SG = 15530

2.3.3 Intact Core Geometry

Main characteristics of the core

- Number of fuel bundles of type 15x15 = 177
- Active core length = 3.66 m
- Total core length = 4.0 m (from core bottom: 0.15 m + 3.66 m (active length) + 0.19 m)
- Type of fuel lattice = square, pitch = 0.01443 m
- Number of fuel rods per assembly = 208
- External diameter of fuel rod = 0.0109 m
- Fuel pellet radius = 0.0047 m
- Fuel rod cladding thickness = 0.000673 m

Initial core material inventory

- UO2 mass = 93650 kg (over the 3.66 m of core active length)
- Zircaloy mass = 23050 kg
- H2 total mass if converted from total zircaloy = 1011 kg (Zircaloy mass / 22.8)
- AIC mass (Ag + In + Cd) = 2750 kg

2.3.4 Vessel and internal structures

- Core baffle internal diameter = 3.28 m
- Core baffle external diameter = 3.33 m
- Core barrel internal diameter = 3.584 m
- Core barrel external diameter = 3.683 m
- Thermal shield internal diameter = 3.683 m
- Thermal shield external diameter = 3.753 m
- Vessel wall internal diameter = 4.36 m
- Vessel wall external diameter = 4.86 m

2.3.5 Vent valve operation

These valves, between the upper plenum and the top of the downcomer, are designed to avoid a direct loss of water by the hot leg. They should be modeled, as they were shown to have an influence on the transient. Simplified simulation of these valves is defined as follows:

- If $\Delta P < 414$ Pa, the valves are closed.

- If $\Delta P > 1724$ Pa, the valves are fully open, which corresponds to a total section of 0.794 m^2.
- If 414 Pa $< \Delta P < 1724$ Pa, the valves are considered partly open, with a cross section area increasing linearly with ΔP.

2.4. Initial TMI-2 plant conditions

2.4.1 Nominal TMI-2 steady-state

The nominal steady-state of the TMI-2 plant is the one defined in the "Pressurizer Water Reactor Main Steam Line Break (MSLB) Benchmark" Final Specifications [2]. The nominal values of the main TMI-2 plant parameters for both primary and secondary systems are listed in Table 2.4.

Table 2.4: Nominal TMI-2 steady-state conditions at transient initiation

Parameter	Unit	TMI-2 steady-state
Reactor core power	MW	2772
Pressurizer pressure (dome)	MPa	14.96
Temperature hot leg A & B	K	591.15
Temperature cold leg A & B	K	564.15
Mass flow rate loop A & B	kg/s	8800
Pressurizer collapsed level	m	5.588
Pressurizer water mass	kg	13710
Total primary mass	kg	222808 (**)
Steam pressure SG A & B (outlet nozzle)	MPa	6.41
Steam temperature SG A & B	K	572.15
Riser collapsed level SG A & B	m	3.28 – 4.03 (*)
Downcomer collapsed level SG A & B	m	5.1 – 5.6 (*)
Liquid mass SG A & B	kg	13140 – 19210 (*)
Feedwater flow rate SG A & B	kg/s	761.1
Feedwater Temperature SG A & B	K	511.15

(*) Range of values used by participants in the ATMI Benchmark
(**) According to primary volumes in Table 2.5

2.4.2 Primary coolant mass inventory

The coolant mass inventory in the primary system has been evaluated according to the primary component volumes defined in Ref. [2]. The calculation of the primary mass inventory is illustrated in Table 2.5 below.

Table 2.5: Coolant mass inventory in the primary system

Component	Vol. (m^3)	N°	Tot. vol. (m^3)	Temp. (K)	Density (kg/m^3)	Mass (kg)
Pressurizer water volume	22.7	1	22.7	615.1	604.0	13710
Pressurizer steam volume	19.8	1	19.8	615.1	96.1	1903
Surge line	0.566	1	0.566	603.15 (*)	649.3	368
Cold leg (each)	6.73	4	26.92	564.15	744.1	20030
Reactor coolant pump (each)	1.59	4	6.36	564.25	744.1	4732
Hot leg (each)	13.3	2	26.6	591.15	684.6	18209
Reactor vessel water volume: - *Lower plenum = 8.27 m^3* - *Core = 20.4 m^3* - *Downcomer = 34.69 m^3* - *Upper plenum = 21.97 m^3* - *Upper head = 14.4 m^3*	113.6	1	113.6	575.22 (*)	721.8	81992
SG primary side volume (each): - *Upper plenum = 7.96 m^3* - *Lower plenum = 7.84 m^3*	57.12	2	114.24	577.65 (*)	716.5	81858
Total			330.79			222808
Total without pressurizer			288.29			207189

(*) Estimated average temperature values

References

1. F. Fichot, O. Marchand, G. Bandini, H. Austregesilo, M. Buck, M. Barnak, P. Matejovic, L. Humphries, K. Suh, S. Paci, “Ability of Current Advanced Codes to Predict Core Degradation, Melt Progression and Reflooding - Benchmark Exercise on an Alternative TMI-2 Accident Scenario”, NEA/CSNI/R(2009)3, July 2009.
2. K.N. Ivanov, T. M. Beam, A. J. Baratta, “Pressurised Water Reactor Main Steam Line Break (MSLB) Benchmark”, Volume 1: Final Specifications, NEA/NSC/DOC(99)8, April 1999.

3. SBLOCA accident calculation with MELCOR

3.1 Brief description of the MELCOR code

MELCOR is a fully integrated, engineering-level computer code able to model the progression of severe accidents in LWR nuclear power plants [1]. It is being developed at SNL for the U.S.N.R.C. as a second generation plant risk assessment tool and the successor to the Source Term Code Package. The spectrum of severe accident phenomena, including reactor coolant system and containment thermal-hydraulic response, core heat-up, degradation and relocation, and fission product release and transport, is treated in MELCOR in a unified framework for both BWR and PWR reactors. MELCOR has especially been designed to facilitate sensitivity and uncertainty analyses. The code has been under development since 1982 and the latest version is the 2.1, released in 2008.

Thermal-hydraulic behavior is modeled in MELCOR in terms of control volumes and flow paths. All hydrodynamic material (and its energy) resides in control volumes. Hydrodynamic material includes the coolant and non-condensable gases. These materials are assumed to separate under the influence of gravity within a control volume to form a pool beneath and an atmosphere above. Each control volume is characterized by a single pressure and two temperatures, one temperature for the pool and one for the atmosphere. The control volumes are connected by flow paths through which materials may move without residence time, driven by a momentum equation. Based on the elevations of the pool surfaces in the connected control volumes relative to the junctions with the flow paths, both pool and atmosphere may pass through each flow path. Appropriate hydrostatic head terms are included in the momentum equation for the flow paths, allowing calculation of natural circulation.

The MELCOR COR-package calculates the thermal response of the core and lower plenum structures, including the portion of the lower head directly beneath the core. In addition, the relocation of core materials during melting, slumping, and debris formation are modeled. Fuel pellets, cladding, grid spacers, canister walls, other core structures (e.g. control rods), and particulate debris are modeled separately with individual cells. Cells are the basic nodalization units in the COR-package. All important heat transfer processes are modeled in each COR cell. Thermal radiation within a cell and between different cells in both axial and radial direction is accounted for, as well as radiation to boundary structures. Radiation to a liquid pool and to steam is also included. Radial conduction across the fuel cladding gap and axial conduction between cells is modeled. Convection to the control volume fluids is simulated for a wide range of fluid conditions and structure surface temperatures, including nucleate and film boiling. Oxidation of zircaloy and steel is modeled for both the limiting cases of solid state diffusion of oxygen through the oxide layer and gaseous diffusion of steam or oxygen through the mixture. The core degradation model treats eutectic reactions, dissolution reactions, candling of molten core materials and the formation and relocation of particulate debris.

MELCOR calculates both the release and transport behavior of fission products and control rod materials. It tracks the masses of these materials by grouping them into classes. Each material class represents a group of one or more elements or compounds with similar physical properties. Each class has its own set of values of parameters, such as release coefficients and vapor pressure. Aerosols and vapors can deposit directly on surfaces such as heat structures and water pools. In addition, aerosols can agglomerate and settle.

3.2 Standard physical parameters of the code

Main core degradation physical parameters used in the standard calculation with MELCOR are summarized in the Table 3.1. The physical parameters used in the standard calculation are the MELCOR default recommended values [2].

For Zircaloy oxidation, the solid-state diffusion of oxygen through an oxide layer to unoxidized metal is represented by a parabolic rate equation, whose rate constant is evaluate using the Urbanic-Heidrick correlation. For very low oxidant concentrations, gaseous diffusion may limit the reaction rate, and a mass transfer coefficient is calculated via a heat-mass transfer analogy from the heat transfer correlations.

Candling, that is the downward flow of molten core materials and the subsequent refreezing of these materials as they transfer latent heat to cooler structures below, is addressed with a semi-mechanistic model, based on fundamental thermal/hydraulic principles. Relocation of core materials may result in a reduction of area and increase of flow resistance, or even total blockage of flow, within various parts of the core. A model is also implemented for an oxide shell to hold up molten material until the shell is breached. Molten material is held up within a component if the oxide thickness is greater than a critical value hold, if the component temperature is less than a critical value, and if no candling from the component in that cell has yet taken place.

MELCOR contains several simple models that consider the structural integrity and support of intact components, and convert them to particulate debris when either is lost. Most are logical models rather than structural models; no stress calculations are performed for any component other than supporting structure. All components other than fuel rods are immediately converted to particulate debris whenever the unoxidized metal thickness is reduced below a user defined minimum value. The thickness criterion is also used for cladding, which is assumed to support fuel pellets, but other criteria are also considered for fuel rods. Oxidized rods are assumed to retain their identity until the cladding reaches 2500 K, and to collapse unconditionally if the fuel temperature reaches 3100 K (the approximate melting temperature of UO2).

Table 3.1: Main assumptions on main degradation models for the reference calculation

Parameter	MELCOR
Zircaloy oxidation kinetics	Urbanic-Heidrick
Cladding failure criteria *(with molten material candling)*	Tclad > 2173 K No candling (holdup) when: ZrO2 thickness >10 µm and Tclad < 2500 K
Melting point of UO2-ZrO2 ceramic material	UO2 Tm = 3100 K ZrO2 Tm = 2990 K
Debris formation criteria	For other materials than fuel rods: thickness < 100 µm Fuel rod failure and debris formation when: Zr thickness < 100 µm and T_{fuel} > 2500 K or T_{fuel} > 3000 K
Molten core relocation into the lower plenum	After failure of grid-supported plate that can initially support fuel assemblies and particulate debris above it. Thus, everything resting on that ring of the plate will fall, but the plate will remain in place until it melts (1273 K). This event corresponds to failure of the plate portion with survival of the grid
Reactor pressure vessel failure (**)	Failure of the lower head will occur if any of four criteria is met: 1. the temperature of a penetration (or the temperature of the innermost ode of the lower head) reaches a failure temperature (1273 K) 2. a failure logical control function is found to be true (not used) 3. overpressure (20 MPa) from the falling-debris quench model occurs 4. creep-rupture failure of a lower head segment occurs, in response to mechanical loading at elevated temperatures

3.3 Initial TMI-2 plant conditions

3.3.1 Nominal TMI-2 steady-state

The nominal steady-state of the TMI-2 plant is the one defined in the “Pressurizer Water Reactor Main Steam Line Break (MSLB) Benchmark” Final Specifications. The nominal values of the main TMI-2 plant parameters for both primary and secondary systems are listed in Table 3.2. The TMI-2 initial conditions are obtained by a steady-state code run lasting 2000 s and starting from plant thermal-hydraulic parameter values close to the ones

specified for TMI-2. During the steady-state calculation, some regulations in the primary and secondary sides are activated to facilitate the achievement of stable conditions.

The regulated parameters are:

- the pressurizer pressure by turning on the heaters when the pressure is lower than the nominal value;
- the pressurizer liquid mass, by water injection or draining, in order to obtain the precise liquid level;

The TMI-2 plant initial conditions calculated by the MELCOR code are compared with TMI-2 accident data at turbine trip in the Table 3.2 below. The primary circuit conditions are very well reproduced by the code, the larger mismatch being the mass core flow rate which resulted about 3% lower with respect to reference plant parameters.

Table 3.2: Nominal TMI-2 steady-state conditions at transient initiation

Parameter	Unit	TMI-2 steady-state	MELCOR
Reactor core power	MW	2772	2772
Pressurizer pressure (dome)	MPa	14.96	14.95
Temperature hot leg A & B	K	591.15	589.9
Temperature cold leg A & B	K	564.15	561.8
Mass flow rate loop A & B	kg/s	8800	8863
Pressurizer collapsed level	m	5.588	5.56
Pressurizer water mass	kg	13710	14347
Total primary mass	kg	222808	220489
Steam pressure SG A & B (outlet nozzle)	MPa	6.41	6.41
Steam temperature SG A & B	K	572.15	570.0
Riser collapsed level SG A & B	m	3.28 – 4.03	6.12
Downcomer collapsed level SG A & B	m	5.1 – 5.6	7.79
Liquid mass SG A & B	kg	13140 – 19210	25957
Feedwater flow rate SG A & B	kg/s	761.1	761.1
Feedwater Temperature SG A & B	K	511.15	511.15

3.3.2 TMI-2 plant model

The same nodalization used to simulate the first two phases of the TMI-2 accident has been used for this benchmark, with proper boundary conditions. Moreover, minor changes were performed with respect to this benchmark, in order to reduce stratification in the primary side and improve heat transfer through steam generators.

The nodalization of the TMI-2 primary system for the MELCOR 1.8.6 code is presented in the Figure 3.1. Both primary loops have been modelled simulating each SGs and

considering a single equivalent main pump and cold leg. The secondary system is modelled only up to the main feed and isolation valves, while the SGs were modelled with a high level of detail. The secondary side is connected to an imposed pressure control volume and to a "spill & feed" level control, which assure the desired imposed boundary conditions.

Particular care has also been devoted to core simulation (Figure 3.2). The core schematization is constituted by five radial rings and twelve axial levels; four thermal-hydraulic levels are used in each ring of the core region, with three core cells axially in each thermal-hydraulic control volume. Radial and axial flow paths in the core region allow for the prediction of 2-D flow patterns. Heat structures representative of the control rod guide tubes and upper tie plate in the upper plenum have been added to the MELCOR model to permit condensation heat transfer and coolant recirculation inside the vessel. The input deck was developed using standard default MELCOR modeling parameters as long as possible, and allows for a complete description of an eventual severe progression of an accidental transient.

The VENT valves are also explicitly modeled between the cold and hot collectors. The plant geometry, the boundary conditions and the accident scenario have been strictly defined according to TMI-2 scenario benchmark specifications.

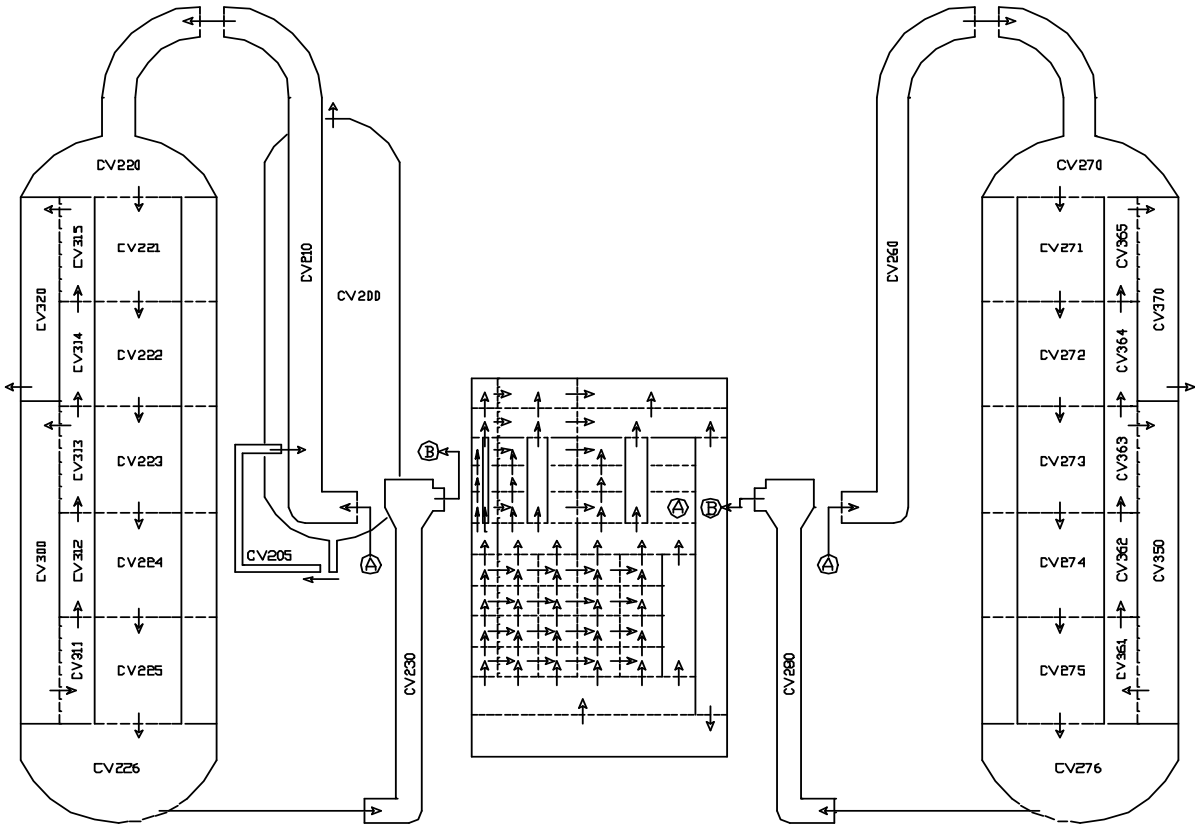

Figure 3.1: TMI-2 plant nodalization scheme

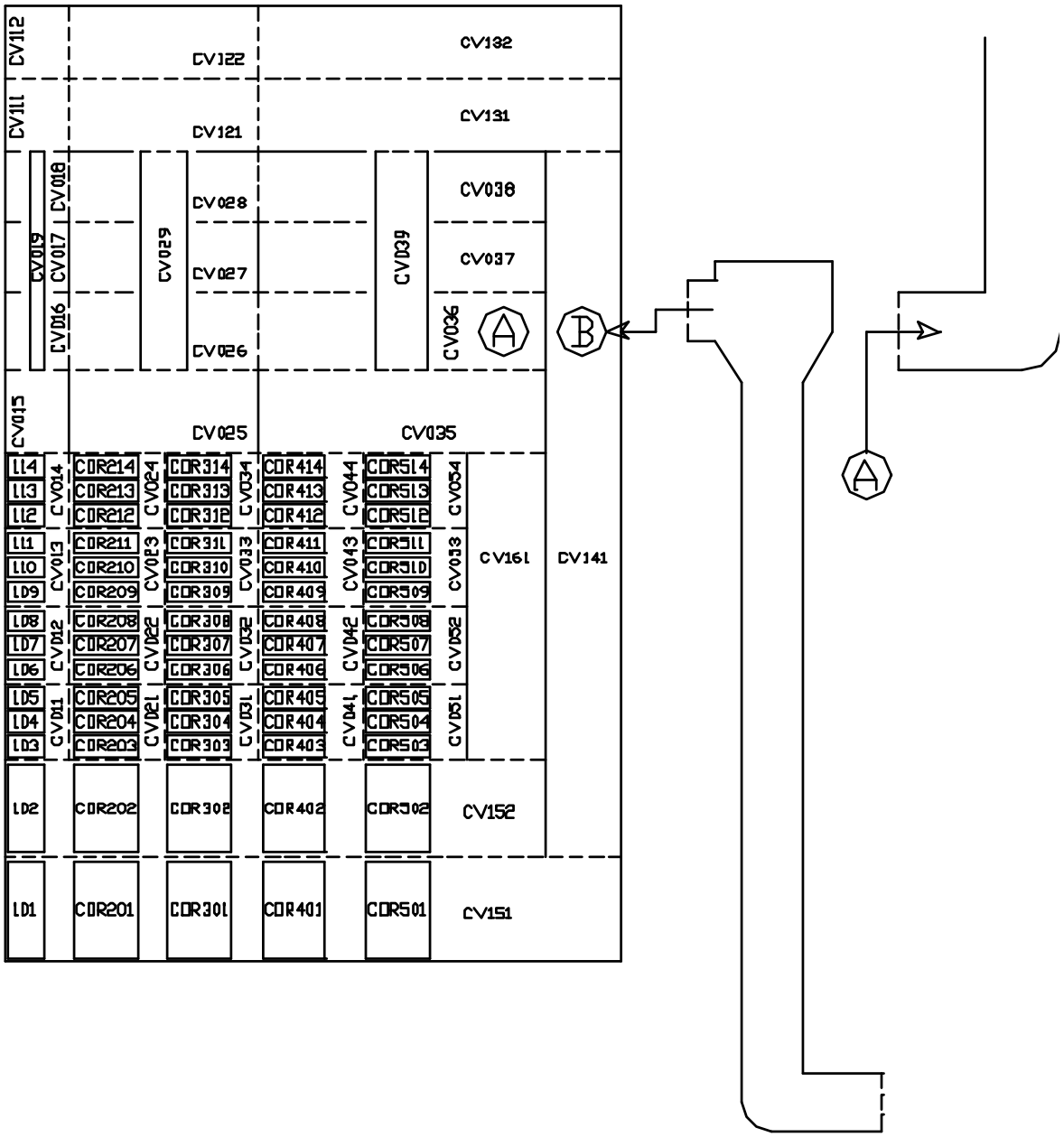

Figure 3.2: TMI-2 core simulation with MELCOR

3.3.3 Primary mass inventory

The coolant mass inventory in the primary system has been evaluated according to the primary component volumes defined in Ref. [3]. The calculation of the primary mass inventory is illustrated in Table 3.3.

Table 3.3: Coolant mass inventory in the primary system

Component	Vol. (m^3)	MELCOR (m^3)	Mass (kg)	MELCOR (kg)
Pressurizer water volume	22.7	22.7	13710	14347
Pressurizer steam volume	19.8	19.8	1903	1867
Surge line	0.566	0.9078	368	599
Cold leg	26.92	32.148	20030	24049
Reactor coolant pump	6.36		4732	
Hot leg	26.6	24.66	18209	16943
Reactor vessel water volume - *Lower plenum = 16.23 m^3* - *Core = 21.57 m^3* - *Downcomer = 25.62 m^3* - *Upper plenum = 30.16 m^3* - *Upper head = 13.573 m^3*	113.6	107.16	81992	75746
SG primary side volume (each) - *Upper plenum = 10.9 m^3* - *Lower plenum = 10.9 m^3*	57.12	60.78	81858	86938
Total	330.8	328.9	222808	220489
Total without pressurizer		281.6	207189	204275

3.4 Parameters and results

The chronology of major events calculated by MELCOR is presented in Table 3.4 and discussed in the following.

Boundary conditions on the SGs secondary side (Figures 3.3 to 3.4) are maintained during the whole transient, by connecting each steam generator secondary side to a control volume with imposed pressure and using a “spill&feed” level control. So, changes in pressure and in liquid level due to steam evaporation/condensation which takes place during the transient are continuously corrected by injecting/spilling saturated steam and water from/to the two controlled source.

The initial feedwater trip and the consequent heat removal loss through the two steam generators causes the primary pressure to rapidly reach the opening PORV set-point and after about 27 s the reactor scram is actuated. The primary pressure (Figure 3.5) rapidly approaches saturation as a consequence of the break on the hot leg and remains almost constant at a value of 7.6 MPa up to the trip of the pumps which takes place after 2593 s. Almost at the same time the break uncovers and pressure starts increasing due to reduced removed power through the steam generators and the break. After 10 minutes the pressure decreases again, due to the

beginning of core uncovery, reaching a minimum value of about 6.8 MPa. Finally, the primary pressure slightly decreases up to the time of vessel failure.

Table 3.4: Chronology of main events (code output)

Parameter	Time (s)
Break opening and total loss of main feedwater	0
Pressurizer PORV opens (P > 15.56 MPa)	17.03
Reactor scram (P > 16.30 MPa)	26.68
Pressurizer PORV closes (P < 14.96 MPa)	33.02
Full steam generator dryout	47.22
Startup of auxiliary feedwater	100.00
Pressurizer is empty	287.0
Stop of primary pumps (primary mass (liquid + steam) < 85000 kg)	2593
First fuel rod clad perforation/burst	(-)
First clad oxidation	4180
First clad melting and dislocation (also considering control rods)	5450/5700
First ceramic melting and dislocation	6310
First molten material slumping in the lower plenum	5480
Vessel failure	9680

Formation of a void fraction is predicted in the primary system (Figure 3.6) reaching almost the 50% when the main pumps trip, due to the low primary mass. Heat transfer through the two steam generators (Figure 3.7) is directly correlated to the primary system saturation temperature up to the trip of the main pumps, when heat removal steeply decreases to zero.

The mass of water in the primary system (Figure 3.8) decreases with an almost constant rate during liquid flow rate through the break. The calculation of break mass flow rate (Figure 3.9) is performed using RETRAN correlations for choked flow, that is the Moody model for saturated water and the Henry-Fauske model for the subcooled phase. After break uncovering the mass inventory decreases more slowly reaching a minimum value of about 37 tons at the end of the calculation.

The mass flow rate through the two primary loops (Figure 3.10) is predicted to be rapidly reduced due to void formation inside the primary system. A void degradation factor has been also applied in order to simulate the decrease of pumps head as a function of the void fraction.

The core starts to uncover at 2800 s (Figure 3.11) as a consequence of the break and pumps trip, while core heatup starts at 2900 s at the core top, because the core decay power is no more removed by natural circulation in the primary circuit. Core level is predicted to reach the bottom of the active fuel after 5300 s since the beginning of the transient and it remains to this level up to the vessel failure.

The temperature in the cold leg (Figure 3.12) remains at saturation during the first part of the transient and undergoes a steep decrease after steam generator emptying. The behavior of the temperature inside the hot leg (Figure 3.13) is similar, even though higher values of steam superheating are evaluated during the core heatup phase.

The fuel rod temperature in the central ring, as evaluated by MELCOR at three different core elevations (Figures from 3.14 to 3.16), shows a steep increase during the oxidation phase. At the bottom of the core, a weaker fuel rod heatup is anyway predicted during the phase where the core level goes to zero.

Fuel rod melting starts just before the main oxidation phase. Melting of control rods materials starts after 5400 s since the beginning of the transient, while zircaloy starts melting at about 5700 s also causing a partial dissolution of the fuel. The total mass of molten metals is predicted to be about 34 tons (Figure 3.17), while about 23.7 tons of debris is predicted to relocate towards the vessel bottom (Figure 3.18).

The main oxidation phase takes place (Figure 3.19) between 4200 s and 6900 s since the beginning of the transient. During this phase almost 516 kg of hydrogen are generated (Figure 3.20), with a maximum rate of about 0.7 kg/s at 6000 s (Figure 3.21).

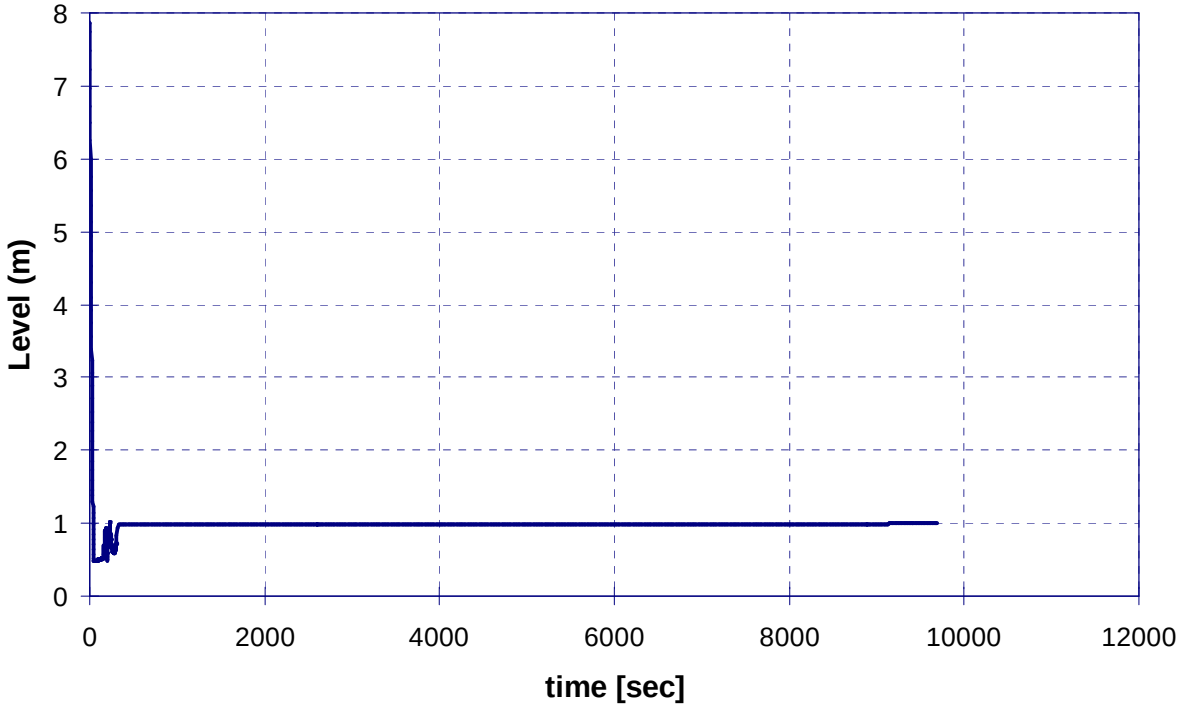

Figure 3.3: Steam generator A level

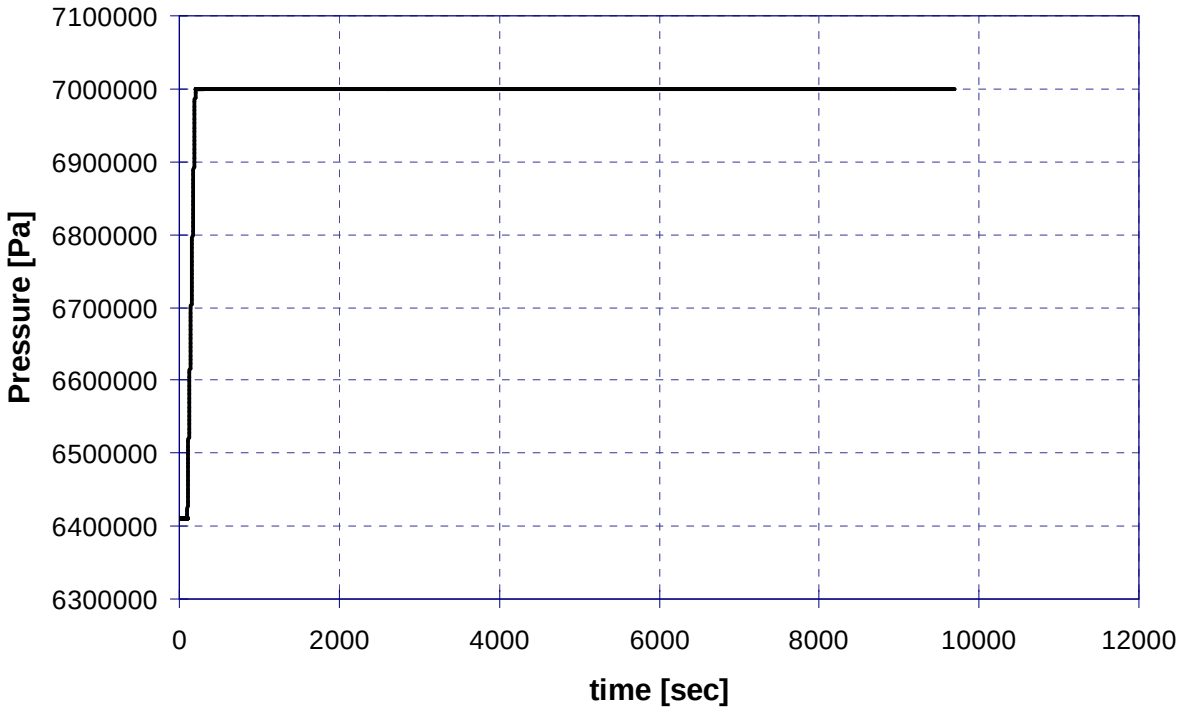

Figure 3.4: Steam generator A pressure

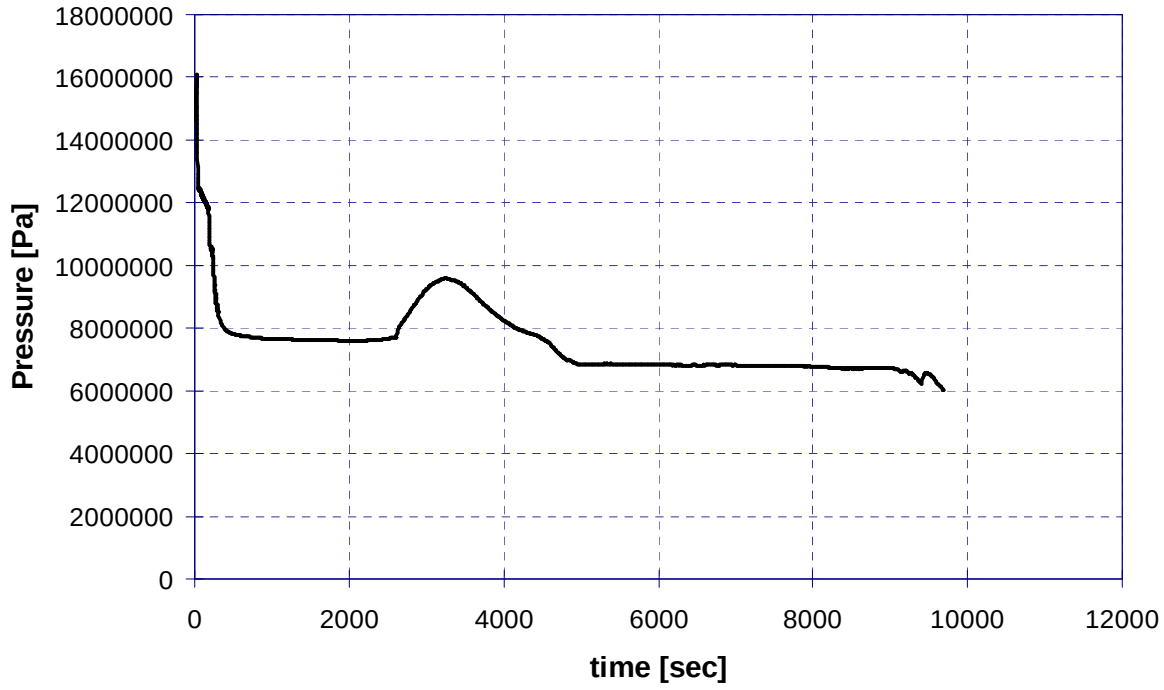

Figure 3.5: Pressurizer pressure

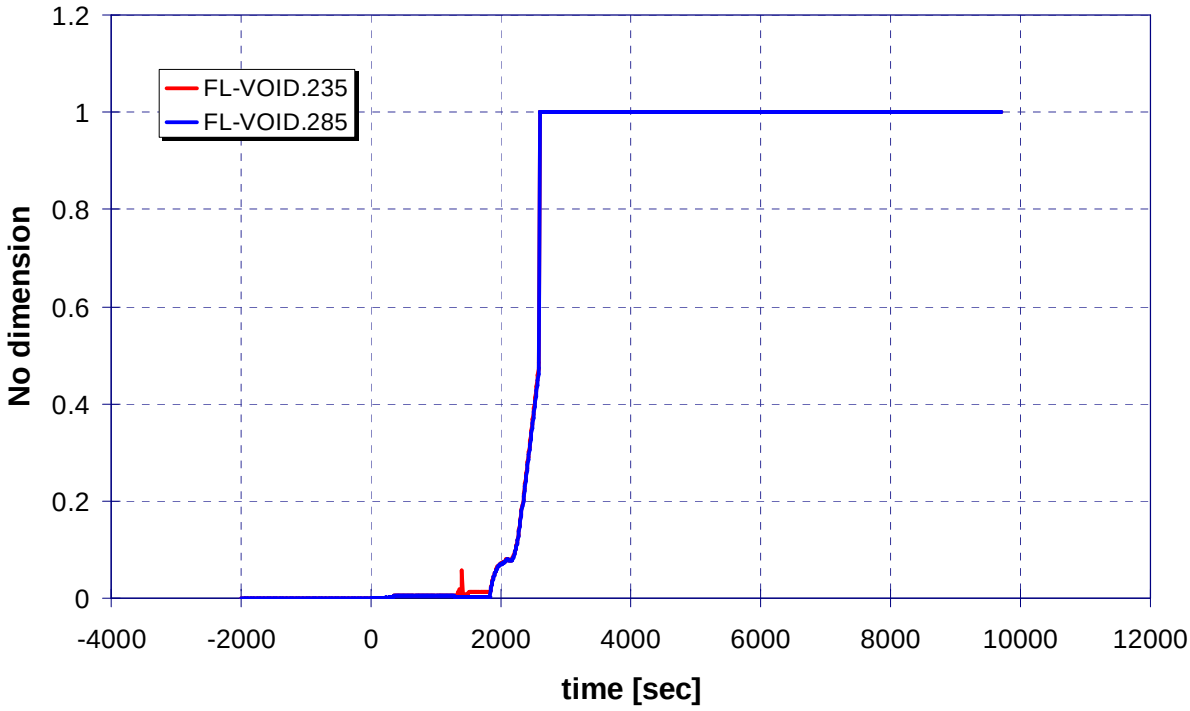

Figure 3.6: Main pumps void fraction

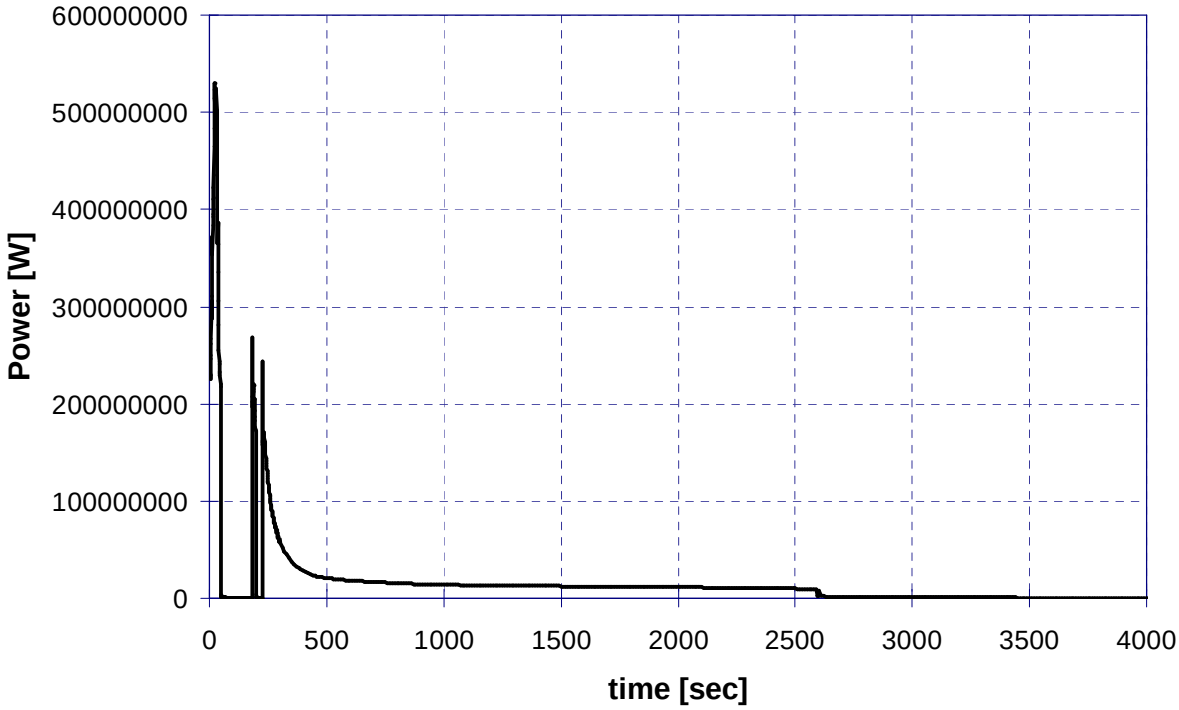

Figure 3.7: Steam generator A removed power

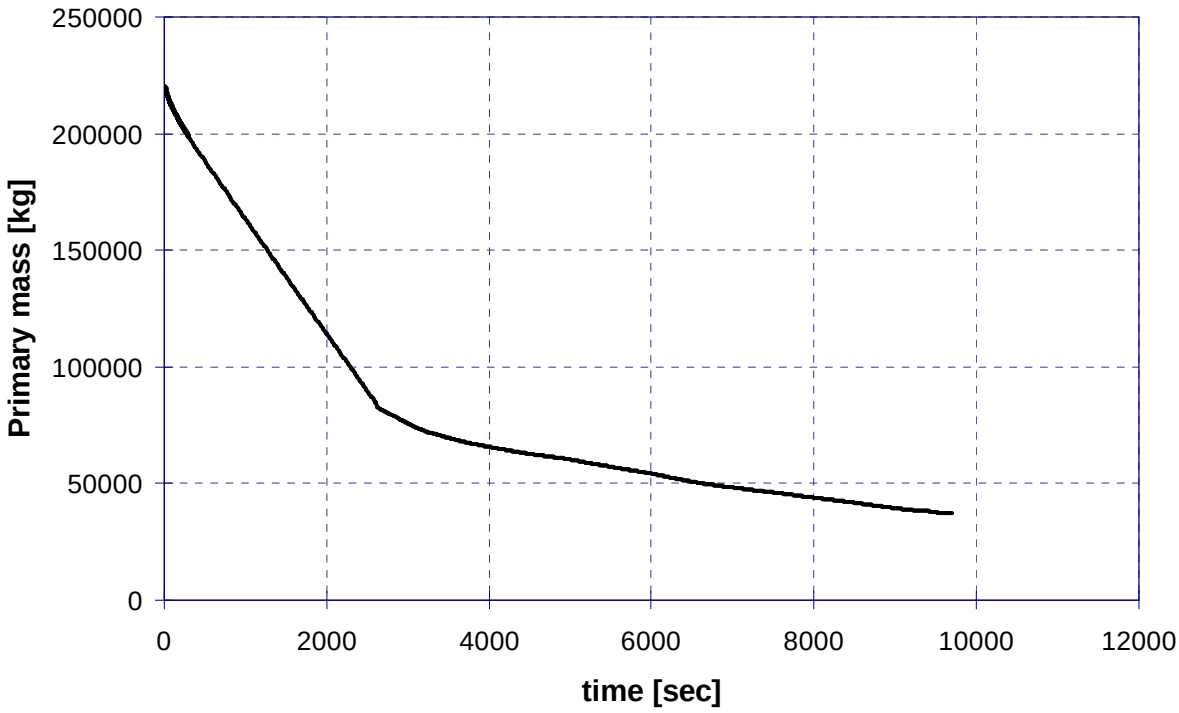

Figure 3.8: Total primary water mass

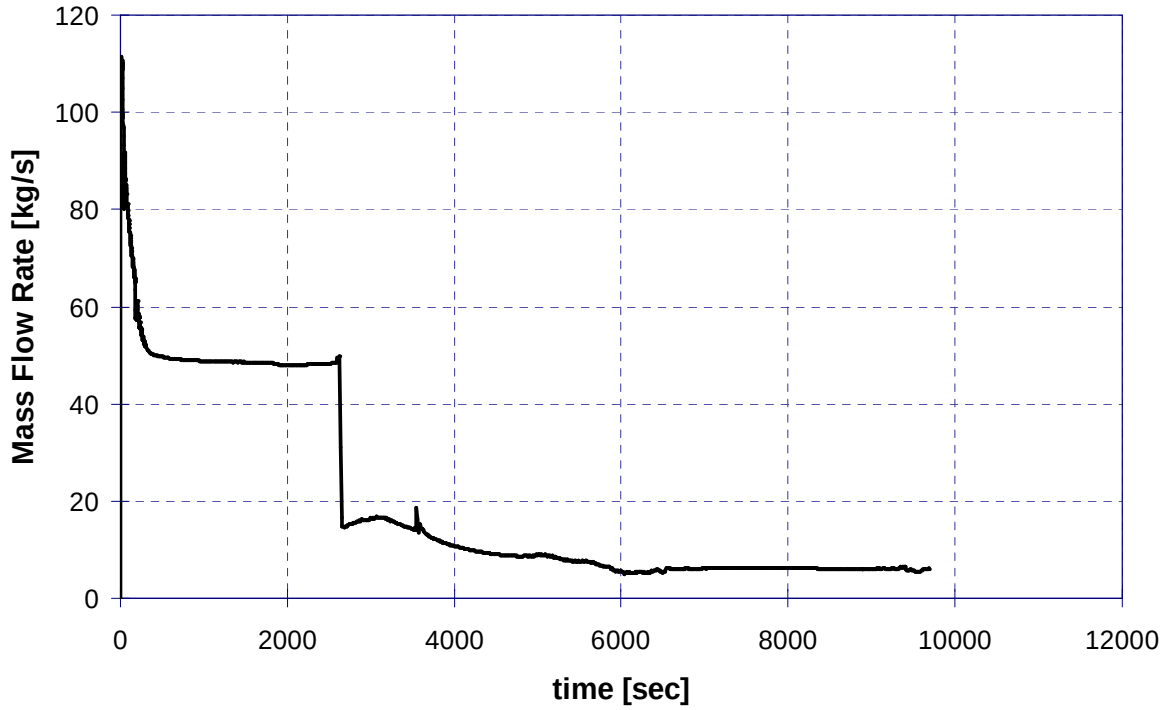

Figure 3.9: Break mass flowrate

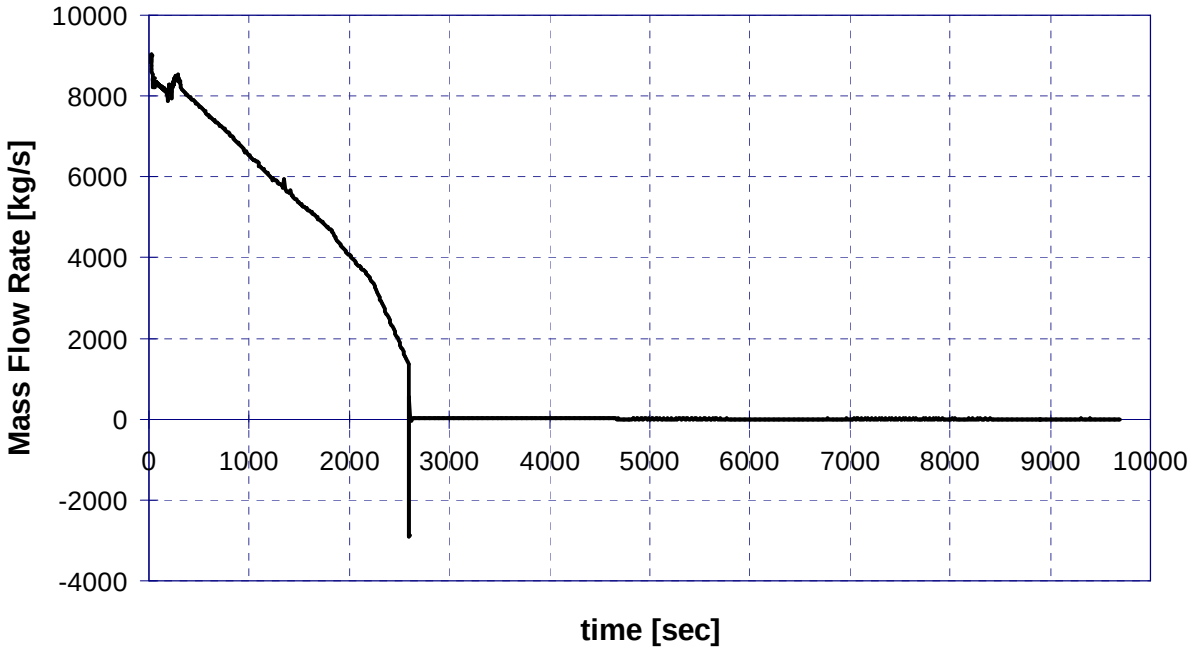

Figure 3.10: Loop A mass flowrate

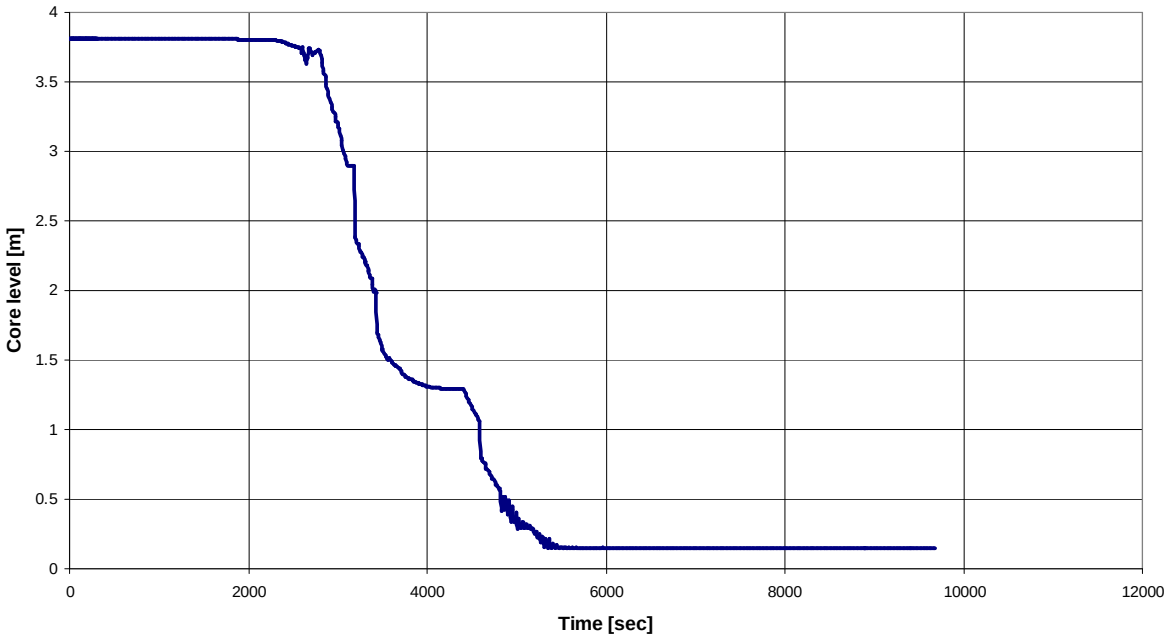

Figure 3.11: Core swollen water level

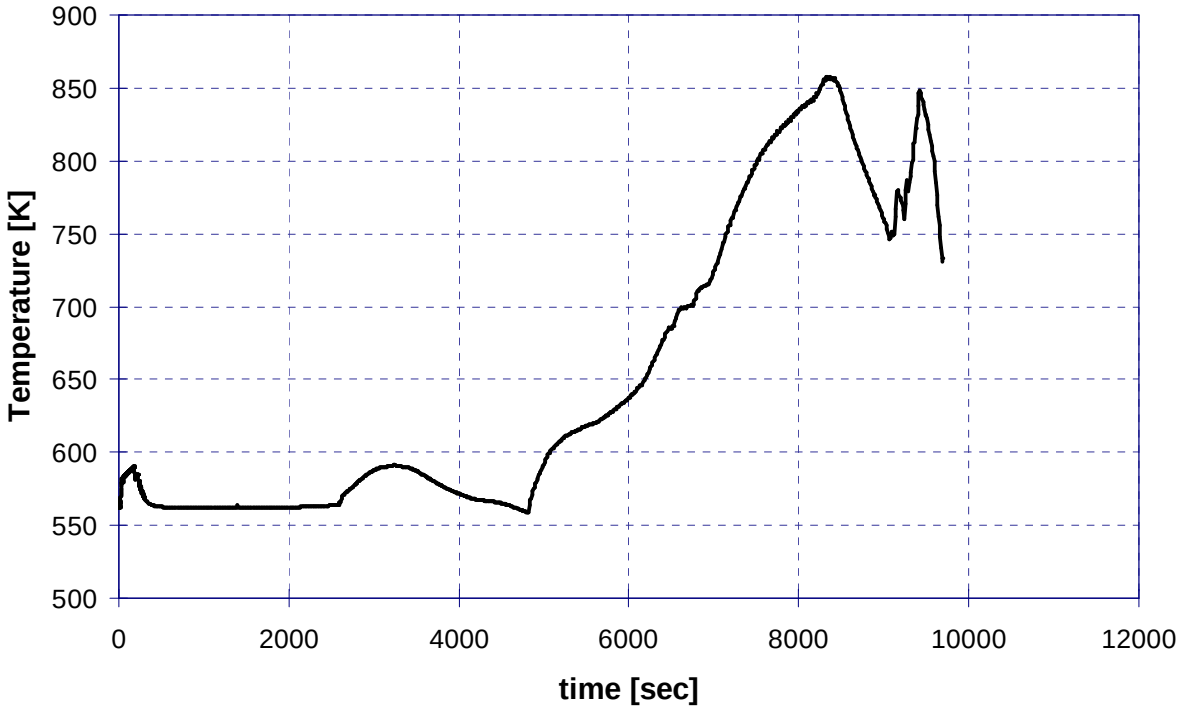

Figure 3.12: Cold leg A temperature

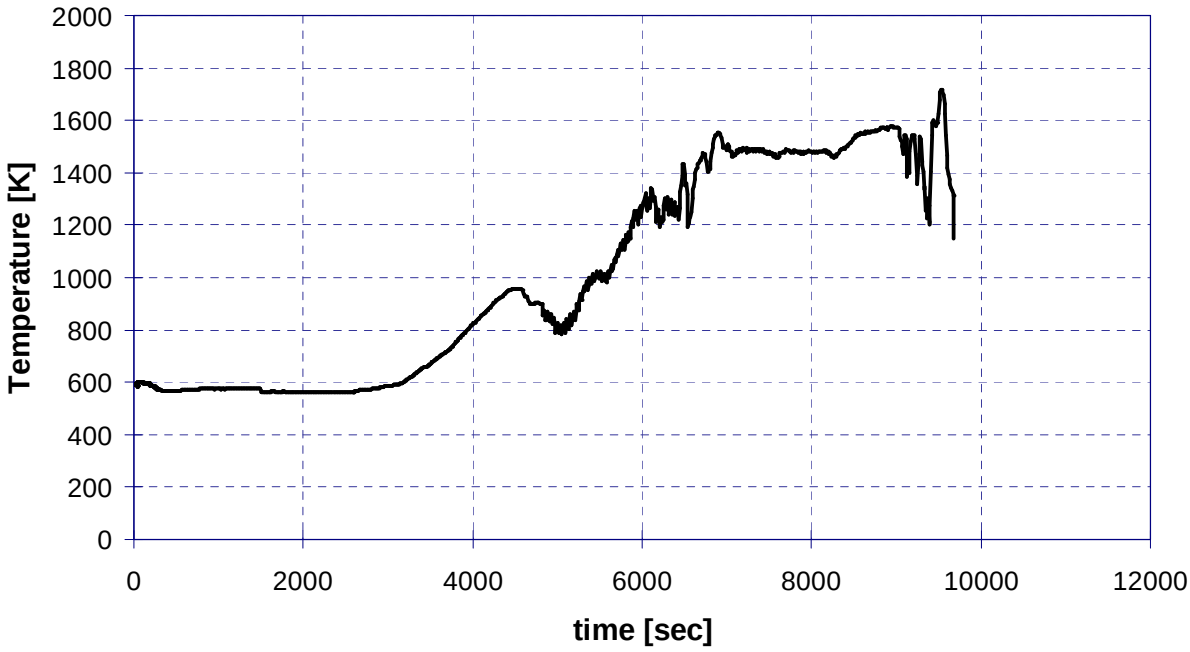

Figure 3.13: Hot leg A temperature

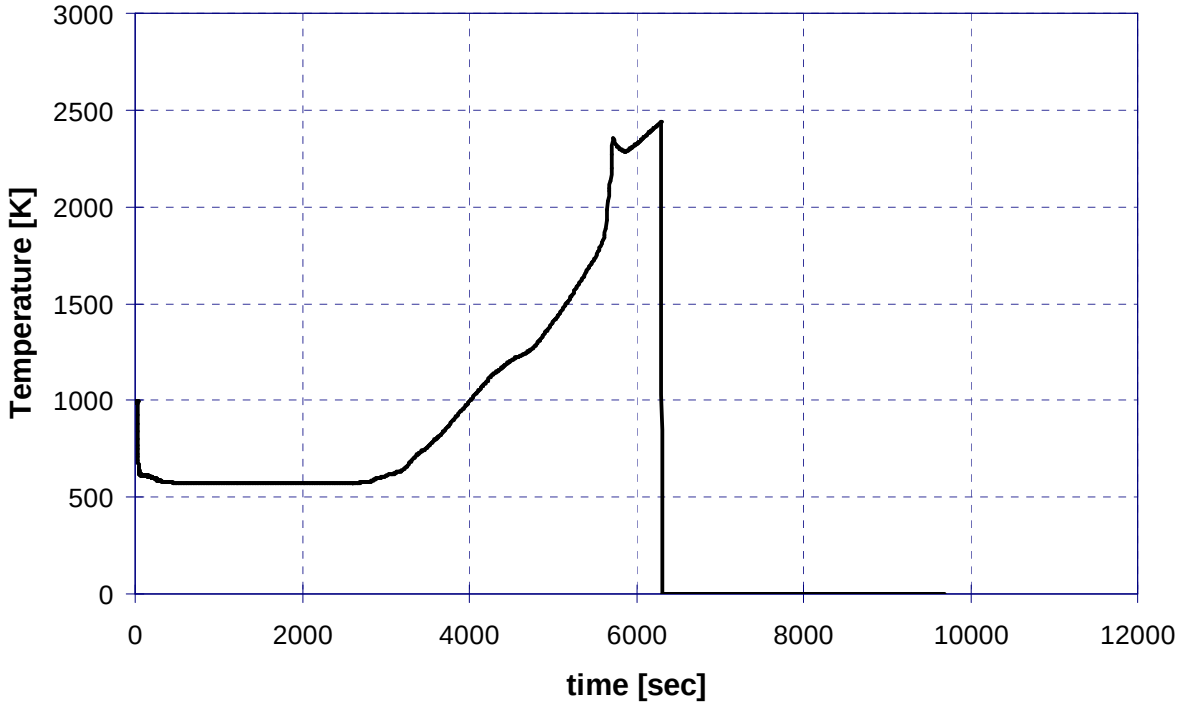

Figure 3.14: Fuel rod temperature at the top of the core

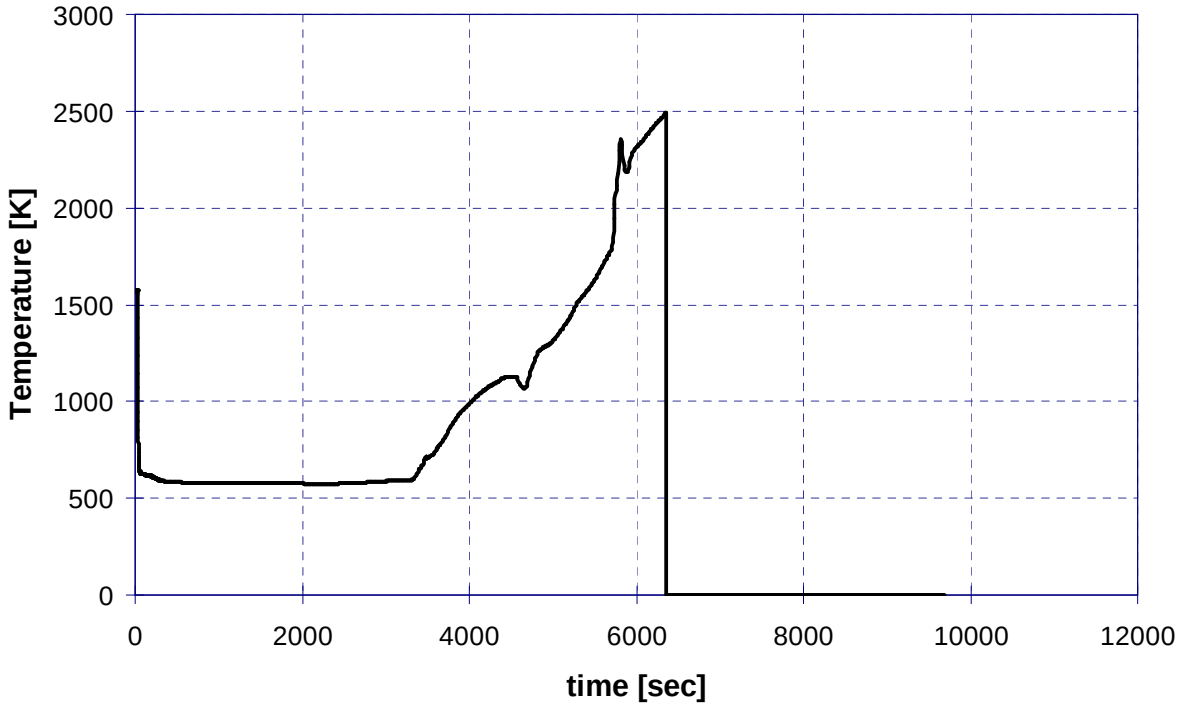

Figure 3.15: Fuel rod temperature at the middle of the core

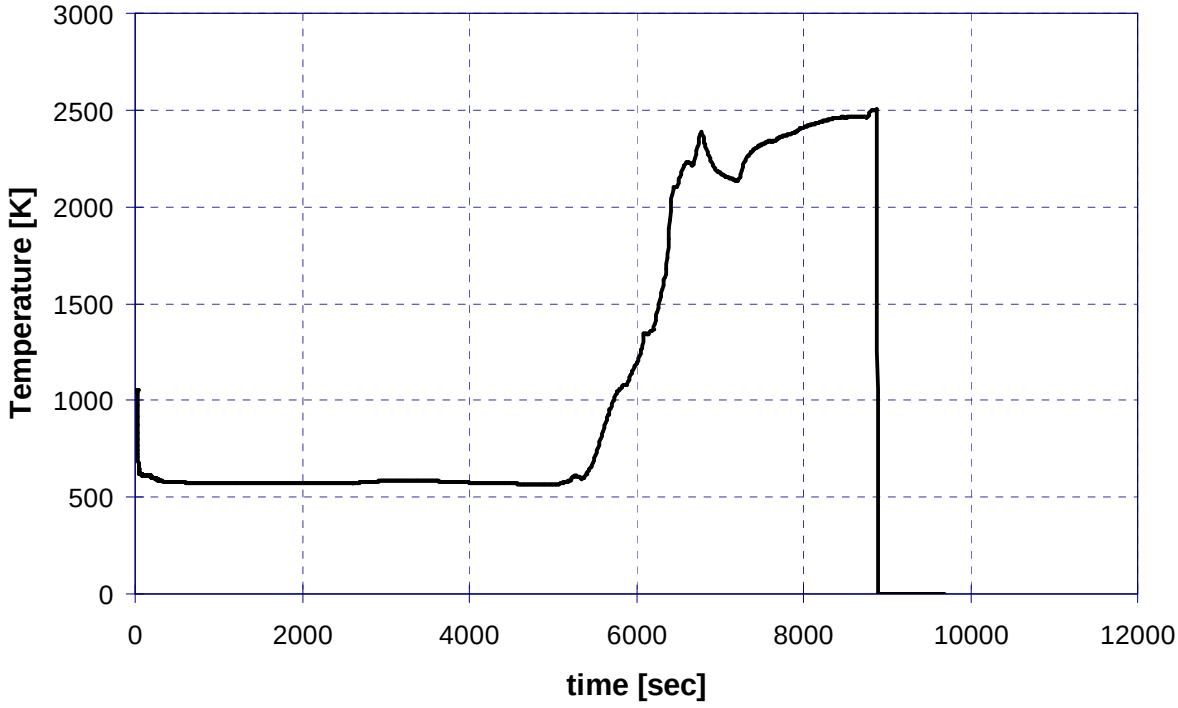

Figure 3.16: Fuel rod temperature at the bottom of the core

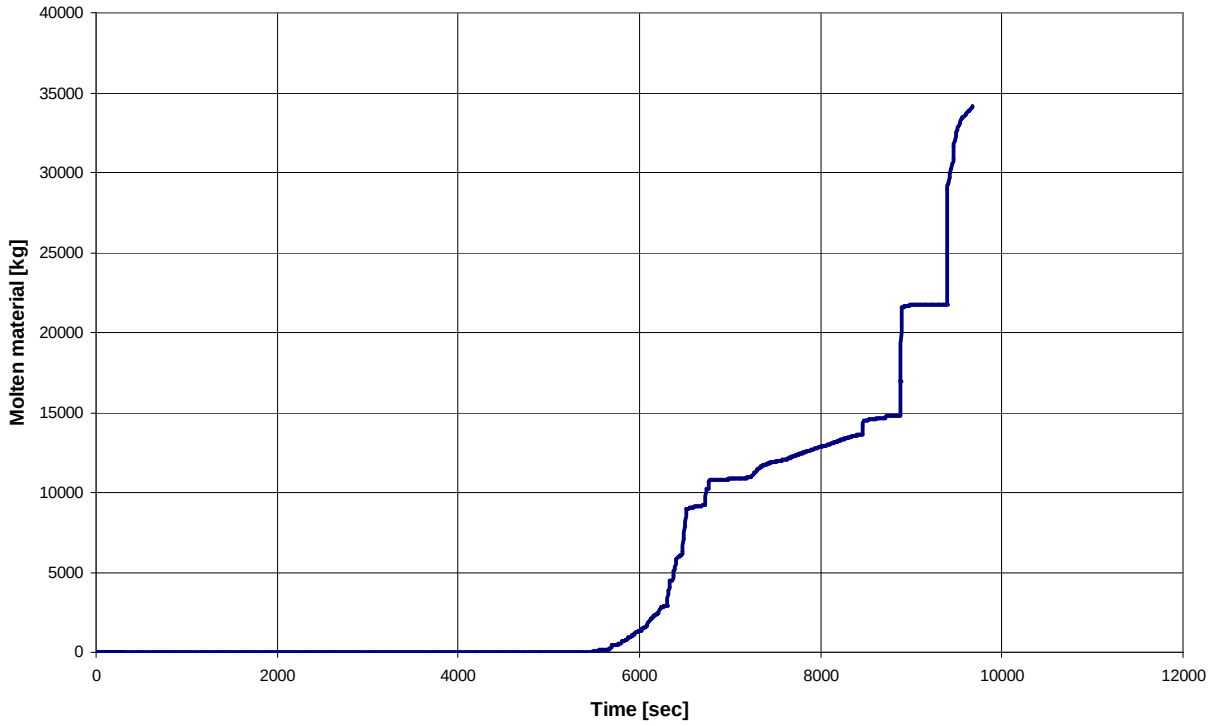

Figure 3.17: total mass of molten metals

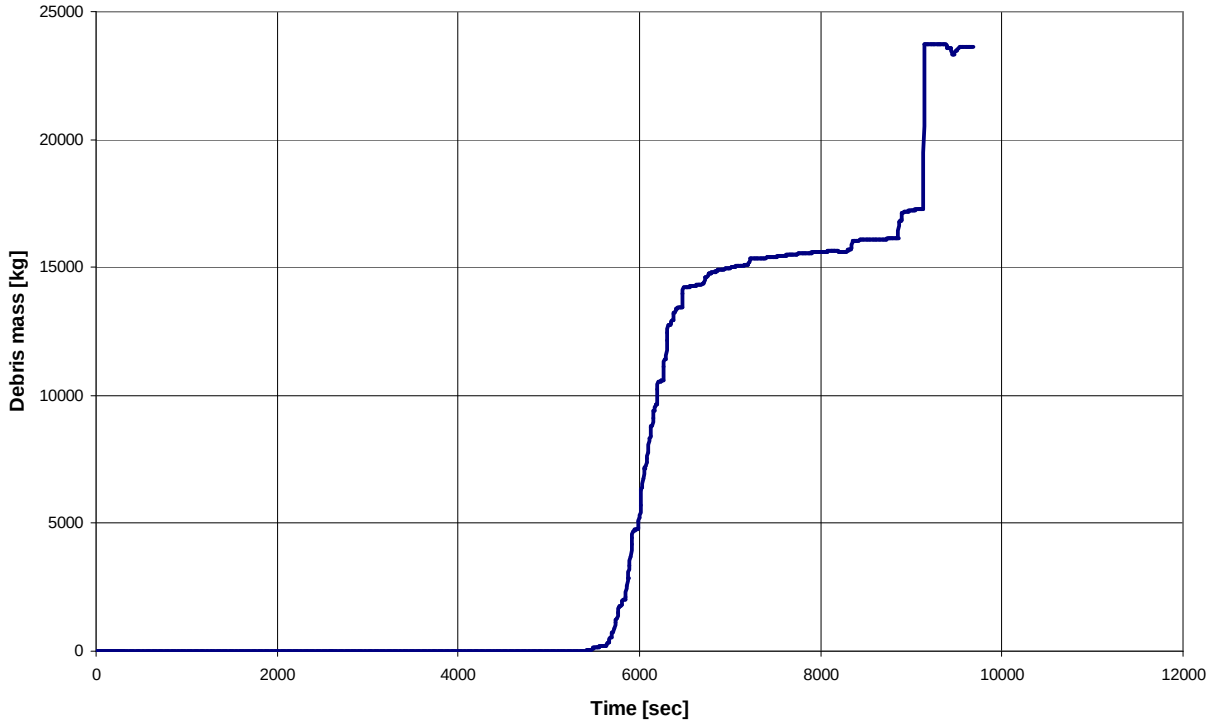

Figure 3.18**:** total mass of debris

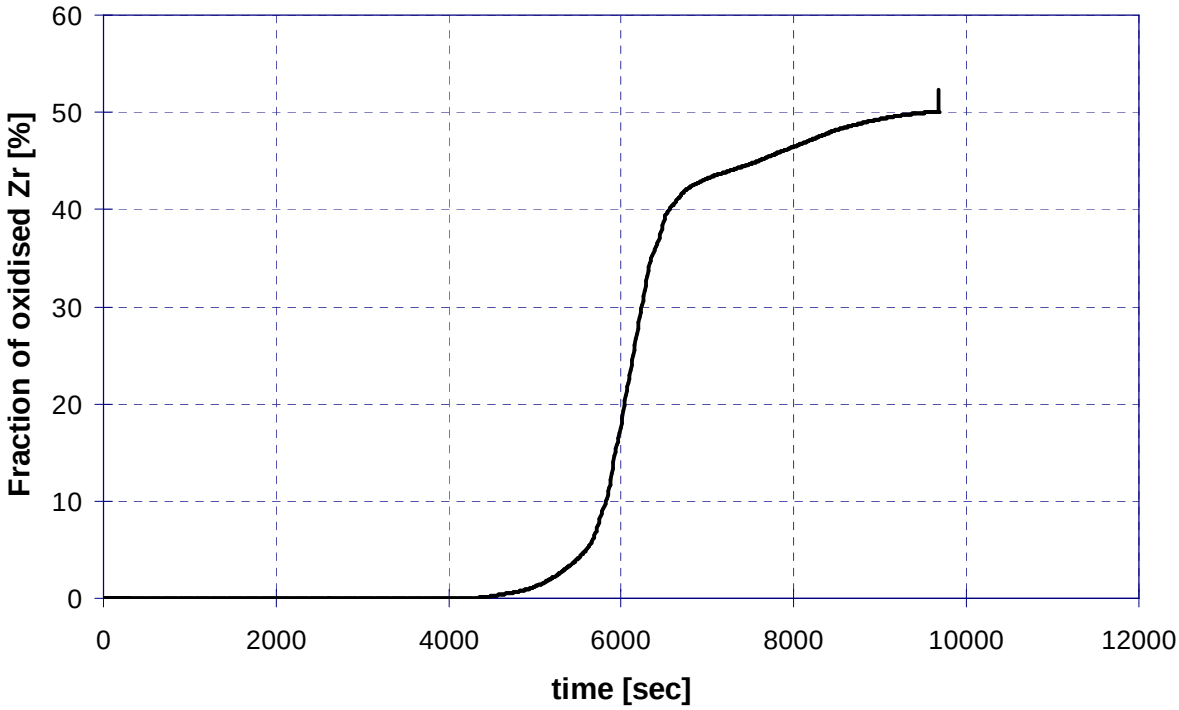

Figure 3.19: Fraction of non-oxidized Zr

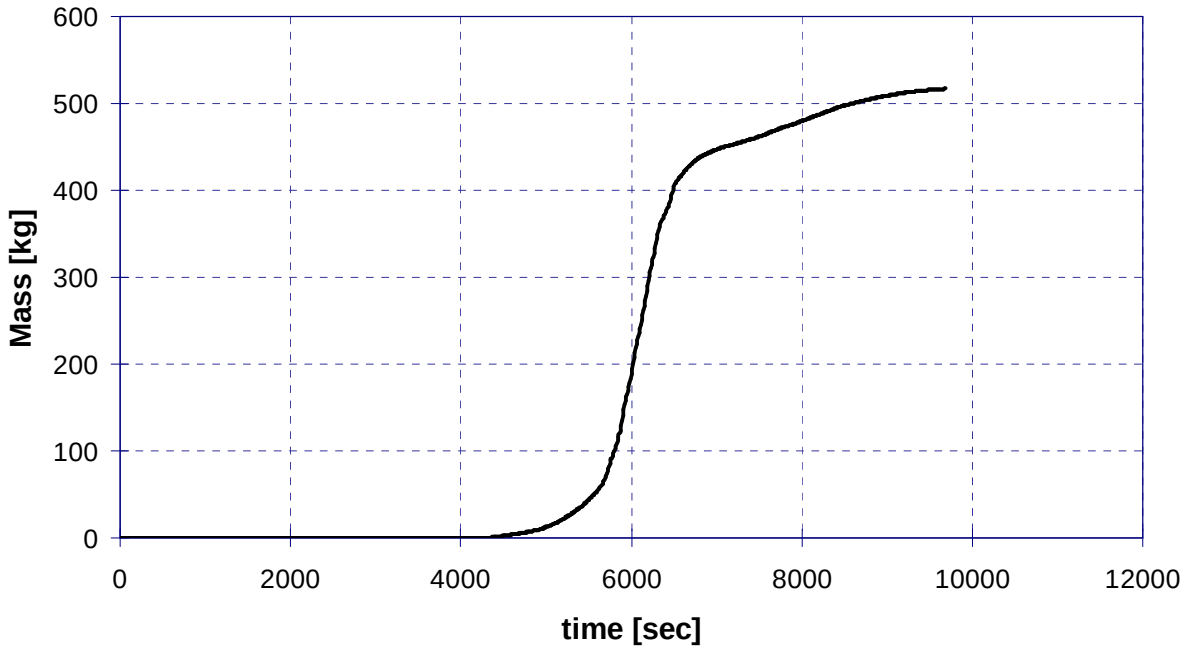

Figure 3.20: Cumulated mass of hydrogen

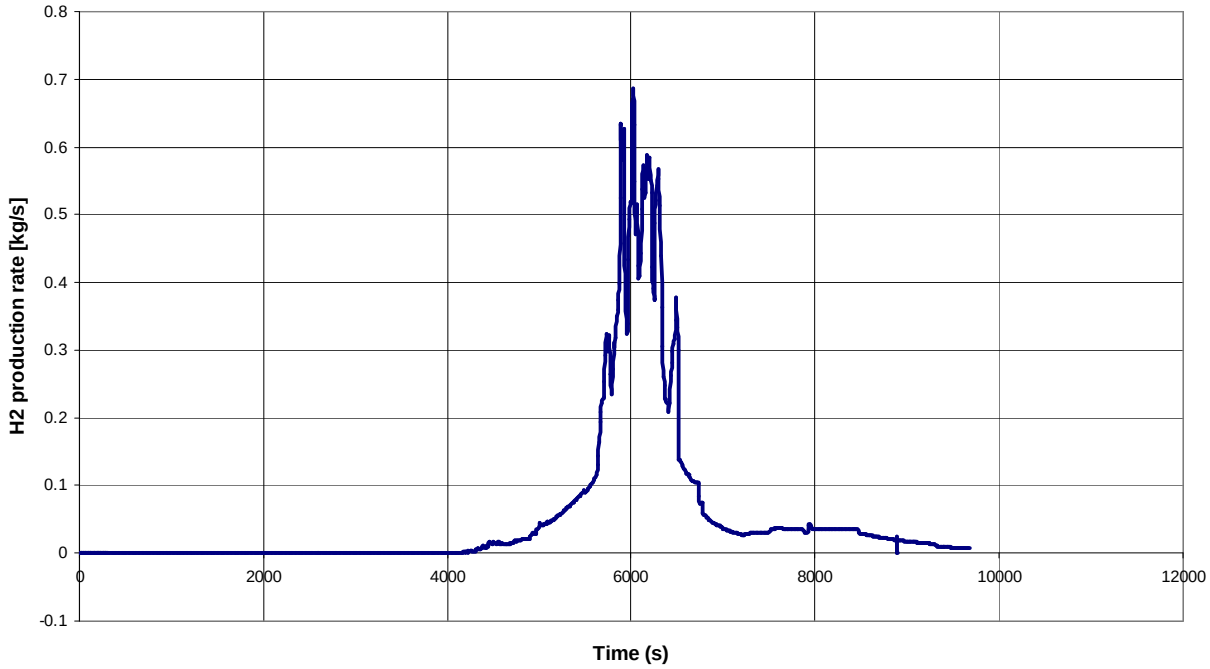

Figure 3.21: Hydrogen production rate

3.5 Synthetic view of the core at selected instants

In the following some of the most significant variables relating to the degradation phase of the core are sketched, as contour plots extended to the active zone of the core (from the bottom support plate to the top of the fuel rods) at different given times.

Figure 3.22 shows the core void fraction from 2000 s to 5000 s during the accidental transient. Up to main pumps trip (at about 2600 s), the amount of voids in the core is quite low and slightly larger in the lower zone due to the progressive emptying of the downcomer as a consequence of the break loss. After pumps trip it is quite evident the stratification in the core with a progressive increase of voids and at 5000 s since the beginning of the transients the whole core shows a void fraction greater than 70%.

As a consequence of the increase of core void fraction and core decay power, the cladding temperature (Figure 3.23) starts to increase in the central upper zone of the core, reaching the value of 1000 K after 4000 s. At this time oxidation of zircaloy starts adding a new thermal power source to the fuel rods and at about 6000 s the melting point of zircaloy is reached in quite a large fraction of the core. The last two sketches of the Figure 3.23 shows the relocation of the material that is molten or transformed in debris from the upper and central zones of the core towards the lower plate.

Finally the Figures from 3.24 to 3.28 show the contour plots of the linear mass (kg/m) of the most significant core materials at five different times during the transient. The use of linear mass allows for the comparison between the cells of different size which model the core. At about 5000 s the oxidation of zircaloy starts in the hottest (central and upper) parts of the core, leading to a slight depletion of the zircaloy in the same location, while neither molten metal nor any degradation of the fuel is still detected (Figure 3.24).

After 6000 s since the beginning of the transient, zircaloy begins to melt and almost disappear from the upper and central zone (largely is still being converted to oxide) and is relocated by candling towards the lowest zone of the core, where refreeze or radially flows towards the external zone of the core. At this time some of the upper part of a little number of fuel rods are also failed and have been converted to debris and relocated downward (Figure 3.25).

After 7000 s almost half of the zircaloy initially present inside the core has been oxidized and the remaining is located in the lower-external zones of the core (and partly has also flowed through the support plate to the lower plenum). A larger number of fuel rods is predicted to fail in the upper zone and is relocated downward where it seems to create a sort of crucible collecting other downward flowing molten materials (Figure 3.26).

The transient then shows an increasing extension of the degraded core (Figure 3.27), even though natural circulation still present inside the vessel is able to prevent the failure of the more external zones of the core, up to the time when the relocated materials join the lower support plate (Figure 3.28) causing after a short time its partial failure, with a consequent massive transfer of materials on the vessel lower head.

3.5.1 Core void fraction

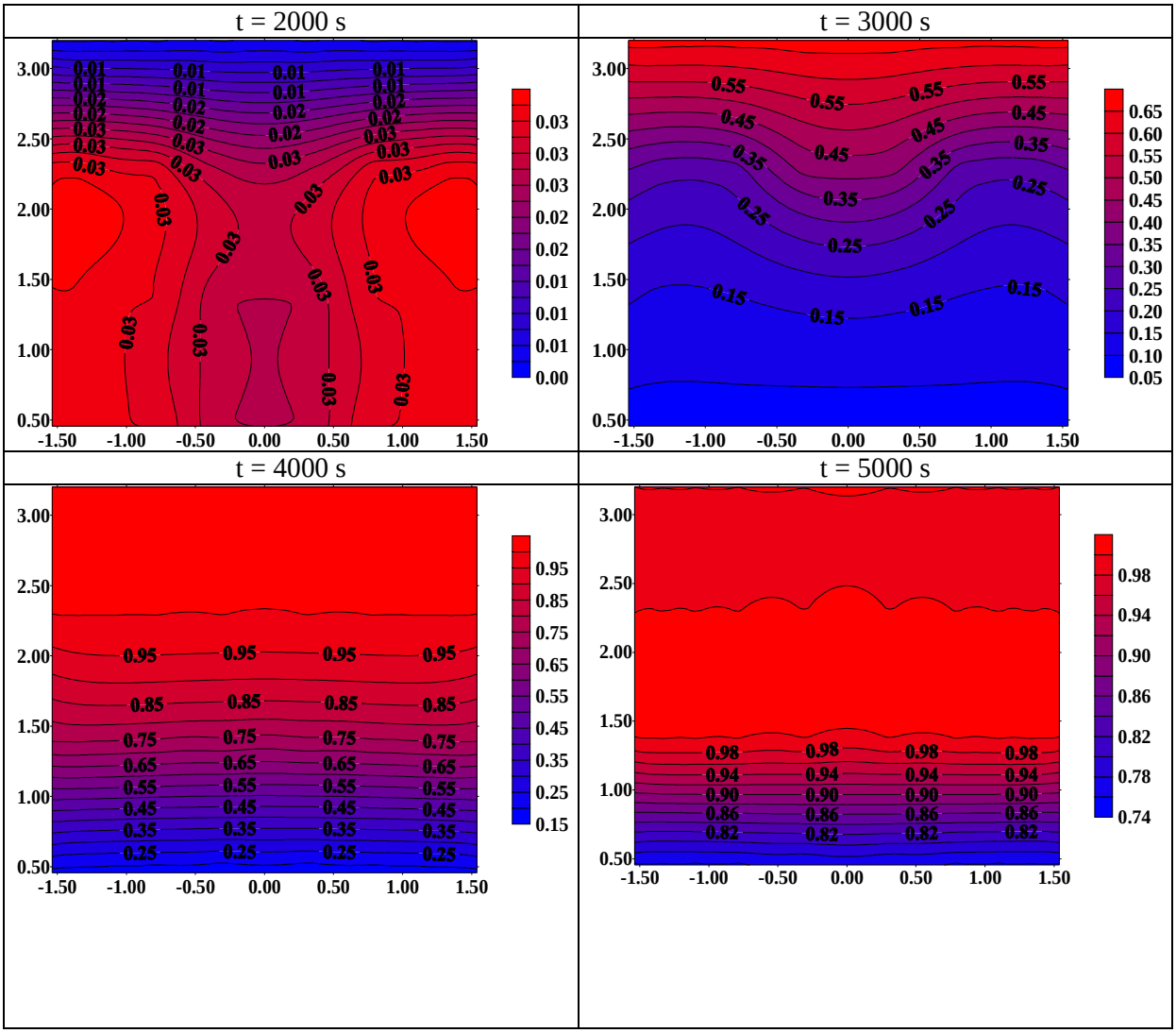

Figure 3.22**:** Core void fraction (t = 2000 - 5000 s)

3.5.2 Cladding temperature maps

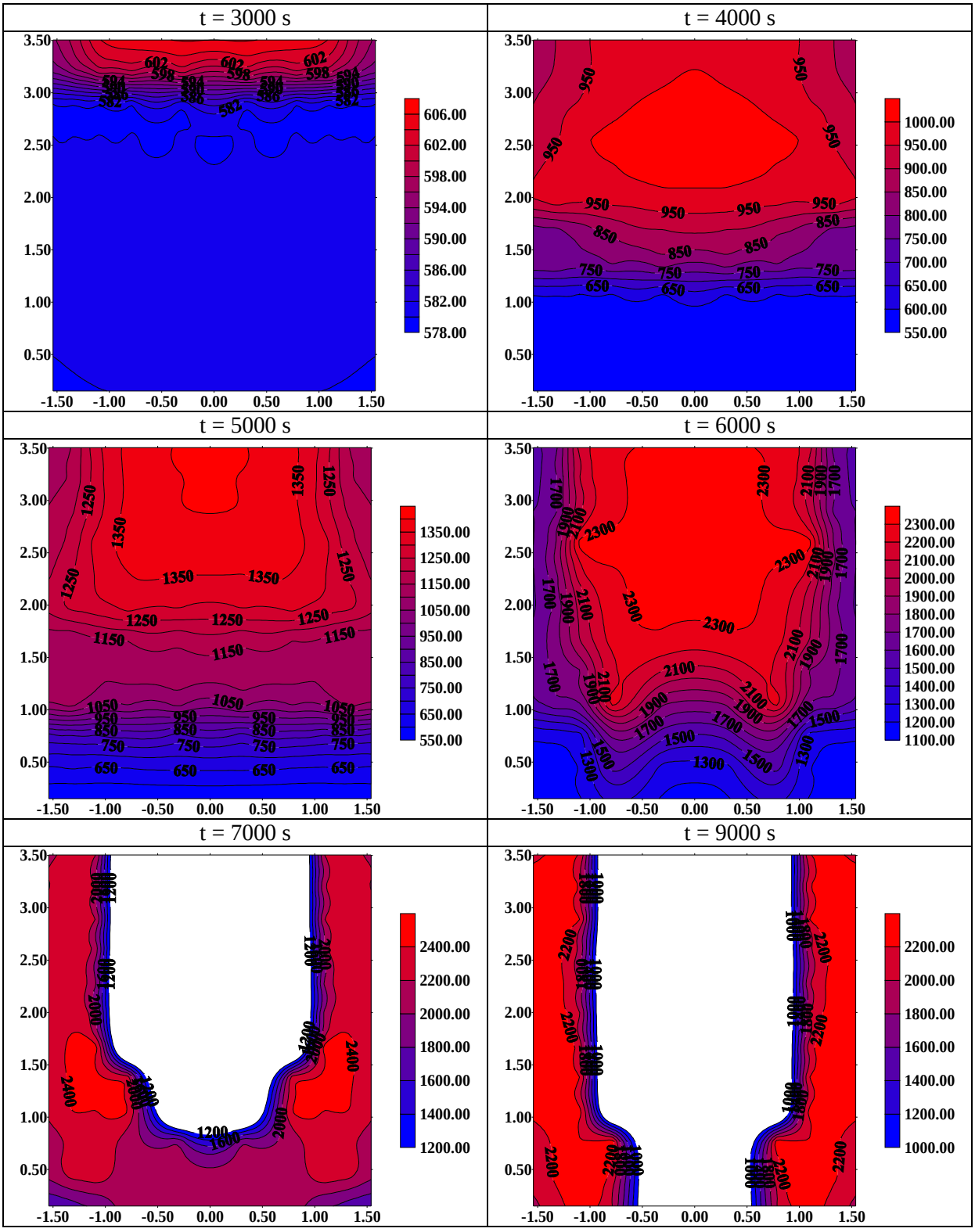

Figure 3.23**:** Cladding temperature (t = 3000 - 9000 s)

3.5.3 Linear mass of materials at different instants

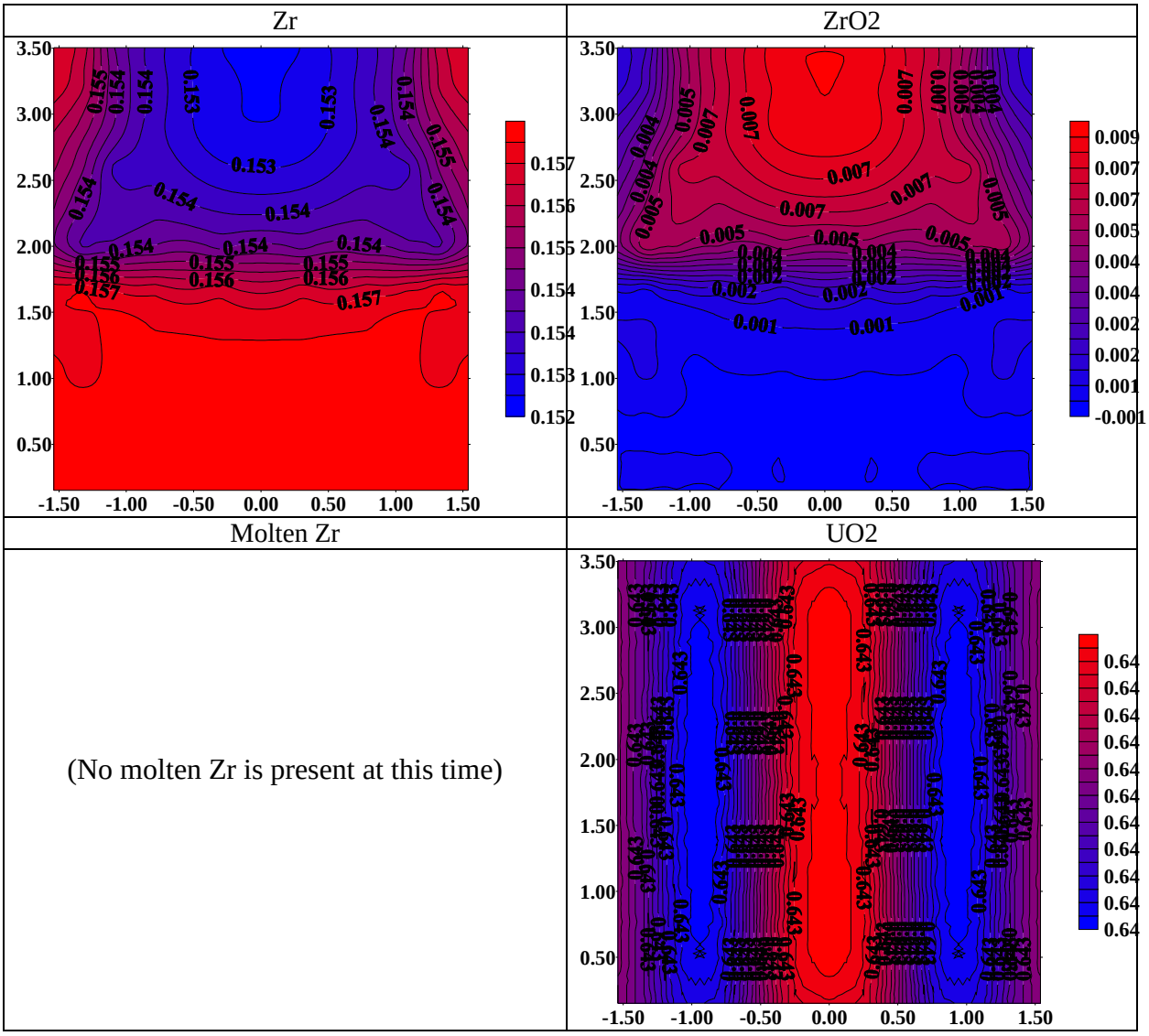

Figure 3.24: Linear mass of core materials at t = 5000 s

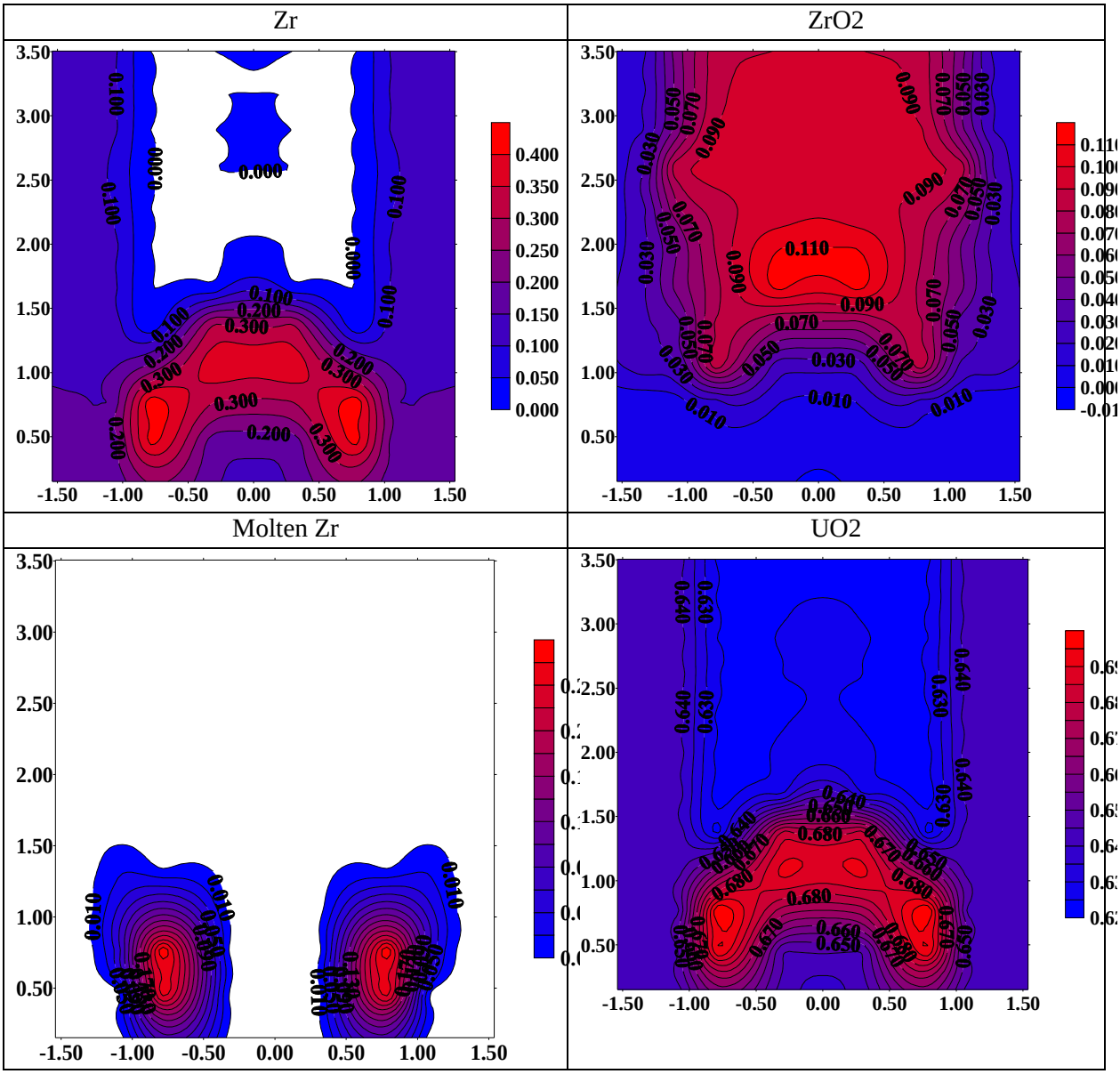

Figure 3.25: Linear mass of core materials at t = 6000 s

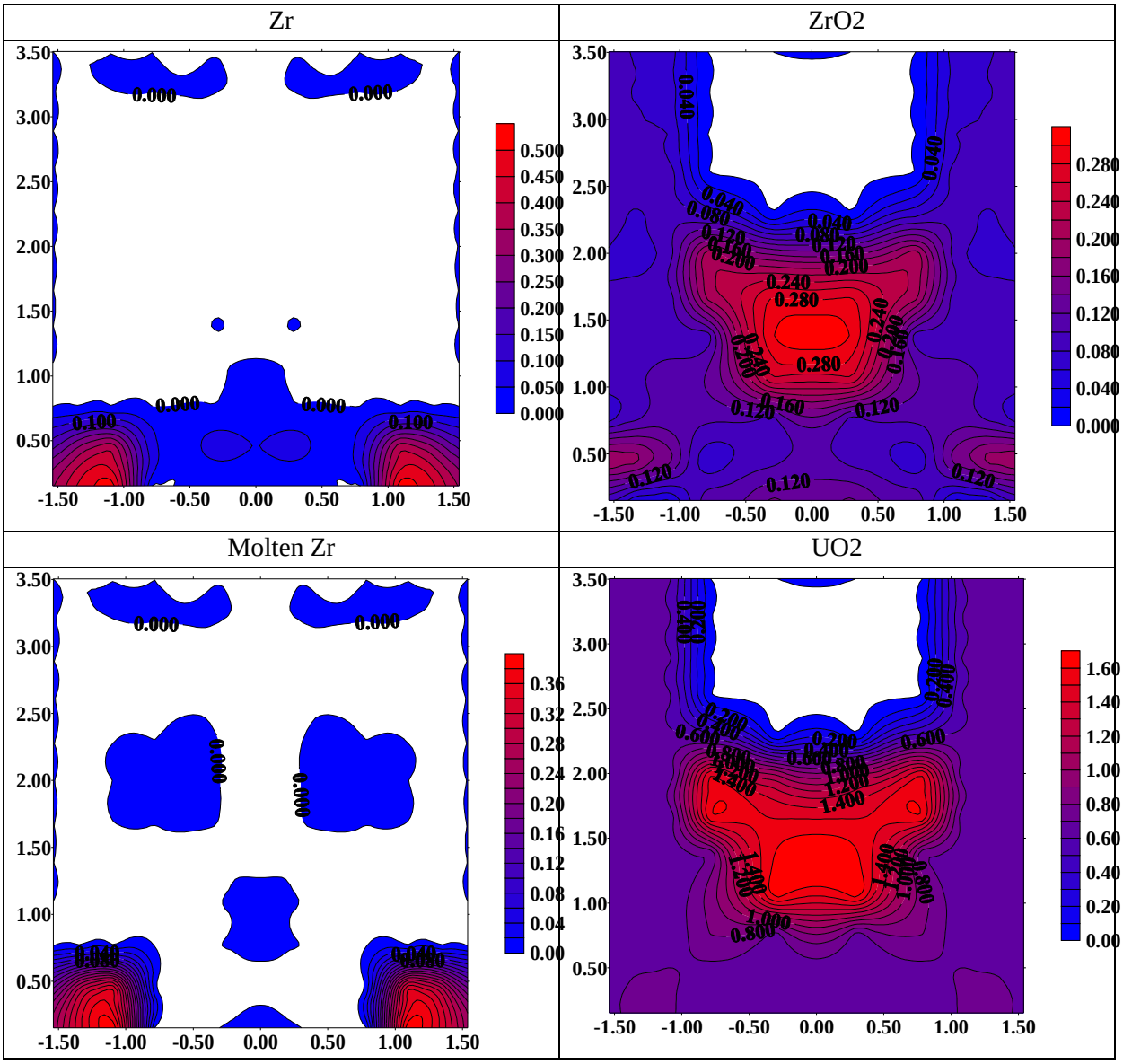

Figure 3.26**:** Linear mass of core materials at t = 7000 s

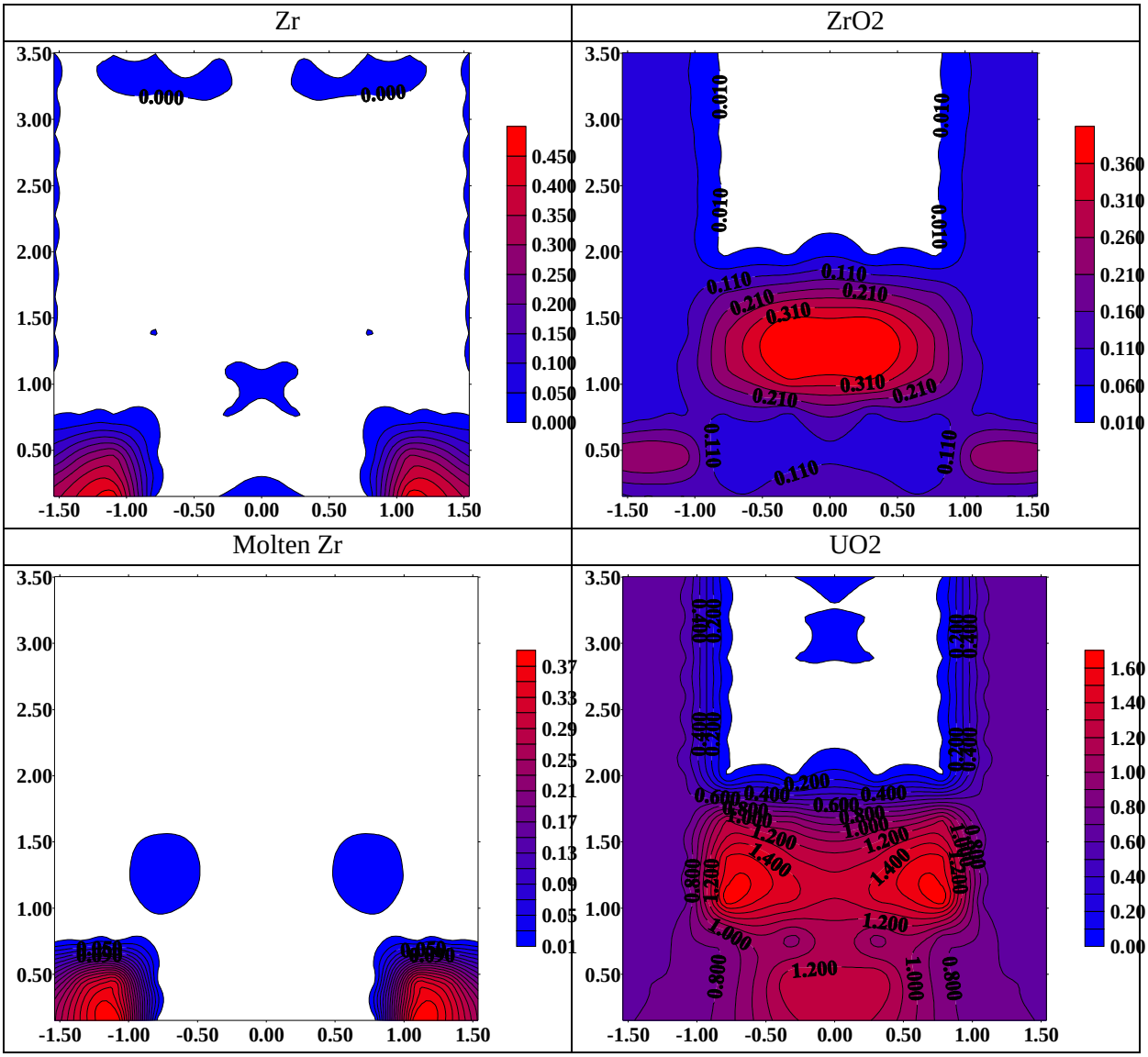

Figure 3.27**:** Linear mass of core materials at t = 8000 s

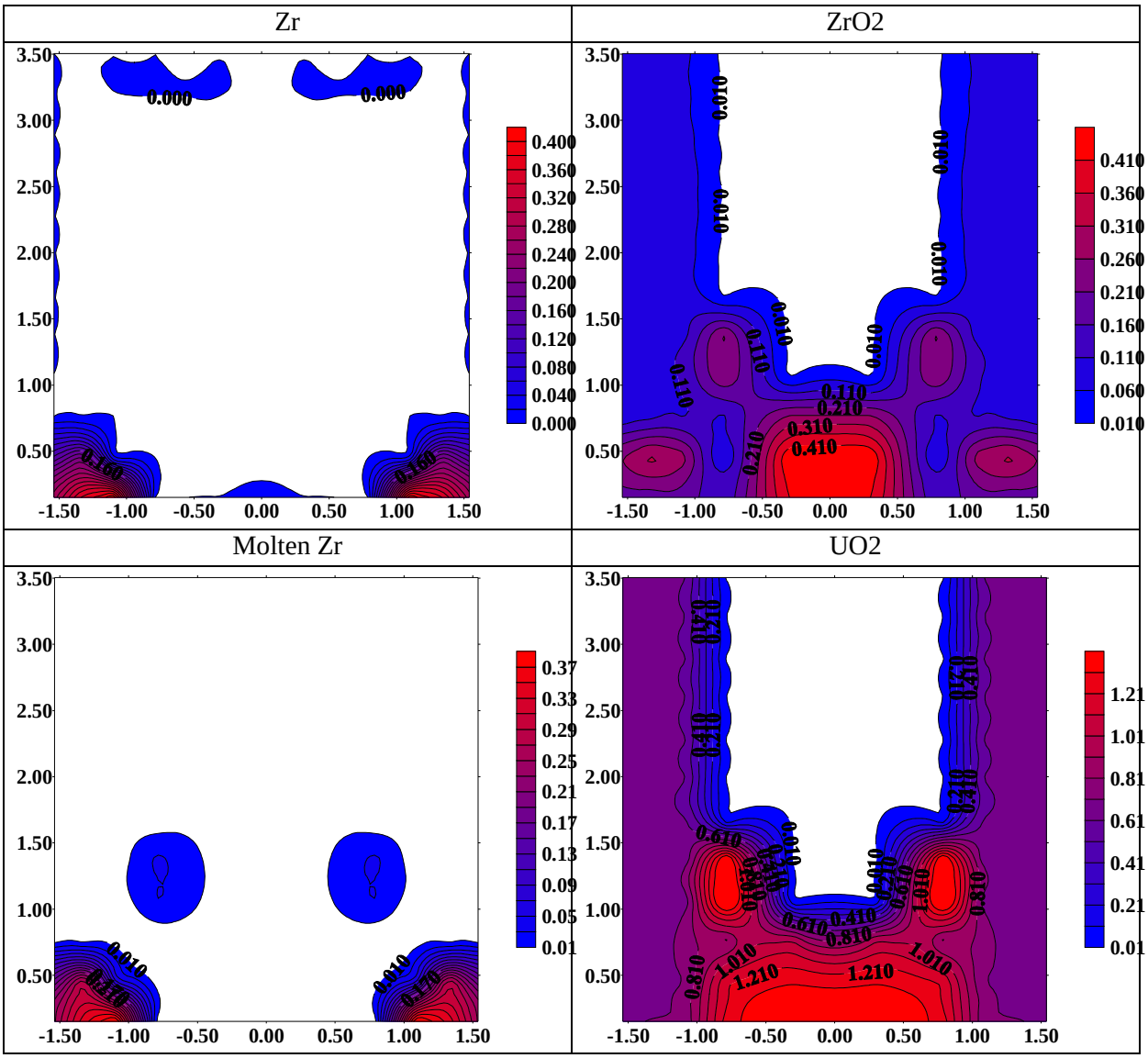

Figure 3.28**:** Linear mass of materials at t = 9000 s

3.6 Final remarks

The results obtained using the MELCOR 1.8.6 code in the simulation of a reference severe accident scenario with prescribed boundary conditions have been presented and analyzed. This exercise follows a similar activity promoted by NEA since almost 30 years to assess the capacity of current codes to predict severe accidents. In order to allow for a comparison with other codes results a reference severe accident scenario, starting with a small break LOCA with prescribed boundary conditions was defined. The transient is supposed to take place in a plant similar to the TMI-2 reactor and a model of the primary system of this plant was set up for MELCOR. Moreover some parameters allowing to judge the quality of

the predicted results were proposed, in order to assess the predictive quality of the code and the adequate capacity of the code user.

The same nodalization used to simulate the first two phases of the TMI-2 accident has been used for this benchmark, with proper boundary conditions. Moreover, minor changes were performed with respect to this benchmark, in order to reduce stratification in the primary side and improve heat transfer through steam generators. Particular attention was devoted to the modelling of the primary vessel, in order to allow natural circulation flows, which TMI-2 evidence showed as extremely important in the correct simulation of core degradation.

Relating to the thermal-hydraulics phase, up to pump stops, the predicted results are in good qualitative agreement with those of the first phase of the TMI-2 accident. The states of the core and the primary circuit at the time of pump stops is strictly related to the break mass flow rate and to the related models employed to simulate the characteristics of the fluid upstream the break and the critical flow rate through the break.

For the degradation phase, the MELCOR code includes assessed models to describe the main physical processes of degradation as well as robust and consistent numerical schemes which make it reliable to predict a severe accident sequence with acceptable results. In particular MELCOR succeeded in calculating the scenario from the beginning to the end, without any tuning of parameters or optimization of input decks, showing the robustness of the code. Most of the parameters significant from a safety point of view (such as the hydrogen production rate and the mass of molten materials) are evaluated by the code, even though some difficulties arise when cumulative values have to be obtained.

Some weaknesses of the MELCOR code have also been identified. The first one is the melting of UO2 and its interaction with molten corium. The second one is the evaluation of structural integrity of penetrations and lower vessel head. The weaknesses to predict those phenomena are not surprising because those are areas for which experimental data are scarce and the physical understanding is still incomplete.

References

1. K. N. Ivanov, T. M. Beam, A. J. Baratta, “Pressurised Water Reactor Main Steam Line Break (MSLB) Benchmark”, Volume 1: Final Specifications, NEA/NSC/DOC(99)8, April 1999.
2. MELCOR Computer Code Manuals – Vol. 1 Primer and Users’ Guide Version 1.8.6 September 2005 - R. O. Gauntt, J.E. Cash, R. K. Cole et al. - NUREG/CR-6119, Vol. 1, Rev. 3 - SAND 2005-5713
3. MELCOR Computer Code Manuals – Vol. 2 Reference Manuals Version 1.8.6 September 2005 - R. O. Gauntt, J.E. Cash, R. K. Cole et al. - NUREG/CR-6119, Vol. 2, Rev. 3 SAND 2005-5713

4. SBLOCA accident calculation with ASTEC

The evolution of the severe SBLOCA accident sequence has been studied until molten core slumping in the lower plenum and possible lower head vessel failure. The entire transient was analyzed by mean of ASTEC V2r2p2 code. To get the steady operating condition of the plant, a steady-state calculation has been performed, to establish the initial conditions of the transient. The core degradation phenomena was simulated adopting two different models; the first taking into account of the debris bed formation (by mean of the STRUCTURE DEBRIS), while the second using the standard 2D magma model.

4.1 Brief description of the ASTEC code

The Accident Source Term Evaluation Code (ASTEC) is a severe accident code developed in common by IRSN and GRS [1]. The code calculates the transient sequences from the initiator events until the eventual radioactive fission product releases to the atmosphere, named source term. The ASTEC code is mainly used for safety analyses on nuclear installations and development/specification of severe accidents management guidelines. The code includes several coupled modules that can deal with the different severe accident phenomena: thermal-hydraulics in the reactor system, core degradation and melt release, fission product release and transport, ex-vessel corium interaction, aerosols behavior and iodine chemistry in the containment, etc. Among them, the CESAR module is used to compute the thermal-hydraulics in the primary and secondary systems of the reactor [2]. Such module is coupled to the ICARE2 module that computes core degradation, melt relocation and behavior in the lower head up to vessel failure. The CESAR module allows a detailed representation of all components of primary and secondary circuits including auxiliary, emergency and control systems [3].

CESAR is a two-phase flow thermal-hydraulic code. The gas phase can be a mixture of steam and hydrogen. The solution of the problem is based on two mass equations, two energy equations, one equation for steam velocity, and a drift flux correlation for water velocity. The state variables computed by CESAR are: total pressure, void fraction, steam and water temperature, steam and water velocity, and partial pressure of hydrogen. All hydraulics components can be discretized by volumes (one mesh) or axial meshed volumes and connected by junctions. The volumes can be homogeneous or with a swollen level. Thermal structures are used to model the walls of the components, and compute thermal heat exchange between primary and secondary systems and heat losses to the environment.

The ICARE2 module can simulate the thermal-hydraulics in the part of the vessel below the top of the core: downcomer, lower plenum and the core itself including the core bypass. The model of the lower head of ICARE2 has one single mesh for fluids, three layers for corium (pool, metal and debris), and a 2D meshing for the vessel. The ICARE2 [4] module is activated to compute core heatup and degradation, in coupled mode with CESAR, at the onset of core uncovery. Before ICARE2 activation, the thermal-hydraulics in the vessel and the core is computed by CESAR through an automatic vessel model creation based on

ICARE2 input deck. The convective and radiative heat exchanges between core components and structures are computed by ICARE2.

Most important core degradation phenomena are dealt with in ICARE2 [5] including: core material oxidation and hydrogen generation, control rod material interaction, melting and relocation, zircaloy clad melting and fuel dissolution, fuel rod clad failure and metallic melt relocation, debris bed and molten pool formation and spreading in the late degradation phase. When corium accumulates in the lower plenum, three 0-D layers are represented: oxide, metals, and debris. The heat transfers between neighboring layers, between layers and vessel walls or residual water, use recent literature correlations, depending on layer mean temperature and power. Then, the corium layers heat up the lower head until its possible melt-through or mechanical failure (by plasticity, creep, etc.).

4.2 TMI-2 ASTEC modeling

The input data for ASTEC V2r2p2 code was prepared to simulate only in-vessel phenomena; the transient finishes when molten core slumping occurs and in case of lower head vessel failure.

To perform this kind of simulation, two ASTEC modules were activated:

- CESAR to simulate the thermal-hydraulics in the RCS, secondary circuit and vessel (with simplified core modelling) up to the beginning of core degradation phase;
- ICARE to simulate in-vessel core degradation phenomena, and thermal-hydraulics in the reactor vessel during this phase;

The drawing of the Babcock and Wilcox lowered loop plant and the graphical representation of the ASTEC primary and secondary circuits are given respectively in Figure 4.1 and in Figure 4.2. The primary part of the RCS input model is a coarse node representation of the hydraulic system and structures comprising about 39 hydraulic control volumes, of which 22 cells are used for the shell side of the steam generators. The secondary circuits are discretized in 30 fluid meshes. The plant simulation includes a detailed modelling of the primary coolant system with:

- reactor pressure vessel volumes and structures, including the VENT valve between the cold collector and the hot collector,
- two primary coolant loops (1 hot leg and 2 cold legs in each loop) with once-through steam generators and main coolant pumps,
- pressurizer with surge-line, PORV, heaters, spray-line and valve,
- main emergency and control systems.

The modelling of the secondary systems is limited to the pipe side of the steam generators, the steam lines with isolation valves, and main feedwater and auxiliary feedwater injections. The simplified reactor vessel adopted by CESAR, to compute the steady state

conditions, consists of four volumes: the core, the bypass and the downcomer volumes discretized into 20 axial meshes, and the lower plenum volume.

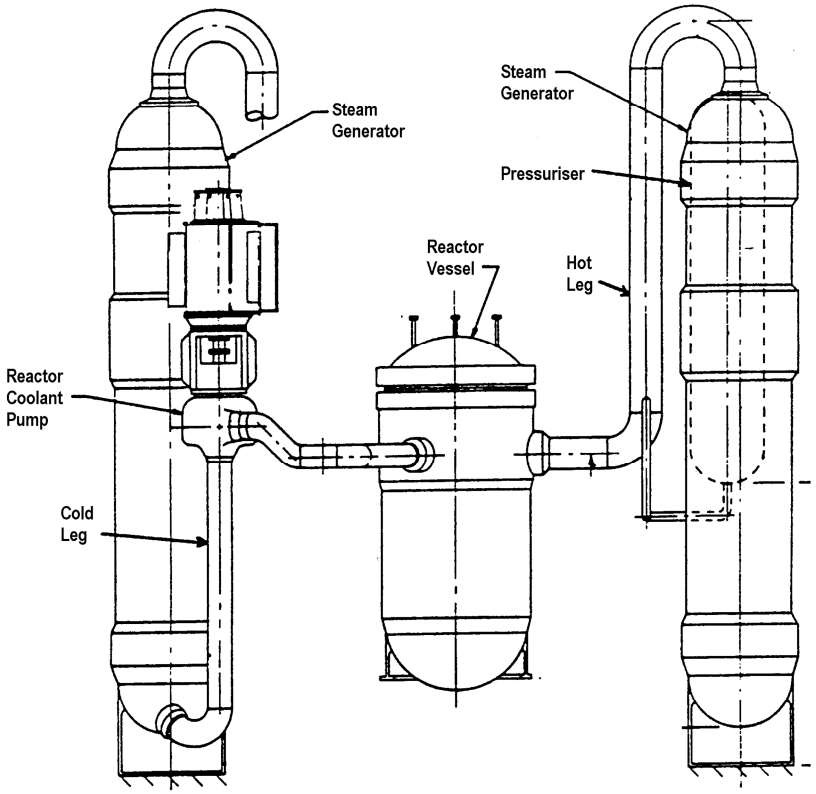

Figure 4.1: Babcock & Wilcox Lowered loop

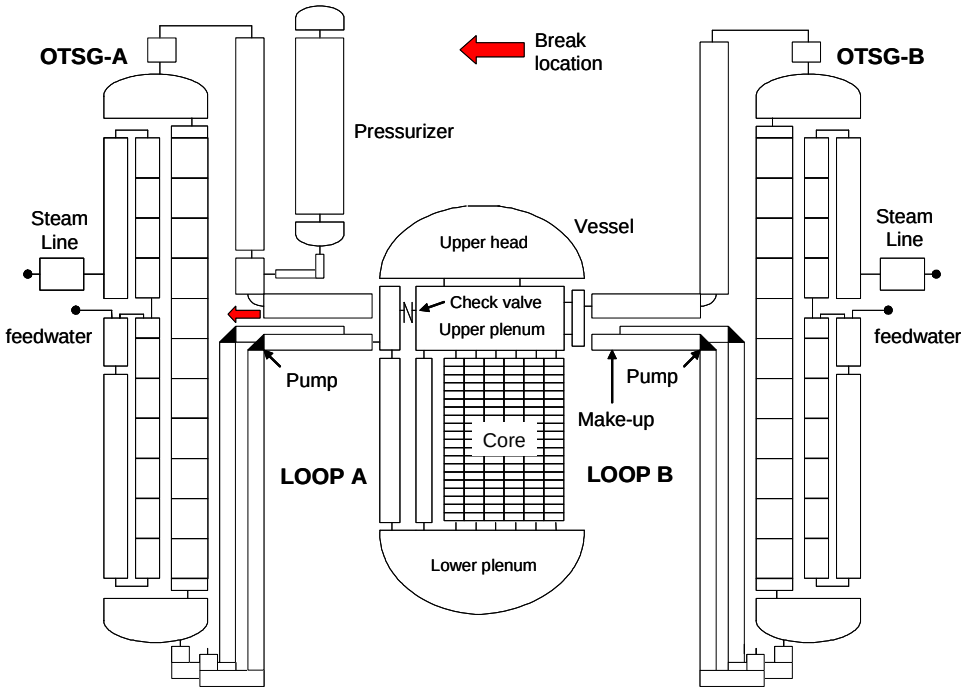

Figure 4.2: Babcock & Wilcox ASTEC nodalization

The ICARE core model shares the same volumes and axial nodalization with the CESAR simplified model, but in this case, the core is further subdivided in 6 radial rings for a total of 161 mesh. In each ring, only one representative component of the fuel and control rods is considered, weighted by the number of rods. The baffle, the barrel and the thermal shield at the core periphery are also represented. The control rod component simulates all the full and part-length control rods, all the guide tubes (including those containing burnable poison rods) and all the instrument tubes. Mass and energy rates of change for core materials are calculated for each core node. The radial peaking factor are fixed for each ring, and an axial peaking factor is assigned for each row.

4.2.1 DEBRIS and NO DEBRIS models

The core degradation process is characterized by the high complexity of phenomena to be considered and geometry to be accurately presented, with a permanent appearance and disappearance of a large number of components in each control volume by e.g. melting, failure, relocation, and chemical reactions. The geometry of a degraded core is very complex and heterogeneous: rod bundles with spacer grids, fluid channels possibly blocked with molten/frozen mixtures of materials, corium molten pool with crusts, debris beds, peripheral and lower/upper core structures (e.g. horizontal plates, vertical surrounding walls such as barrels or shrouds), also partly or totally molten. In this work, two different models were adopted to reproduce the core degradation phenomena, the first called (in this work) NO DEBRIS case and the second called DEBRIS case (6). The first one use a special macro-component, called magma, which is especially devoted to deal with the 2D movement and relocation of the molten materials. The magma can be either liquid corium or liquid/solid corium. The second simulation (DEBRIS) also use the magma macro-component, but it takes also into account the formation of a debris bed by mean of the activation of the model DEBRIS. In this case, the user can define the threshold values of some variables, which, once achieved, will lead to the debris bed collapse.

The user criteria regard the following variables:

- the debris bed porosity: if the debris are heated up and melt down, the void fraction in the medium can become too high for the debris to stay in place,
- the debris bed mass: for the same reason than previously, the debris mass will decrease
- thresholds which can lead to the collapse of the particles,
- the debris bed temperature: when a certain temperature is reached, almost all the debris are liquid and the remaining solid phase can fall down.

In the input data file, the user can introduce criteria on these local variables to trigger the debris bed collapse as well as an instant of the transient. When the criteria are reached the solid particles are supposed to be able to fall down onto a receiver component that has to be determined (note that, as usual in ICARE, debris particles are regarded as spherical particles).

4.2.2 Adopted parameters and criteria

The Table 4.1 below illustrates the parameters and the models used to analyze the transient. These criteria have been established by mean of the interpretation of several separate-effect and integral experiments.

Table 4.1: Parameters and criteria adopted

PARAMETER	ASTEC (*) DEBRIS MODEL	ASTEC (*) NO DEBRIS MODEL
Zircaloy oxidation kinetics	BEST-FIT correlation: Cathcart-Pawel in the low temperature range and Prater-Courtright in the high temperature range	BEST-FIT correlation: Cathcart-Pawel in the low temperature range and Prater-Courtright in the high temperature range
Cladding failure criteria	Tclad > 2300 K and ZrO2 thickness < 0.3 mm; or T > 2500 K	Tclad > 2300 K and ZrO2 thickness < 0.3 mm; or T > 2500 K
Melting point of UO2-ZrO2 ceramic material	2550 K (PHEBUS FP tests)	2550 K (PHEBUS FP tests)
Debris formation criteria	Fuel rod temperature > 2500 K	Fuel rod temperature > 2500 K
Molten core relocation into the lower plenum	Baffle melting (relocation through core by-pass) or melting at core bottom (relocation through core support plate)	Baffle melting (relocation through core by-pass) or melting at core bottom (relocation through core support plate)
Reactor pressure vessel failure	Vessel wall melting (100%)	Vessel wall melting (100%)
Debris bed	Permeability: Carman model Correlation for debris conductivity Yagi Gas conductivity constant 0.01 W/m²/K	
Debris moving criteria	Porosity > 0.6	

4.3 Primary mass inventory

The coolant mass inventory in the RCS is illustrated in Table 4.2 according to the primary component volumes defined in Ref. [2] and the repartition of coolant mass inventory in Table 2.5 of Section 2.4.2.

Table 4.2: Coolant mass inventory in the ASTEC V2 model

Component	Vol. (m^3)	N°	Tot. vol. (m^3)	Temp. (K)	Density (kg/m^3)	Mass (kg)
Pressurizer water volume	24.03	1	24.03	614.93	605.6	14552.5
Pressurizer steam volume	18.468	1	18.468	614.93	52.59	971.23
Surge line	0.566	1	0.566	611.792	618.528	348.34
Cold leg (each)	8.32	4	33.28	563.1	745.45	24880
Reactor coolant pump (each)		4		563.62	745.996	
Hot leg (each)	11.3	2	22.6	591.280	683.17	15440
Reactor vessel water volume - *Lower plenum = 25.52 m^3* - *Core = 22.55 m^3* - *Downcomer = 28.12 m^3* - *Upper plenum = 21.97 m^3* - *Upper head = 14.4 m^3*	112.56	1	112.56	579.52 (*)	711.106	80048
SG primary side volume (each) - *Upper plenum = 9.96 m^3* - *Lower plenum = 7.84 m^3*	59.57	2	119.14	576.92 (*)	716.123	85319
Total			330.65			221559
Total without pressurizer			287.59			206035

(*) Estimated average temperature values

As it is possible to see in the table the ASTEC model values are in good agreement with the reference values. The biggest discrepancy is on pressurizer steam mass. This difference is due the steam gas density, which behaves as a perfect gas (a necessary requirement when the CESAR and ICARE modules are run in a coupled mode) in ASTEC. It is well known that the perfect law underestimates the density close to the saturation point which explains the lower pressurizer steam mass.

4.4 Steady-state calculation

Before any transient calculation, it is necessary to run a steady state calculation. The aim of this calculation is to bring the initial state of the reactor, defined in the input deck, to the physical state at which the reactor is operating in normal conditions.

This is performed through the use of regulations which act on the pressurizer heater and spray, etc., in order to reach the desired physical values such as the primary and secondary mass and pressure, the loop flow rate, the SG water level just to name a few. The steady-state conditions at nominal power calculated by ASTEC are presented in the next Section 4.5.

4.5 Parameters and results

The parameters and results to be provided for comparison are:

1. Nominal steady-state parameters as shown in Table 4.3
2. Chronology of main transient events for DEBRIS model as listed in Table 4.4
3. Chronology of main transient events for NO_DEBRIS model as listed in Table 4.5
4. Time evolution of main parameters for code result comparison
5. Picture of the final state of core degradation and corium relocation in the lower head, just before vessel failure.

Table 4.3: Nominal TMI-2 steady-state (ASTEC V2 DEBRIS and NO_DEBRIS model)

Parameter	Unit	Value
Reactor core power	MW	2772.0
Pressurizer pressure (dome)	MPa	14.93
Temperature hot leg A	K	591.28
Temperature hot leg B	K	591.28
Temperature cold leg A	K	563.23
Temperature cold leg B	K	563.23
Mass flow rate loop A	kg/s	8800.4
Mass flow rate loop B	kg/s	8800.4
Pressurizer collapsed level	m	5.588
Total primary mass	kg	221559
Steam pressure SG A (outlet nozzle)	MPa	6.7815
Steam pressure SG B (outlet nozzle)	MPa	6.7815
Steam temperature SG A	K	570.76
Steam temperature SG B	K	570.76
SG A collapsed level	m	3.203
SG B collapsed level	m	3.203
Feedwater flow rate SG A	kg/s	784.398
Feedwater flow rate SG B	kg/s	784.392
Feedwater Temperature SG A & B	K	511.15

Table 4.4: Chronology of main events (ASTEC V2 with DEBRIS model)

Parameter	Time (s)
Break opening and total loss of main feedwater	0
Pressurizer PORV opens (P > 15.56 MPa)	16.20
Reactor scram (P > 16.30 MPa)	19.79
Pressurizer PORV closes (P < 14.96 MPa)	24.36
Full steam generator dryout	24.35
Startup of auxiliary feedwater	100
Pressurizer is empty	142.29
Stop of primary pumps (primary mass (liquid + steam) < 85000 kg)	2907.29
First fuel rod clad perforation/burst	4646
First clad melting and dislocation	5131.3
First ceramic melting and dislocation	5169.3
First molten material slumping in the lower plenum	5613
Vessel failure	11887.2

Table 4.5: Chronology of main events (ASTEC V2 without DEBRIS model)

Parameter	Time (s)
Break opening and total loss of main feedwater	0
Pressurizer PORV opens (P > 15.56 MPa)	16.20
Reactor scram (P > 16.30 MPa)	19.79
Pressurizer PORV closes (P < 14.96 MPa)	24.36
Full steam generator dryout	24.35
Startup of auxiliary feedwater	100
Pressurizer is empty	142.29
Stop of primary pumps (primary mass (liquid + steam) < 85000 kg)	2907.29
First fuel rod clad perforation/burst	4646
First clad melting and dislocation	4942.3
First ceramic melting and dislocation	5459
First molten material slumping in the lower plenum	5705
Vessel failure	At 25000 s no lower head vessel failure

The chronology of the major events during the transient is described in Table 4.4 and in Table 4.5 for the two simulations with the timings. The break occurs on the hot leg at t = 0 s (Figure 4.3) along with the total loss of the feedwater pumps. Given the characteristics of the once-through steam generator (short dryout time), the failure of the feedwater system directly triggers a significant fall of the water inventory in the shell side of the steam generator (Figure 4.4**)**. At the beginning phase of the accident, the effect of the small break LOCA is negligible. The transient is completely dependent by the feedwater loss to the secondary system, which leads to a rapid increase of the primary circuit pressure (Figure 4.5**)**. Neither the subsequent opening of the PORV valve cannot limit the rise of pressure caused by the loss of cooling. Once the pressure reaches 163 bar at t = 20 s the reactor scram occurs.

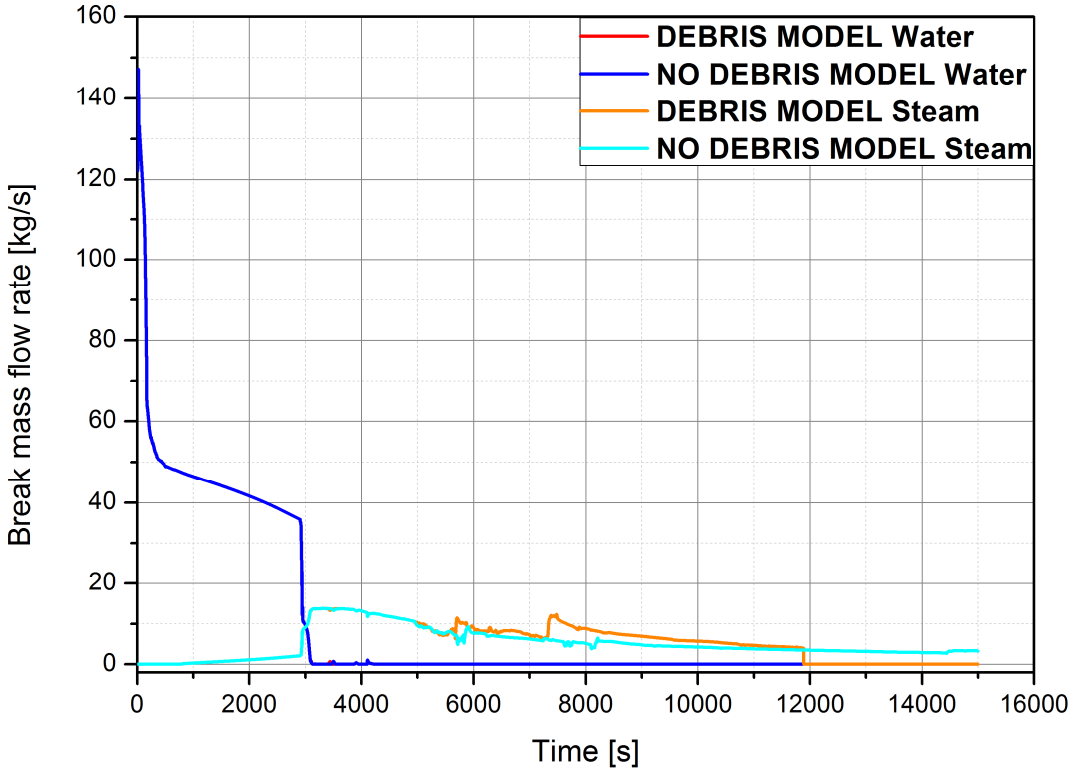

Figure 4.3: Break mass flow rate

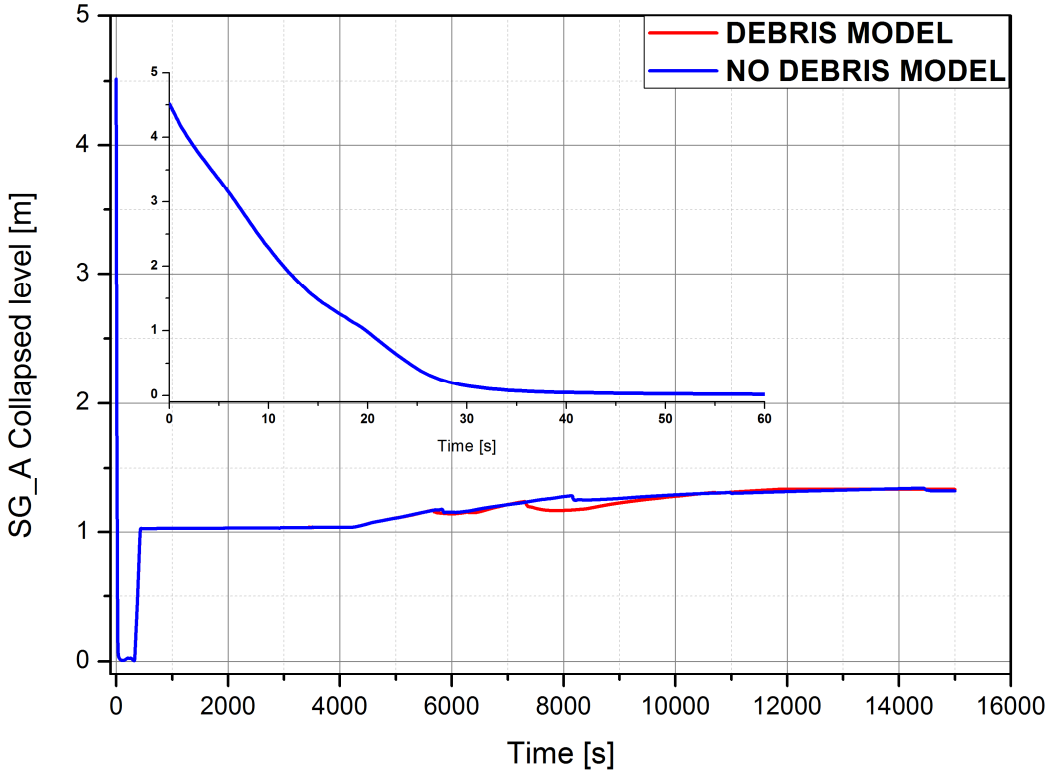

Figure 4.4: Steam generator A collapsed level

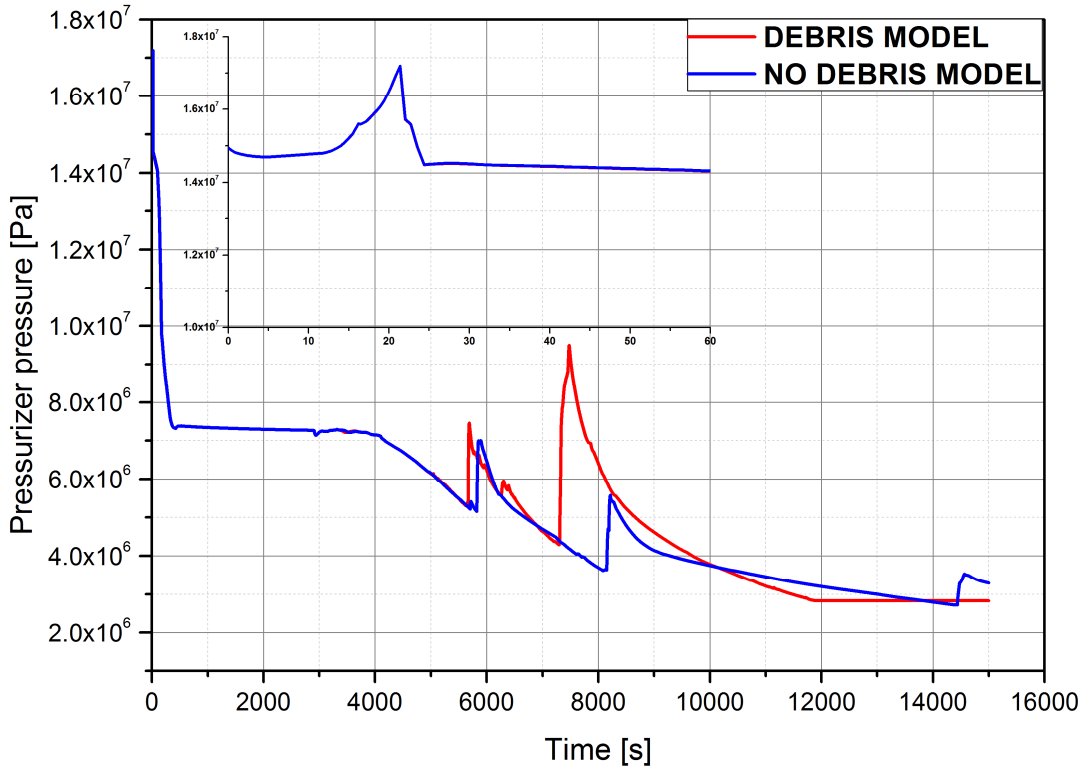

Figure 4.5: Pressurizer pressure

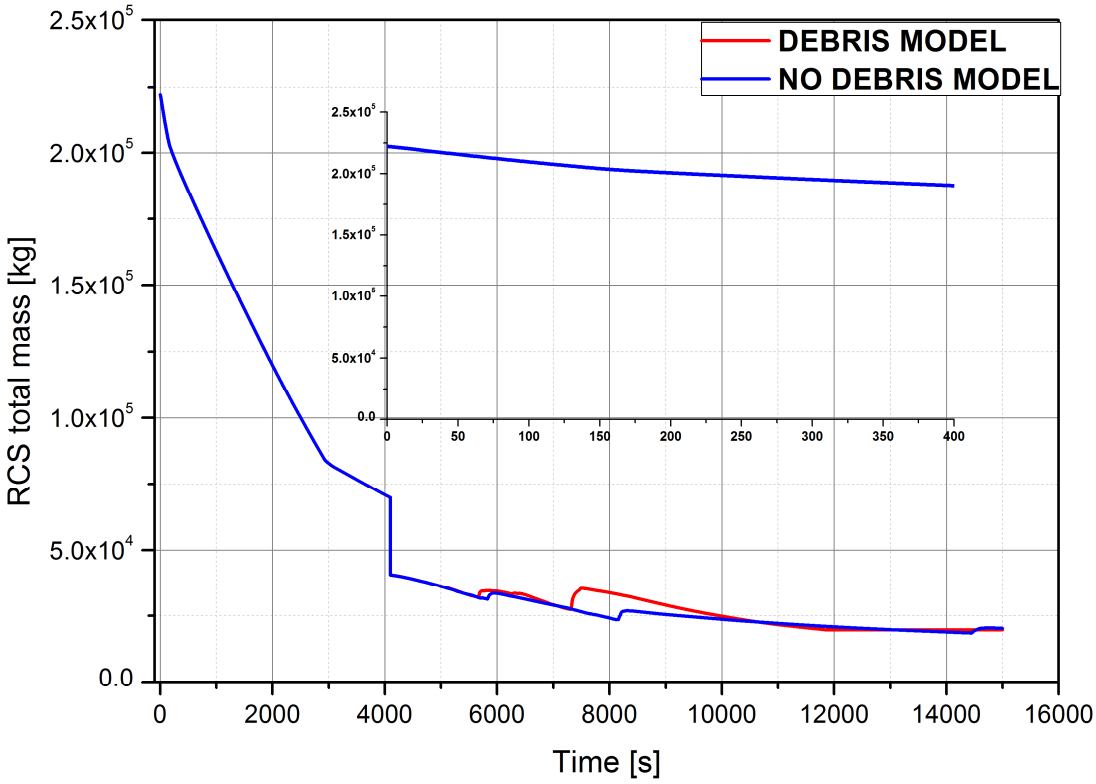

Figure 4.6**:** RCS total inventory

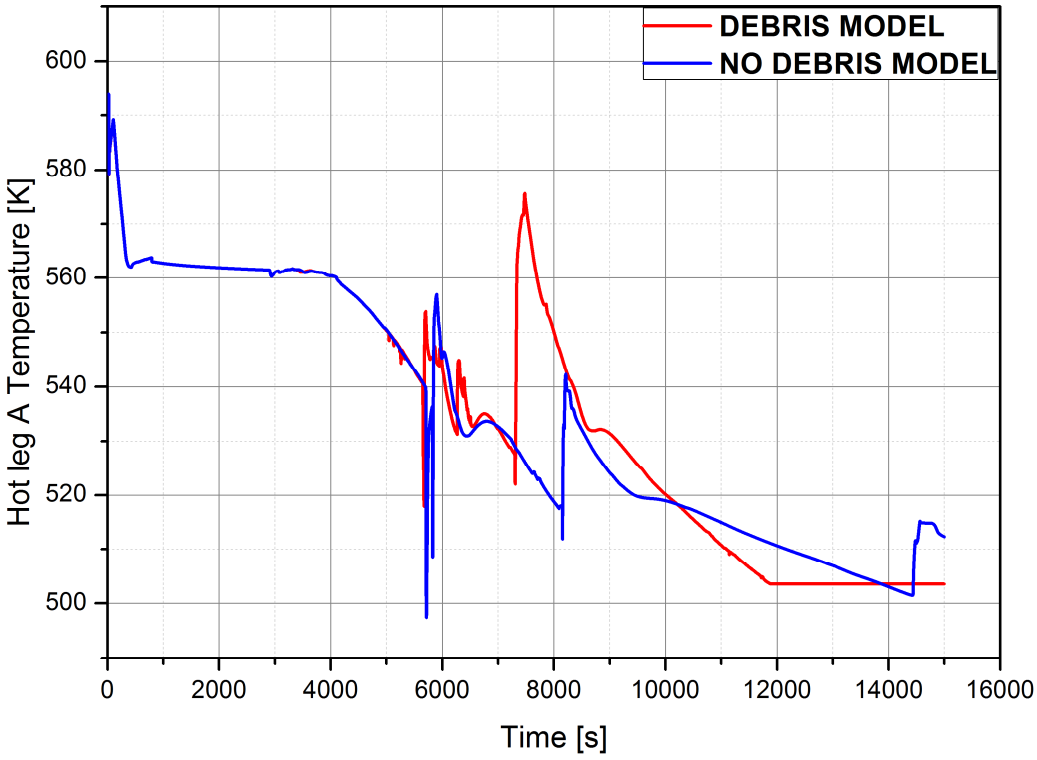

Figure 4.7**:** Hot leg A temperature (*at the vessel outlet nozzle*)

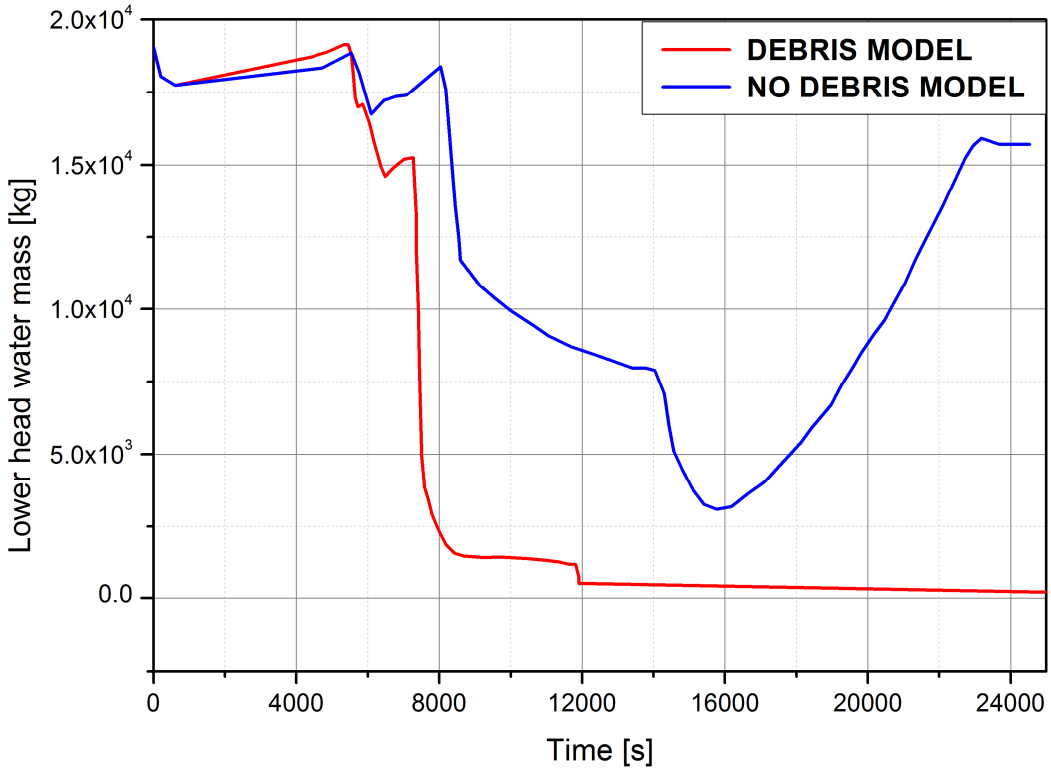

Figure 4.8: Water mass inside the Lower-head

The computed results show the same evolutions of the primary system main thermal-hydraulic parameters for the DEBRIS model (DM) and NO DEBRIS model (NDB) case, until ICARE module starts, that occurs at 4101 s for both cases. The two simulations show the first discrepancy concerning the primary circuit pressure between 7000 s and 9000 s, where the DM case predicts a rapid increase with a peak around 100 bar, while the case NDM case, compute a shorter and lower peak than DM.

As it can be seen in Figure 4.7, these differences are also evident in the comparison of the temperature in the hot leg A for the two cases. These sudden increases of the primary pressure and temperature are due to the coolant flashing, caused by the melting material relocation, inside the lower head. In Figure 4.8 is possible to note the different behavior predicted by the two simulations concerning the evolution of the water mass inside the lower head. The DM case computes a strong mass decrease around 7000 s confirmed by the peak pressure, while the NDM predicts around 7000 s an abrupt vaporization but shorter than DM case, followed by a continuous mass drop until 14000 s, and another strong vaporization until 15000 s, probably due to a second melting material relocation. The final water mass increase (16000 s – 25000 s) is attributable to the make-up system, which injects 2 kg/s of water during the entire transient into the cold leg.

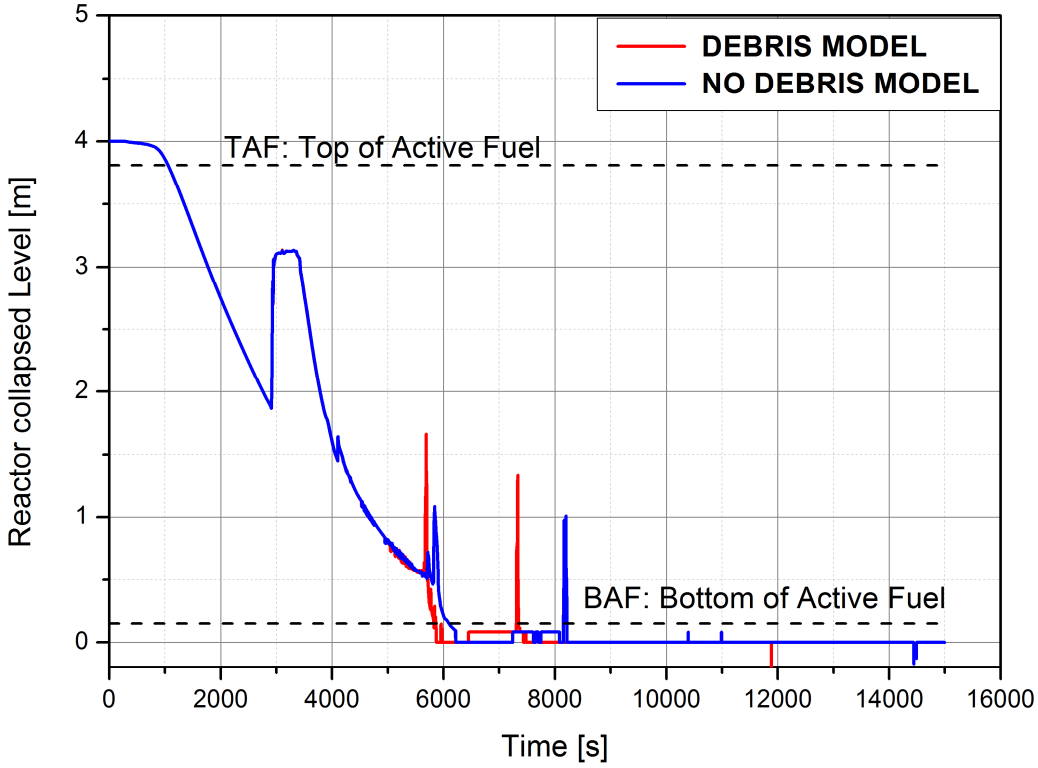

Figure 4.9**:** Core water level

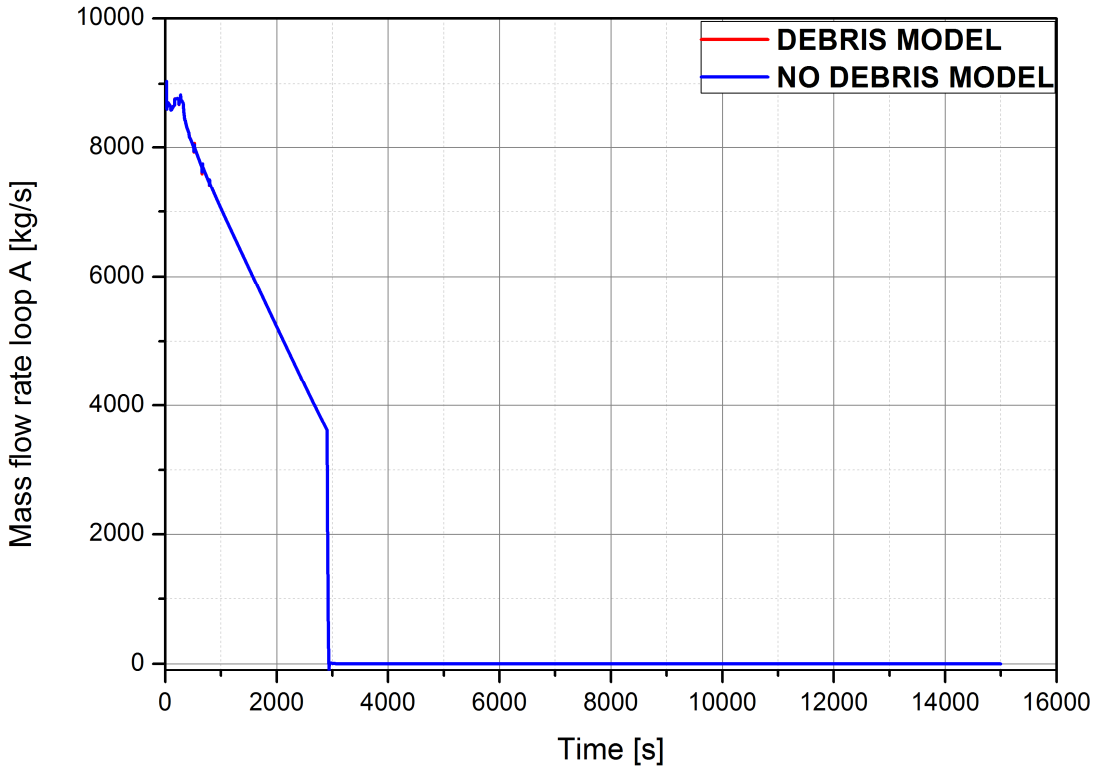

Figure 4.10**:** Mass flow rate loop A

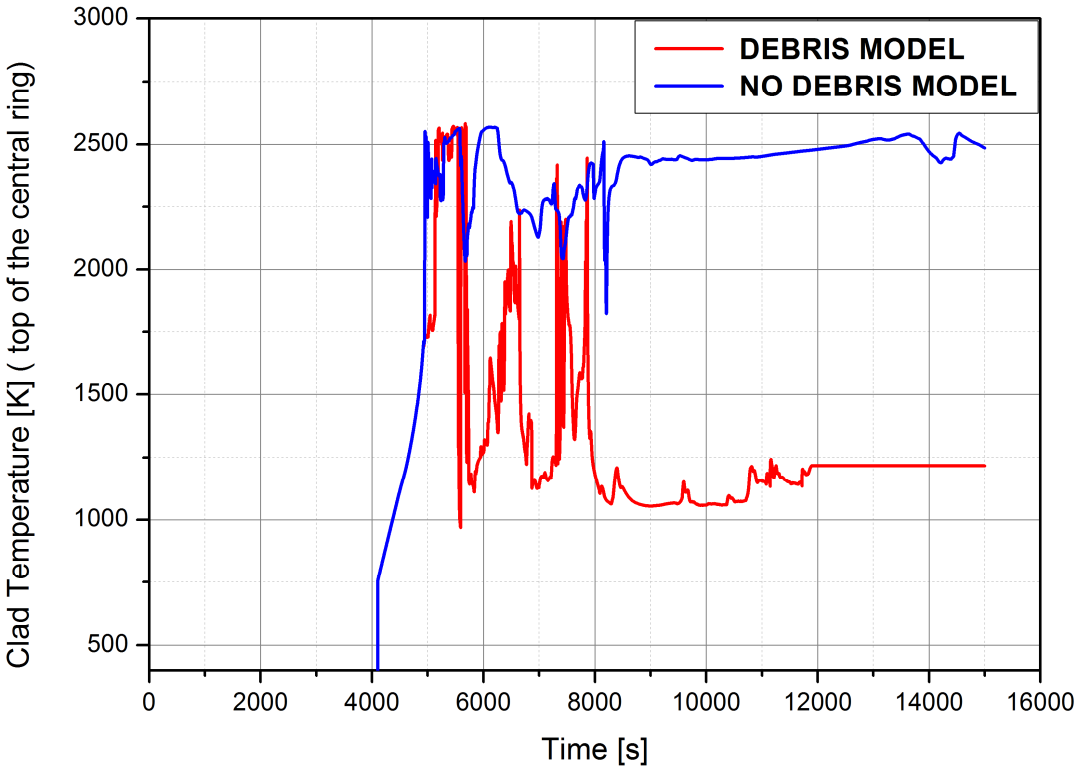

Figure 4.11**:** Cladding temperature (central ring)

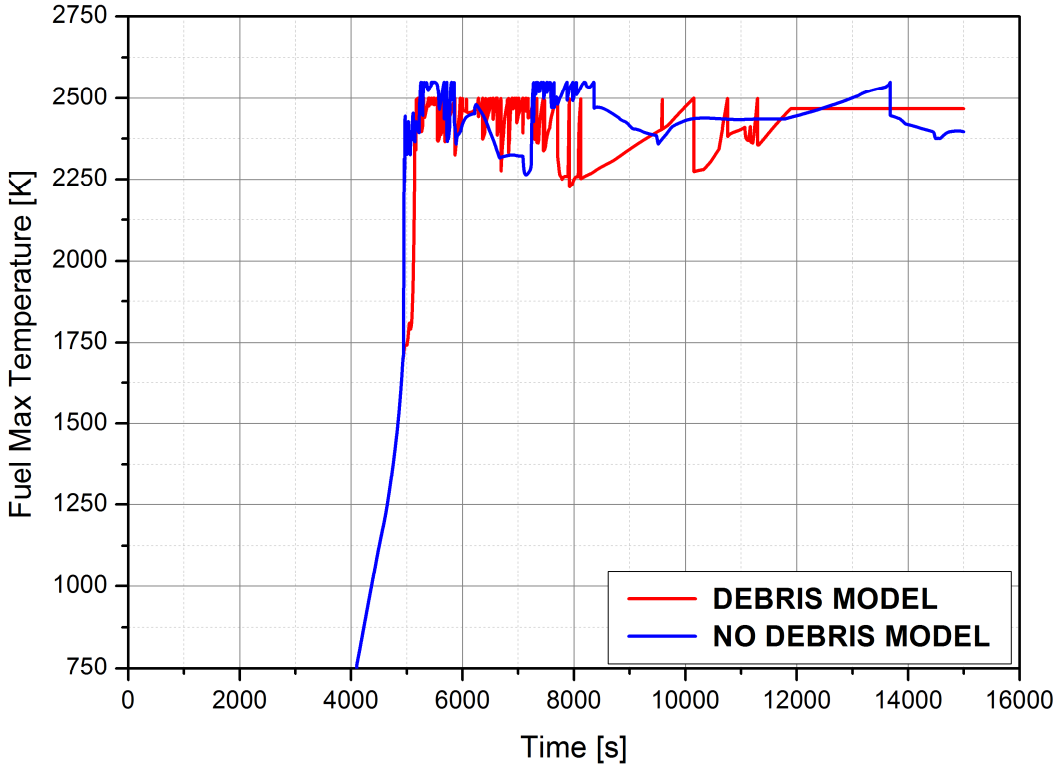

Figure 4.12**: :** Max fuel temperature

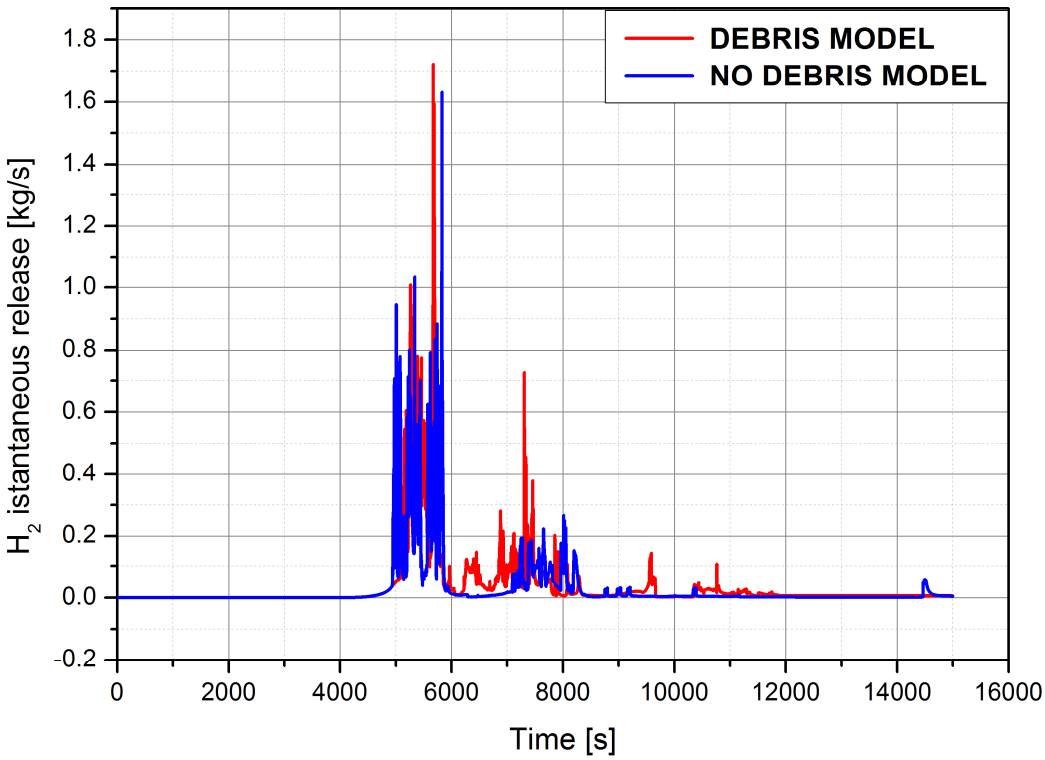

Figure 4.13**:** Instantaneous hydrogen production

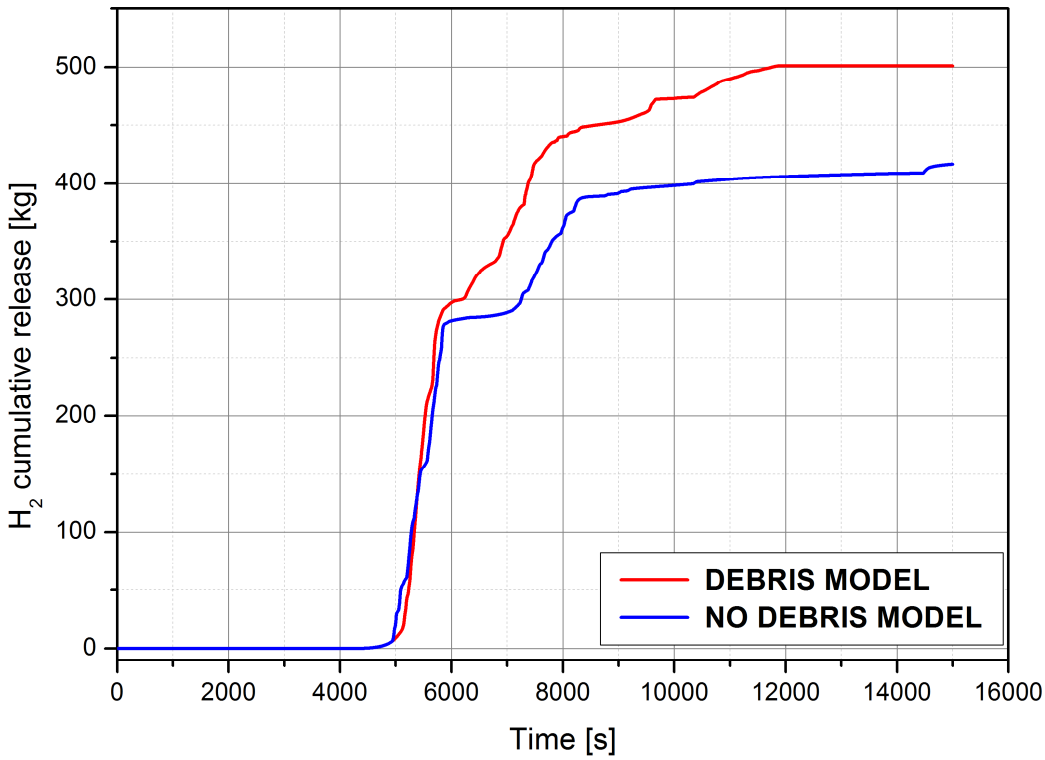

Figure 4.14**:** Cumulated hydrogen production

Figure 4.8 shows the evolution of the water level inside the core, the peak around 3000 s is due to the stop of the main pumps, which causes a rapid decrease of the coolant flow across the core, followed by strong boiling. The imposed criteria for the stop of the primary pumps is satisfied after 2910 s (Figure 10).

However, throughout the entire transient, the core water inventory is almost the same for both analyzed cases, so that the fuel rod and the cladding remain uncovered at the same timing and for the same duration of time.

Figure 11 illustrates the temperature of the cladding in the upper part of the core central ring. Until t = 5500 s, the two cases predict the same thermal behavior, then the cladding temperature computed by NDM shows a little drop and a further peak at the same level of the former, to settle finally at 2400 - 2500 K, while the DM case calculates the failure of the clad at 5800 s. It is not clear the reason why the clad in the NDM case does not fail at that high temperatures.

It is also interesting to observe in Figure 12, as the fuel temperature does not start to increase after start of core uncovery around 2000 s but only 1000 s later the pumps stop. Evidently, the heat transfer from fuel rods to steam in the upper part of the uncovered core is still sufficient to remove the decay heat from that core region.

Anyhow, after 4800 s the increase of fuel rod cladding and guide tube temperature above 1000 K starts the hydrogen production. The excursion of core heat-up accelerates when the temperatures becomes high enough to enhance the oxidation of the claddings.

Both cases predict two oxidation phases, the first one and even the main, are identical, as pointed out in Figure 14, with a maximum of hydrogen generation rate during the period (4800 - 6000 s) equal to 0.80 kg/s. The second oxidation phase is different in the two cases; the DM case computes 200 kg of H_2 produced against only 100 kg for the NDM case, with a total hydrogen generation of about 500 kg for the first case and 400 kg for the second one.

This discrepancy could be explained by the fact that the H_2 produced during the first oxidation come from the fuel cladding when the core is still in rod-like geometry, while the second oxidation phase occurs mainly in the degraded materials, which are in a different configuration in the two cases analyzed.

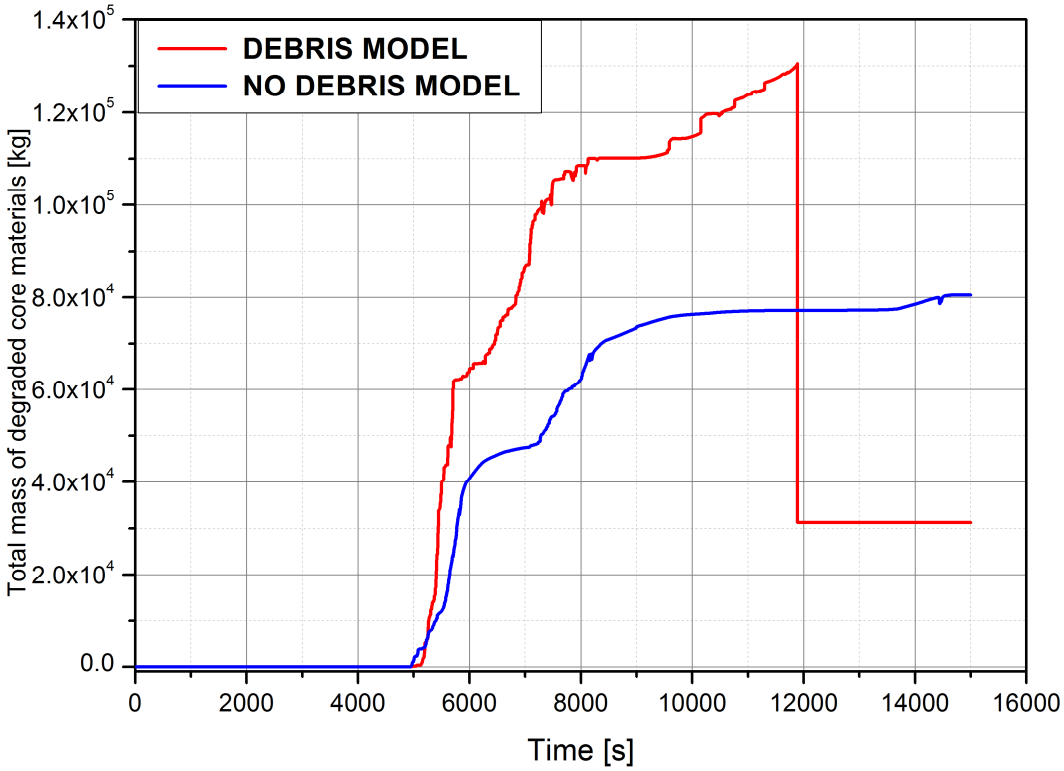

Figure 4.15 **:** Total degraded core materials

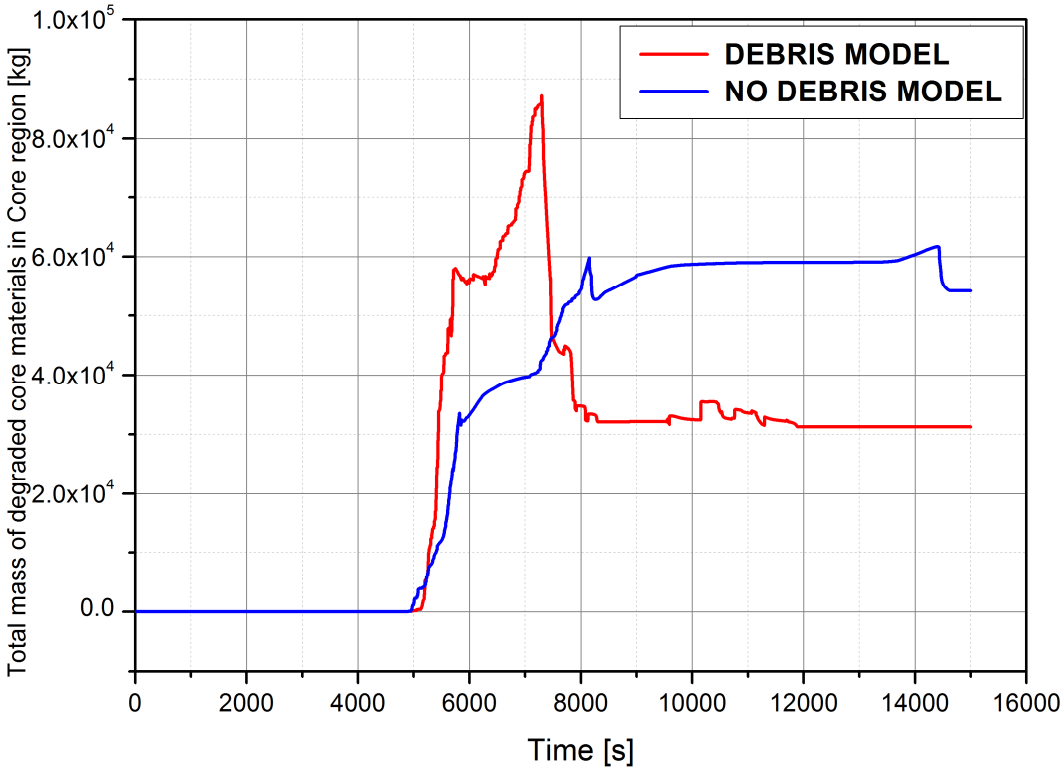

Figure 4.16: Total degraded mass in the core region

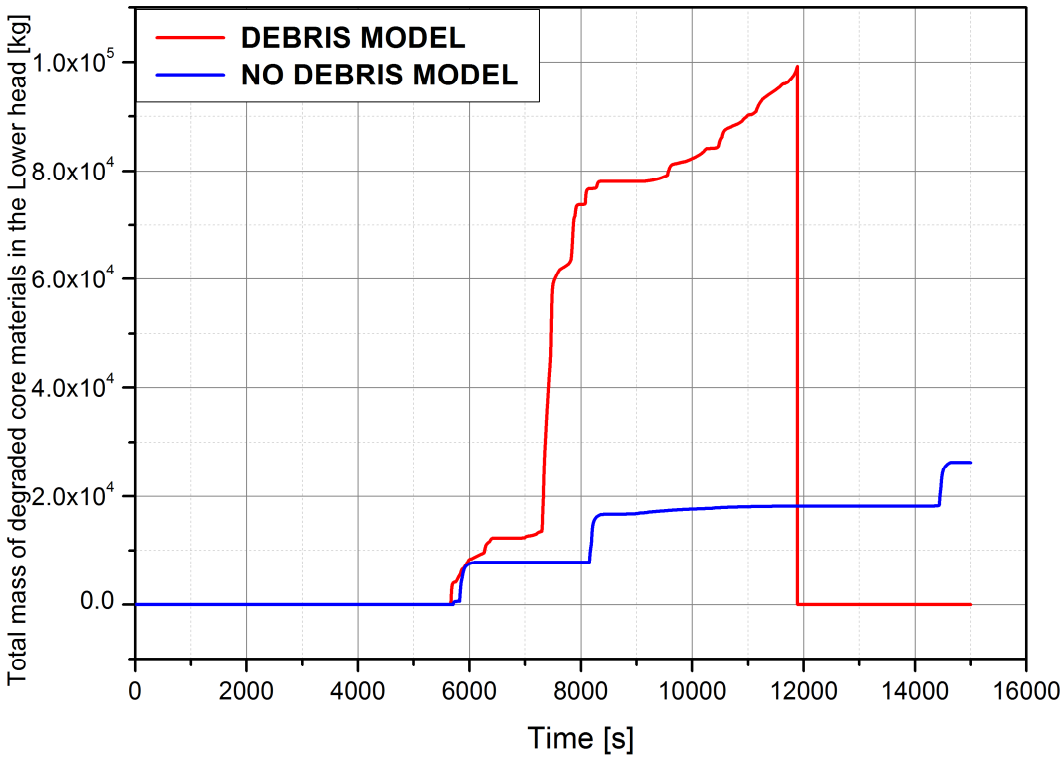

Figure 4.17: Total degraded mass inside the lower head

The total mass amount of melting material formed calculated show a great discrepancy for the two cases (Figure 4.15**)**. The DM case predicts a final value of about 130 t while the NDM case computes 80 t. Observing the Figure 4.16 and Figure 4.17, which illustrate the total mass of degraded materials inside the core and into the lower head, it is possible to note even much more disagreement concerning the mobility of this material.

The DM case predicts a maximum value equal 80 t of degraded material inside the core region before 8000 s, which starts slumping into the lower head before 6000 s and kept on until its failure, for a total final mass accumulation of 100 t in the lower head. The NDM case calculates only 26 t of melting material drops into the lower head. Figure 4.18 and Figure 4.19 provide a graphical representation of the evolution of the melting material at four different time steps.

The massive corium relocation predicted in DM case, causes a strong water evaporation, which explains the peak pressure observed at 7000 s in Figure 4.5, while in the NDM case, the smaller mass of degraded material relocated into the lower plenum cannot evaporate all the water inside.

The DM case predicts a more extensive core degradation in comparison with NDM case; furthermore, the degraded material seems to be less viscous and more penetrative than that calculated by NDM case. The transient analysis for DM case ends at lower head failure

which is predicted to occur at 11887 s; on the contrary in the NDM case the lower head failure is not predicted and the transient was stopped at 25000 s.

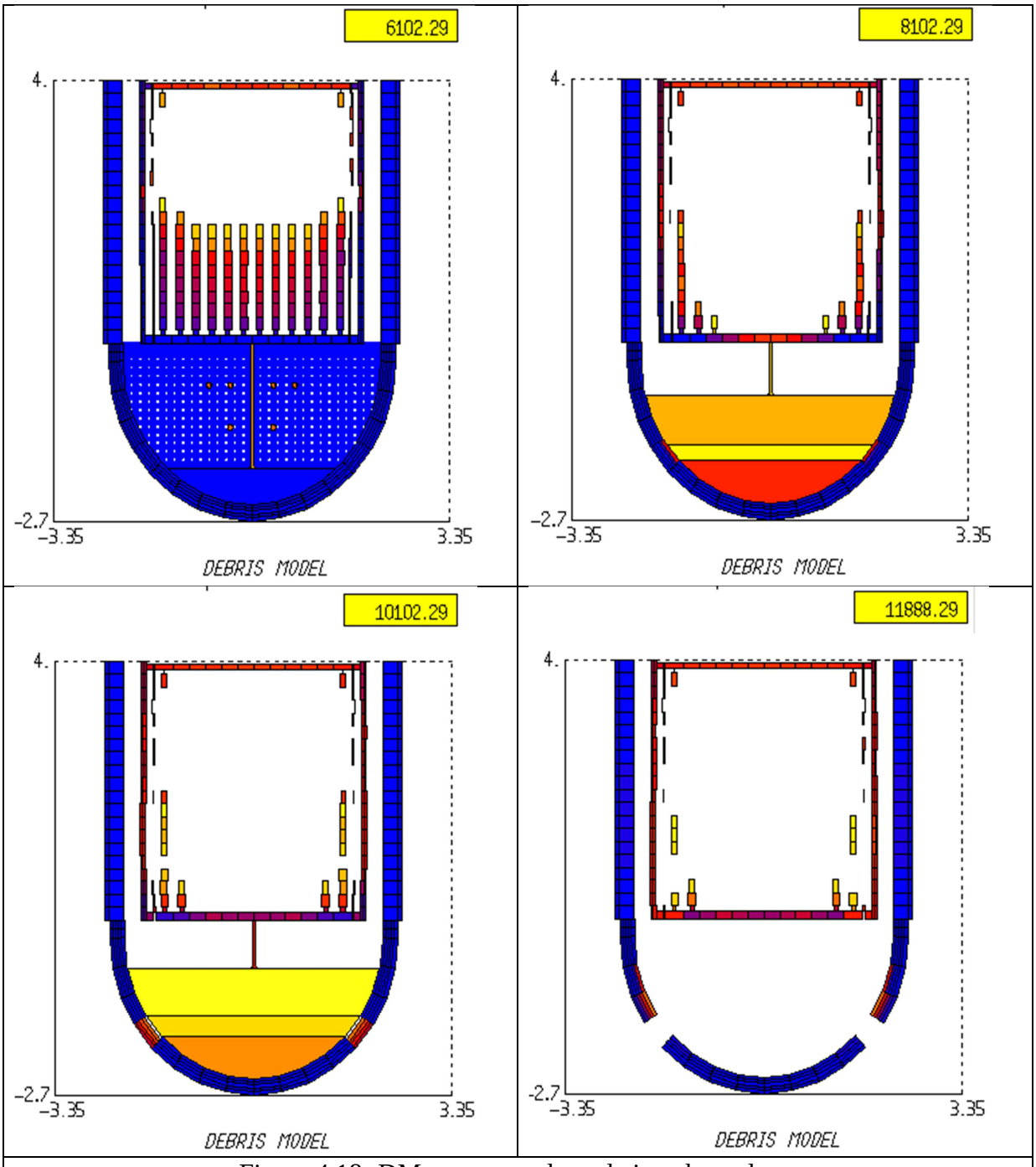

Figure 4.18**:** DM case, core degradation chronology

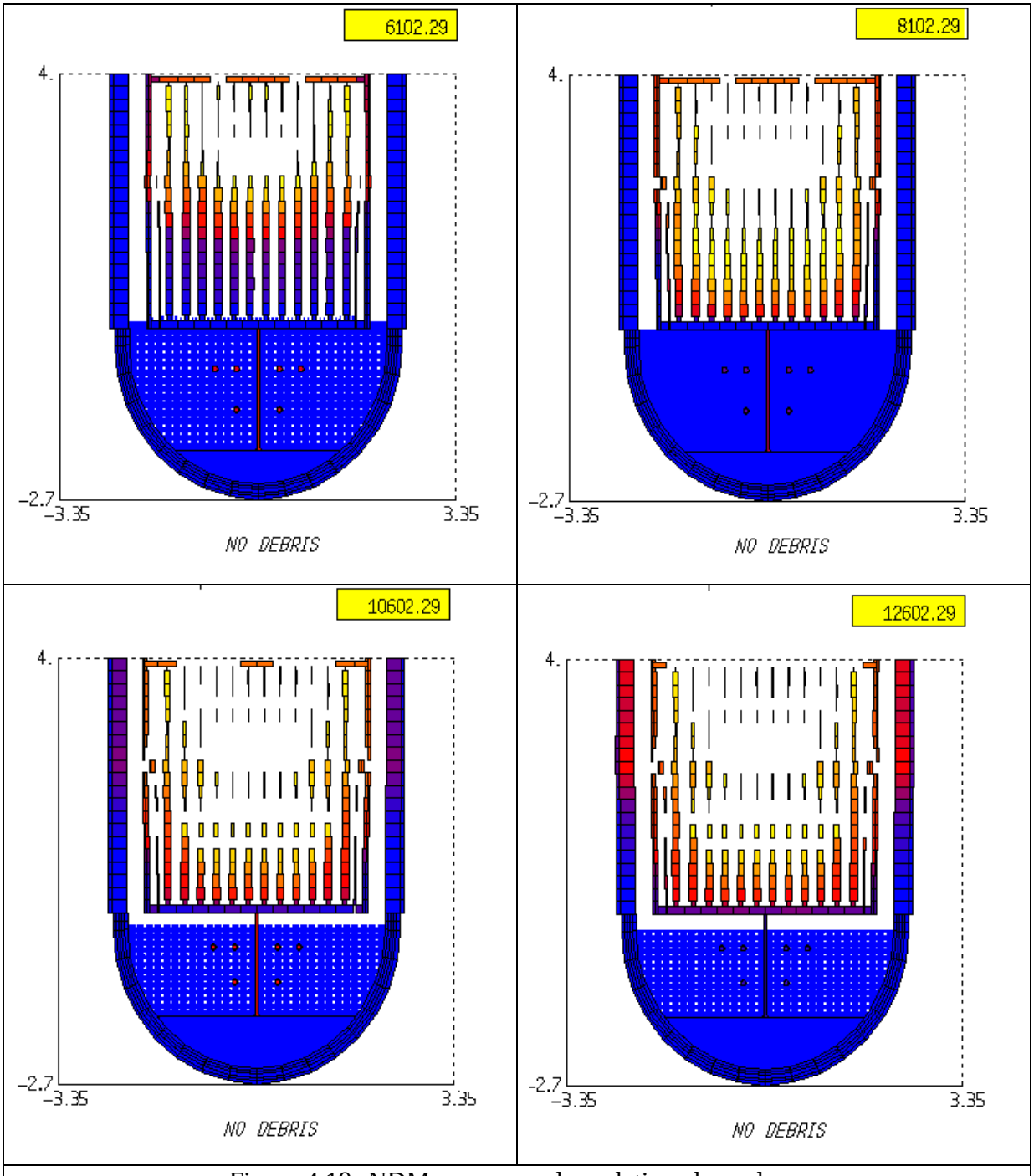

Figure 4.19**:** NDM case, core degradation chronology

4.6 Summary and Conclusion

The work presented, shows some comparisons of results regarding in-vessel phenomena between two simulation using ASTEC V2.0r2p2 codes with different model Babcock and Wilcox lowered loop plant, (the same reactor of the unit 2 of TMI nuclear power plant) severe accident scenarios. Regarding the total hydrogen production calculated for both

cases, the simulations results show a discrepancy of about 20%. However, DM case predicts a larger fraction of hydrogen produced during corium relocation in the lower head, about 200 kg, while in NDM case, the amount of hydrogen produced during the relocation is 100 kg. This cannot be the consequence of the choice of oxidation correlations but of the core degradation model used.

The masses of corium accumulated in the vessel lower head before the vessel failure time of the DM case differs of about 80 t calculations.

Differences are observed between the codes regarding vessel failure and corium slump into the lower head; according to the model adopted, to analyze the core degradation phenomena, the results are completely different. The DM case predicts the failure of the lower head at 11887 s whilst the NDM case does not calculate the failure of the lower head (until 25000 s).

This observation is very important; what is the more correct model to adopt for simulate this kind of accident? The model selected (DEBRIS, NO DEBRIS) affects completely the result.

Further code validation vs. experiments benchmark is needed, in order to assess and to confirm that, which ASTEC model could be used to simulate what really occur inside a core during a severe accident. The user has to pay attention on the quality of the results, and sensitivity analysis has to be performed in order to pointed out what is the model parameters that can strongly affect the results.

References

1. Van-Dorsselaere, J.P., Seropian, C., Chatelard, P., Jacq, F., Fleurot, J., Giordano, P., Reinke, N., Schwinges, B., Allelein, H.J., Luther, W., 2009a. The ASTEC integral code for severe accident simulation. Nuclear Technology 165, 293–307.
2. Trégourès, N., Moal, A., 2007. ASTEC V1 code: CESAR physical and numerical modeling. ASTEC-V1/DOC/07-18.
3. Trégourès, N., et al., 2008. Validation of CESAR thermal–hydraulic module of ASTEC V1.2 code on BETHSY experiments. Journal of Power and Energy Systems 2 (1).
4. Van-Dorsselaere, J.P., et al., 2009. The ASTEC integral code for severe accident simulations Nuclear Technology 165.
5. Carénini, L., Fleurot, J., Fichot, F., 2014. Validation of ASTEC V2 models for the behaviour of corium in the vessel lower head. Nuclear Engineering and Design272, 152–162.
6. P. Chatelard, N. Chikhi, L. Cloarec, O. Coindreau, P. Drai, F. Fichot, B. Ghosh, G. Guillard, ASTEC-V2/DOC/09-04, ASTEC V2 code ICARE physical modelling Rev. 0.

7. Bandini, G., et al., 2013. Status and results of the OECD benchmark exercise on TMI-2 plant. In: 6th European Review Meeting on Severe Accident Research (ERMSAR 2013), Avignon, France, October 2–4.

5. Comparison of MELCOR and ASTEC results

One of main objective of this activity is to highlight the uncertainties in the calculation of a severe accident sequence by the comparison of different code results. Two of the main integral codes actually employed worldwide for severe accident analysis have been considered: the U.S NRC MELCOR code and the European ASTEC code. The MELCOR calculation has been performed by the University of Pisa, while the ASTEC calculation has been performed by the University of Bologna in the frame of CIRTEN activities.

The main results from the SBLOCA transient analysis described in details in the previous sections are compared and discussed, highlighting and trying to explain the main differences observed in code results. The ASTEC results are the ones of the calculation with DEBRIS model applied, for best modelling consistency with MELCOR, which employs a similar DEBRIS modelling in the evaluation of in-core melt progression during the late degradation phase.

5.1 TMI-2 steady-state conditions at nominal power

The steady-state conditions calculated by the two codes are compared with TMI-2 specification data in Table 5.1 below.

Table 5.1:Nominal TMI-2 steady-state

Parameter	Unit	MELCOR	ASTEC	TMI-2
Reactor core power	MW	2772	2772	2772
Pressurizer pressure (dome)	MPa	14.95	14.93	14.96
Temperature hot leg A	K	589.86	591.28	591.15
Temperature hot leg B	K	589.86	591.28	591.15
Temperature cold leg A	K	561.83	563.23	564.15
Temperature cold leg B	K	561.83	563.23	564.15
Mass flow rate loop A	kg/s	8866	8800	8800
Mass flow rate loop B	kg/s	8863	8800	8800
Pressurizer collapsed level	m	5.571	5.588	5.588
Total primary mass	kg	220857	221559	222808
Steam pressure SG A (outlet nozzle)	MPa	6.41	6.78	6.41
Steam pressure SG B (outlet nozzle)	MPa	6.41	6.78	6.41
Steam temperature SG A	K	569.8	570.8	572.15
Steam temperature SG B	K	570.1	570.8	572.15
SG A collapsed level	m	7.86	3.20	-
SG B collapsed level	m	7.87	3.20	-
Feedwater flow rate SG A	kg/s	761.1	784.4	761.1
Feedwater flow rate SG B	kg/s	761.1	784.4	761.1
Feedwater Temperature SG A & B	K	511.15	511.15	511.15

There is a general good agreement between code results and TMI-2 reference data for the primary system. The differences in hot leg and cold leg temperatures is within 1.3 °C and the uncertainty in primary mass inventory is below 1%. The mass flow rates in the two primary loops is just 0.7% overestimated in the MELCOR calculation, while the pressurizer pressure and the pressurizer level in the two calculations are practically coincident with the TMI-2 data.

Some more important deviations are found in the initial conditions of the SG secondary side. In particular, there is a large discrepancy in the SG collapsed level, but unfortunately there is no TMI-2 data available to judge which of the two is the right value. This discrepancy can make a difference in the total mass of water inventory of the SG secondary side and then in its thermal capacity and draining time in the initial phase of the transient following main feedwater trip. Furthermore, the steam pressure at the SG outlet and the main feedwater flow rate at the SG inlet are slightly overestimated in the ASTEC calculation.

5.2 In-vessel core degradation parameters and modelling options

In-vessel core degradation parameters and modelling options used in the two calculations to evaluate the core melt progression during both early and late degradation phases of the SBLOCA transient are compared in Table 5.2. The parameters and model options were mainly selected on the basis of specific code user guidelines and engineering judgment.

Different empirical correlations are used in ASTEC and MELCOR to compute the zircaloy clad oxidation. This leads to faster oxidation kinetics with MELCOR in the lower temperature range, but slower oxidation kinetics in the higher temperature range, with respect to ASTEC.

Both cladding failure criteria are based on oxide layer thickness and clad temperature, even if the reference parameter values are somewhat different. This parameters mainly determine the capability of the oxidized cladding to retain the metallic zircaloy and dissolved fuel during the early degradation phase following oxidation runaway and fuel rod temperature escalation above the melting point of clad material. The different parameter values used might impact on the degree of early phase core degradation and the initial hydrogen source.

The melting point of ceramic UO2 and ZrO2 materials is significantly different. While values close to the ones of pure materials are considered in the MELCOR calculation, the melting point of pure ceramic materials is lowered by several hundreds of degrees in the ASTEC calculation, according to the results of severe fuel damage Phébus FP tests.

The same threshold temperature value is defined for fuel rod collapse and transition to debris bed. This threshold is applied in ASTEC for both oxidized and non-oxidized claddings, while the threshold value is increased up to the melting point of UO2 in MELCOR, when a residual thin metallic layer is still in place.

Table 5.2: In-vessel core degradation parameters/criteria

Parameter	MELCOR	ASTEC (*)
Zircaloy oxidation kinetics	Urbanic-Heidrick	BEST-FIT correlation: Cathcart-Pawel in the low temperature range and Prater-Courtright in the high temperature range
Cladding failure criteria	ZrO2 thickness < 10 mm and Tclad > 2400 K	Tclad > 2300 K and ZrO2 thickness < 0.3 mm; or T > 2500 K
Melting point of UO2-ZrO2 ceramic material	UO2 Tm = 3113 K ZrO2 Tm = 2990 K	2550 K (PHEBUS FP tests)
Debris formation criteria	Rod failure when: Tclad > 2500 K and Zr thickness < 100 mm or T_{UO2} > 3100 K	Fuel rod temperature > 2500 K
Molten core relocation into the lower plenum	After failure of grid-supported plate that can initially support fuel assemblies and particulate debris above it. Thus, everything resting on that ring of the plate will fall, but the plate will remain in place until it melts (1273 K). This event corresponds to failure of the plate portion with survival of the grid	Baffle melting (relocation through core by-pass) or melting at core bottom (relocation through core support plate)
Reactor pressure vessel failure (**)	Failure of the lower head will occur if any of four criteria is met: 1. the temperature of a penetration (or the temperature of the innermost node of the lower head) reaches a failure temperature (1273 K) 2. a failure logical control function is found to be true (not used) 3. overpressure (20 MPa) from the falling-debris quench model occurs 4. creep-rupture failure of a lower head segment occurs, in response to mechanical loading at elevated temperatures	Vessel wall melting (100%)

(*) ASTEC calculation with DEBRIS model applied

(**) Condition 1. took place in MELCOR simulation

Different corium relocation flow paths into the lower plenum of the vessel are considered in ASTEC: laterally through the core bypass after baffle melting and/or through the lower core support plate after fuel rod melting or pool relocation above it. The relocation of corium into the lower plenum is considered in MELCOR after core support plate failure in each one of the radial rings that simulate the core.

Finally, different criteria is applied to assess the instant of vessel failure: the failure of the lower head penetrations applies in this MELCOR calculation, while the whole local wall melting is considered with ASTEC.

5.3 Chronology of main events

The chronology of main events in the SBLOCA sequence calculated by the two codes is presented in Table 5.3 below. The initial phase of the transient evolution is dominated by the combination of primary coolant loss through the break, which tends to depressurize the primary system, and the draining of the SG secondary side following main feedwater trip, which tends to increase the primary pressure due to the progressive loss of heat removal by the secondary circuits.

The prevalent primary pressure increase induced by the main feedwater trip results first in PORV opening and successively in reactor scram.

Table 5.3: Chronology of main events

Parameter	ASTEC (*)	MELCOR
Break opening and total loss of main feedwater	0 s	0 s
Pressurizer PORV opens (P > 15.56 MPa)	16.20 s	17.03 s
Reactor scram (P > 16.30 MPa)	19.79 s	26.68 s
Pressurizer PORV closes (P < 14.96 MPa)	24.36 s	33.02 s
Full steam generator dryout	24.35 s	47.22 s
Start-up of auxiliary feedwater	100 s	100 s
Pressurizer is empty	142 s	287 s
Stop of primary pumps (**)	2907 s	2593 s
First fuel rod clad perforation/burst	4646 s	(***)
First clad melting and dislocation	5131 s	5700 s
First ceramic melting and dislocation	5169 s	6310 s
First molten material slumping in the lower plenum	5613 s	5480 s
Vessel failure	11887 s	9680 s

(*) ASTEC calculation with DEBRIS model applied

(**) Primary mass (liquid + steam) < 85000 kg

(***) Not calculated by MELCOR

The two codes predict the opening of the PORV more or less at the same instant, but the reactor scram and then the PORV closure are delayed in the MELCOR calculation by 7 s and 9 s, respectively. This is clearly due to the large difference in the initial water inventory of the SG secondary side, as highlighted by the discrepancy in the collapsed water levels in Table 5.2. This is further confirmed by the rather large discrepancy observed in the timing of full steam generator dryout (delay of 23 s in the MELCOR calculation with respect to ASTEC).

The start-up of auxiliary feedwater is imposed as boundary conditions at t = 100 s in both calculations.

The full pressurizer draining is delayed in MELCOR calculation, by about 130 s with respect to ASTEC. The main reason for this discrepancy is the difference in the initial break mass flow rate. Another important reason is the largest increase of the pressurizer level observed with MELCOR before reactor scram. Furthermore, the saturation condition in the primary loops is reached before the complete draining of the pressurizer in MELCOR, and thus slowing down the pressurizer level decrease.

The stop of the primary pumps, which is defined according to the depletion of water inventory in the primary system, occurs earlier in the MELCOR calculation. Since the difference in the initial primary mass inventor is very small (0.7 ton) and the water mass lost through the PORV in the initial phase of the transient is negligible, the only reason for this discrepancy is in the different evolution of the integral mass of water lost through the break.

Despite the earlier stop of primary pumps and core uncovery in MELCOR calculation, the onset of fuel rod degradation indicated by the instant of first clad melting and dislocation is slightly delayed with respect to ASTEC, owing to the slowest core heat-up rate. While in the ASTEC calculation the first ceramic material melting and dislocation occurs shortly after first clad melting, in MELCOR calculation this event is significantly delayed, likely because of the large difference in ceramic melting points considered by the two codes (see Table 5.2).

There is a rather good agreement in the onset of the molten material slumping into the lower plenum. In the MELCOR calculation the corium relocation occur through the lower core support plate, while in the ASTEC calculation most of the corium relocation occurs laterally through the core bypass following baffle melting.

The vessel failure is predicted earlier by MELCOR than by ASTEC. The main reasons for this difference is explained in the successive Section 5.4.

5.4 Evolution of main parameters

The main parameters investigated for code results comparison are listed in Table 5.4. They concerns: (1) the boundary conditions on the SG secondary side, (2) the thermal-hydraulic behavior of the primary system, (3) the in-vessel core degradation progression, and (4) the hydrogen source. The time evolution of these parameters, as calculated by the two codes until vessel failure, is compared from Figure 5.1 to Figure 5.18. The major deviations

between code results highlighted in the figures are discussed and tentatively explained in this section of the report.

Table 5.4: List of main parameters to be plotted for code result comparison

Parameter	Index	Unit
Steam generator A pressure	P-sga	Pa
Steam generator A collapsed level	L-sga	m
Pressurizer pressure	P-prz	Pa
Pressurizer level	L-prz	m
Loop A mass flow rate	Q-lpa	kg/s
Hot leg A temperature	T-hla	K
Cold leg A temperature	T-cla	K
Break mass flow rate	Q-brk	kg/s
Total primary mass (liquid + steam)	M-pri	kg
Core power	W-cor	W
Power exchange with SG A	W-sga	W
Power exchange with SG B	W-sgb	W
Core collapsed water level (from core bottom, see also Figure 3)	L-cor	m
Fuel rod clad temperature at core top *(central ring)* (*)	T-cor	K
Instantaneous hydrogen production	H-rat	kg/s
Cumulated hydrogen production	H-cum	kg
Total mass of degraded core materials (debris or molten, cumulated value)	M-tco	kg
Total mass of materials in the lower plenum (cumulated value)	M-tlp	kg

(*) The temperature of fuel rod clad at core top should be taken at the last mesh of the active zone (stop of temperature plot if the clad fails and relocates).

SG secondary side pressure and level

Figure 5.1 and Figure 5.2 show the behavior of the SG secondary side regarding pressure and water level evolution, respectively. While in the MELCOR calculation these values are kept constant during the transient according to the specified boundary conditions, in the ASTEC calculation their time evolution is affected by the condition assumed at the SG outlet, which does not allow the ingress of steam inside the SG dome. As a consequence, the the SG starts to depressurize, below the outlet boundary value of 70 bar, after about t = 4200 s (see Figure 5.1) due to steam condensation on the secondary side. At the same time, as a result of steam condensation, the SG water level start to rise slowly over the reference value of 1 m (see Figure 5.2).

Break flow rate and primary mass inventory

The time evolution of break mass flow rate is shown in Figure 5.3. During the initial depressurization phase the flow rate is over predicted by MELCOR, partly due to the slowest primary system depressurization. Once the primary pressure approaches the secondary pressure after about t = 300 s, the two break flow rate values become practically coincident. After this time the void fraction in the hot leg, and then upstream the break increases progressively according with the depletion vs. time of the primary mass inventory. While this void fraction increase is taken into account in the calculation of water-steam mixture through the break in the ASTEC calculation, mostly liquid water is flowing through the break in the MELCOR calculation, independently on the void fraction behavior, and thus maintaining the break flow rate almost constant until the stop of primary pumps. This is therefore the main reason of the deviation observed in break mass flow rate calculated by the two codes, before primary pumps coastdown is taken into account on the basis of the residual primary mass threshold (< 85 tons).

After the stop of primary pumps with consequent water draining from the upper part of the primary circuit, only steam flows through the hot leg break and the leak calculated by the two codes is consistent; remaining differences are mainly induced by different primary pressure behavior during the core degradation phase.

The Figure 5.4 shows the time evolution of water inventory in the primary system, which depends on the break flow rate and the constant make-up flow rate of 2 kg/s. The rather small deviation in code results is of course dependent on the different break flow rate evolution discussed above.

Primary loop mass flow rate

The time evolution of the mass flow rate in the loop A calculated by the two codes is compared in Figure 5.5. The discrepancy in code results is certainly caused by the different pump model used, since no precise TMI-2 primary pump specification data were available and then provided for the preparation of the respective code input decks. Furthermore, some differences in the void fraction behavior in the cold leg near the pump location might contribute to enlarge the discrepancy in pump flow rate evolution, until its coastdown.

Pressurizer level

Both codes predicts quick draining of the pressurizer in the initial phase of the transient (see Figure 5.6), following hot leg break opening and consequent onset of primary mass inventory depletion. The difference in the instant of full pressurizer draining has been clarified in the previous Section 5.3.

Primary pressure

The time evolution of the pressurizer pressure is compared in Figure 5.7. In both code calculations the primary pressure approaches the secondary pressure and remain constant until primary pump coastdown. During this time interval the core decay power is removed through the SG by forced circulation of liquid-steam mixture in the primary loops. The loss of forced

circulation in the primary loops after pump coastdown results in significant primary pressure increase in the MELCOR calculation, because of sudden interruption of heat transfer through the steam generator. This primary pressure increase is not observed with ASTEC, due to residual heat removal by the SGs after pumps coastdown and hot legs draining.

The primary pressure evolution calculated by ASTEC after t = 4000 s is characterized by a progressive decrease with two sudden pressure spikes around t = 6000 s and t = 7500 s, respectively. These large pressure spikes are consequent to the massive slumping of hot corium in the lower plenum, followed by molten jet fragmentation and strong vaporization of water still present in the lower head of the vessel. Conversely, no pressure spikes are predicted by MELCOR, mainly due to a more continuous and gradual relocation of corium into the lower plenum.

Hot leg and cold leg temperatures

The time evolution of hot leg and cold leg temperatures is compared in Figure 5.8 and Figure 5.9, respectively. The large discrepancy observed in the hot leg temperature behavior is mainly due to the different point where the temperature value is taken. In ASTEC calculation the temperature is taken in the coldest branch between the break and the SG, while in the MELCOR calculation the temperature is taken in the branch between the vessel outlet nozzle and the break, which is heated-up by the hot steam produced in the core and flowing towards the break. The large discrepancy observed in the cold leg temperature behavior is mainly due to different cold leg meshing. The cold leg is simulated by only one volume with MELCOR and then its temperature is strongly influenced by the hot gas temperature inside the vessel. Conversely, the cold leg temperature in ASTEC calculation is the one of the coldest branch in inlet to the primary pump.

Core decay and SG exchanged powers

The decay power decrease with time is shown in Figure 5.10, in agreement with the specification value. The decay power reduction due to noncondensable and volatile fission products release from degraded fuel rods and molten pools in the late phase of the transient is not taken into account in the two code calculations.

The power removal by the SG A and B is illustrated in Figure 5.11 and Figure 5.12, respectively. The large discrepancy in the power exchange before primary pump coastdown is mainly caused by the large amount of heat dissipated by the primary pumps, which is taken into account in the ASTEC calculation, but it is neglected with MELCOR. The power removal by both SGs reduces down to zero after coastdown of all primary pumps in both calculations, even if some residual power is predicted by ASTEC until t = 4000 s. The power peaks observed in the ASTEC calculation around t = 5700 s and t = 7300 s are produced by the condensation of steam produced during the massive slumping of corium into the lower plenum.

Core uncovery and heat-up

The time evolution of core collapsed level is compared in Figure 5.13. The core top elevation is used with ASTEC to calculate the water level, including the axial extension of 19 cm above the top of core fissile zone, which is instead used as reference elevation in MELCOR. This produce the difference of 19 cm observed in Figure 13 at the beginning of the transient. After about t = 1000 s, the core collapsed level calculated by ASTEC reduces significantly below the MELCOR one, owing to a different void fraction calculated inside the core. The effective core uncovery starts as soon as the primary pumps are stopped, the hot legs are drained and then the coolant tends to settle down in the lower parts of the primary circuit. This draining process results in a sudden core water level increase in the ASTEC calculation, while the core is still almost completely filled by water in the MELCOR calculation.

The onset of core uncovery and heat-up at the core top (see clad temperature evolution in Figure 14) is calculated earlier by MELCOR with respect to ASTEC. However, due to the slower core heat-up rate in MELCOR, the oxidation runaway with temperature escalation at the core top is predicted earlier by ASTEC. The reason for this significant discrepancy is likely in the different modeling of the vessel upper plenum. Only one volume is used in ASTEC, while several volumes are used in MELCOR to try to take into account convective movements in the upper part of the vessel that might significantly influence the core heat-up. The clad temperature fall down at t = 6310 s in MELCOR calculation is due to the disappearance of the clad at the core top due to its melting, failure and relocation. For similar reason (debris bed formation and collapse), the clad temperature calculated by ASTEC after t = 5740 s is unreliable.

Hydrogen generation

The time evolution of hydrogen generation rate is presented in Figure 15, while the hydrogen cumulated value is compared in Figure 16. Despite the significant difference in the timing of hydrogen generation, there is a good agreement in the total amount of hydrogen produced at the end of the transient: 501 kg and 516 kg in the ASTEC and MELCOR calculations, respectively. In both calculations, most of the hydrogen, approximately 80%, is produced by oxidation of intact fuel rods during the early degradation phase. About 20% of hydrogen is produced by oxidation of debris and melt during the late degradation phase.

Core degradation and corium relocation into the lower plenum

The progression of core degradation calculated by MELCOR and ASTEC is described in details in Section 3 and Section 4, respectively. The time evolution of the total degraded core mass calculated by the two codes is compared in Figure 17, while the evolution of total amount of materials relocated into the lower plenum is compared in Figure 18. The large discrepancy observed in the total amount of degraded core materials can be explained by the different heat-up of the peripheral rings of the core. The central rings of the core are highly degraded in MELCOR calculations, but the external rings of the core remains substantially intact due to reduced heat-up. Conversely, in the ASTEC calculation the core degradation

extends significantly to the periphery of the core leading to melting and relocation of the baffle structure. Mainly due to different core degradation progression and corium slumping criteria, the amount of materials relocated into the lower plenum is significantly smaller in the MELCOR calculation with respect to ASTEC.

Despite the largest amount of corium in the lower head, with massive corium slumping around t = 7400 s caused by baffle melting in the lower part of the core, the vessel failure is delayed by about 2000 s in the ASTEC calculation with respect to MELCOR. Molten jet fragmentation and debris cooling by residual water in the lower head of the vessel in the ASTEC calculation contributes to delay the vessel failure due to wall melting. Furthermore, the lower head penetration failure in MELCOR calculation leads to early vessel failure before local wall melting.

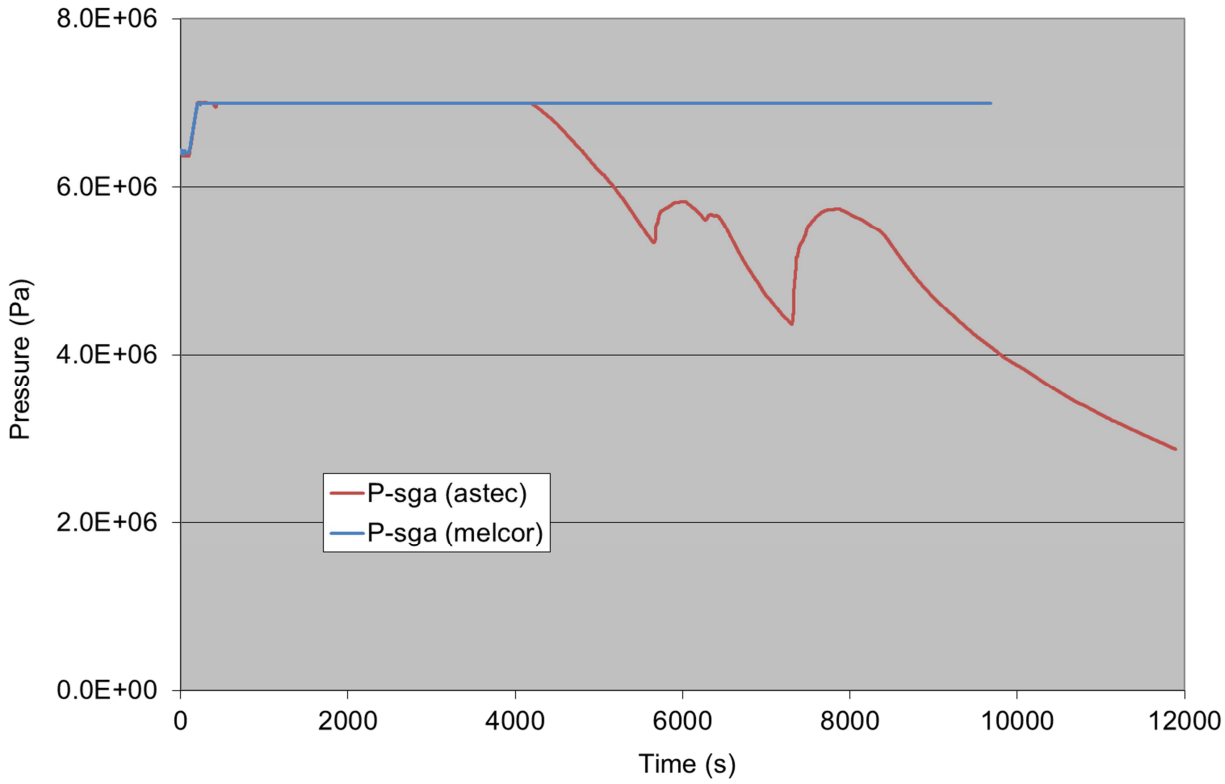

Figure 5.1**:** Steam generator A pressure

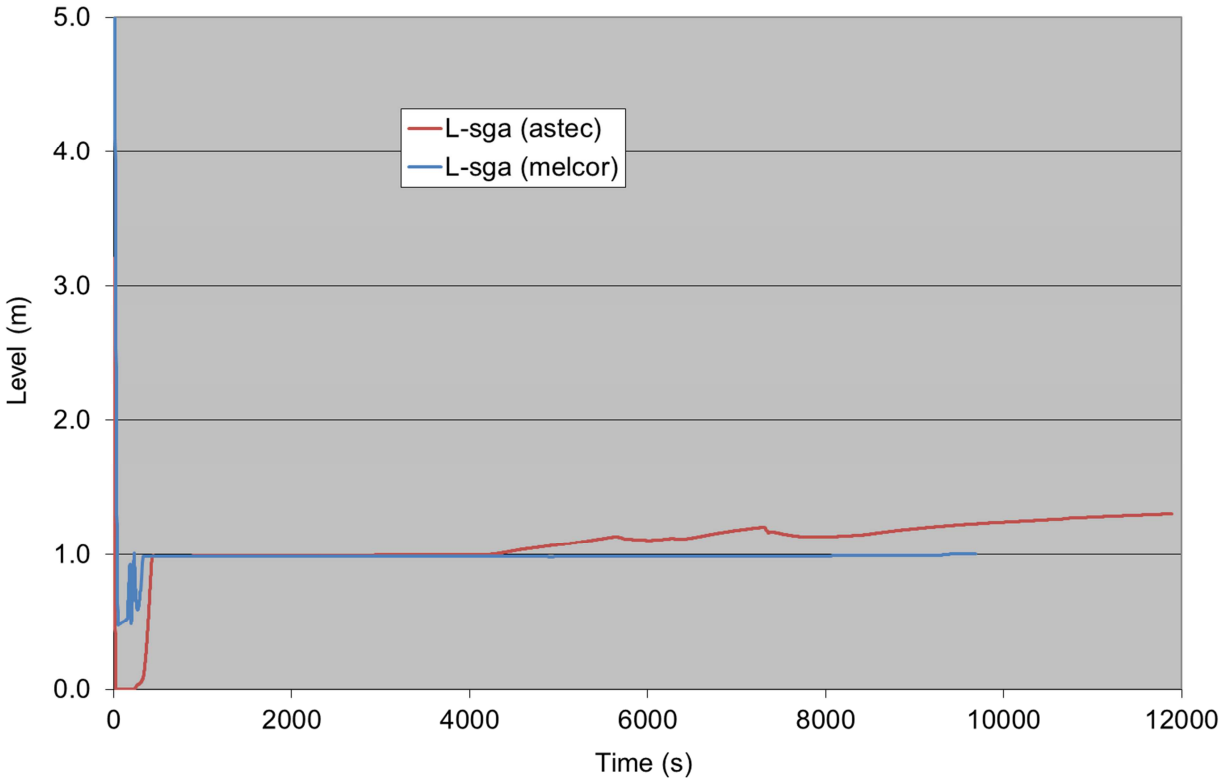

Figure 5.2**:** Steam generator A collapsed level

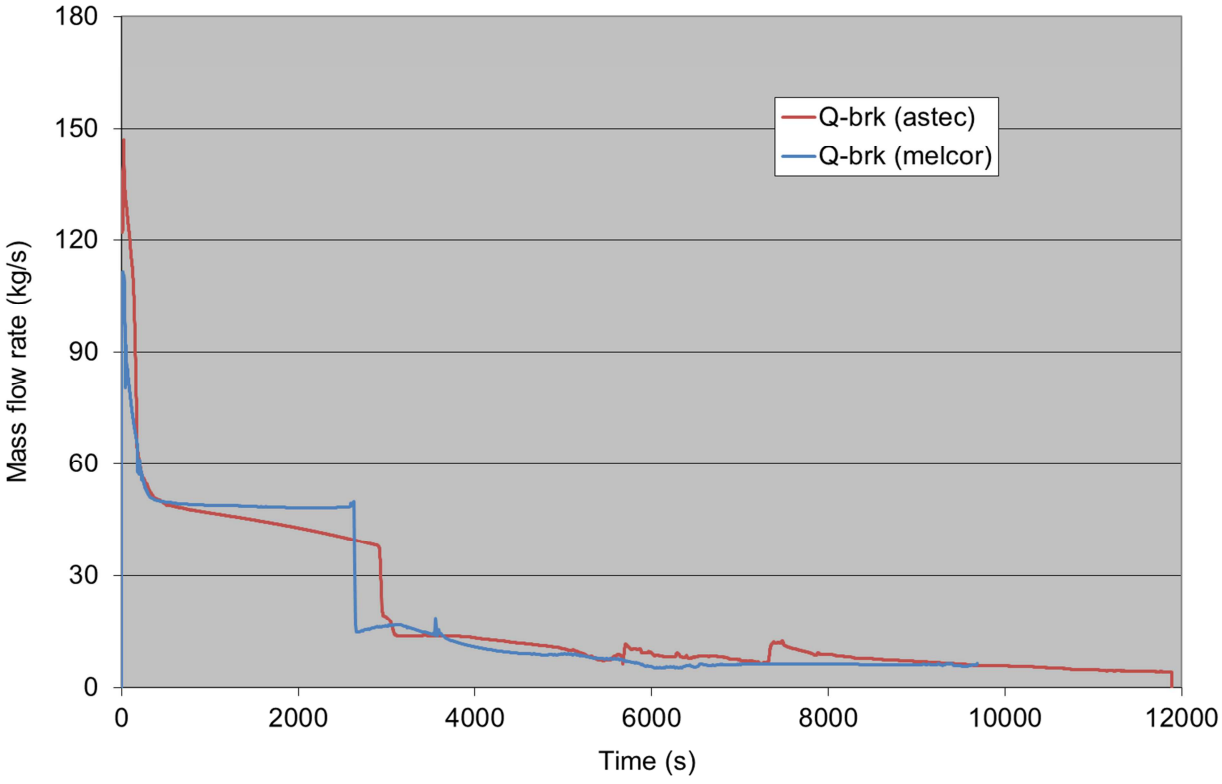

Figure 5.3**:** Break mass flow rate

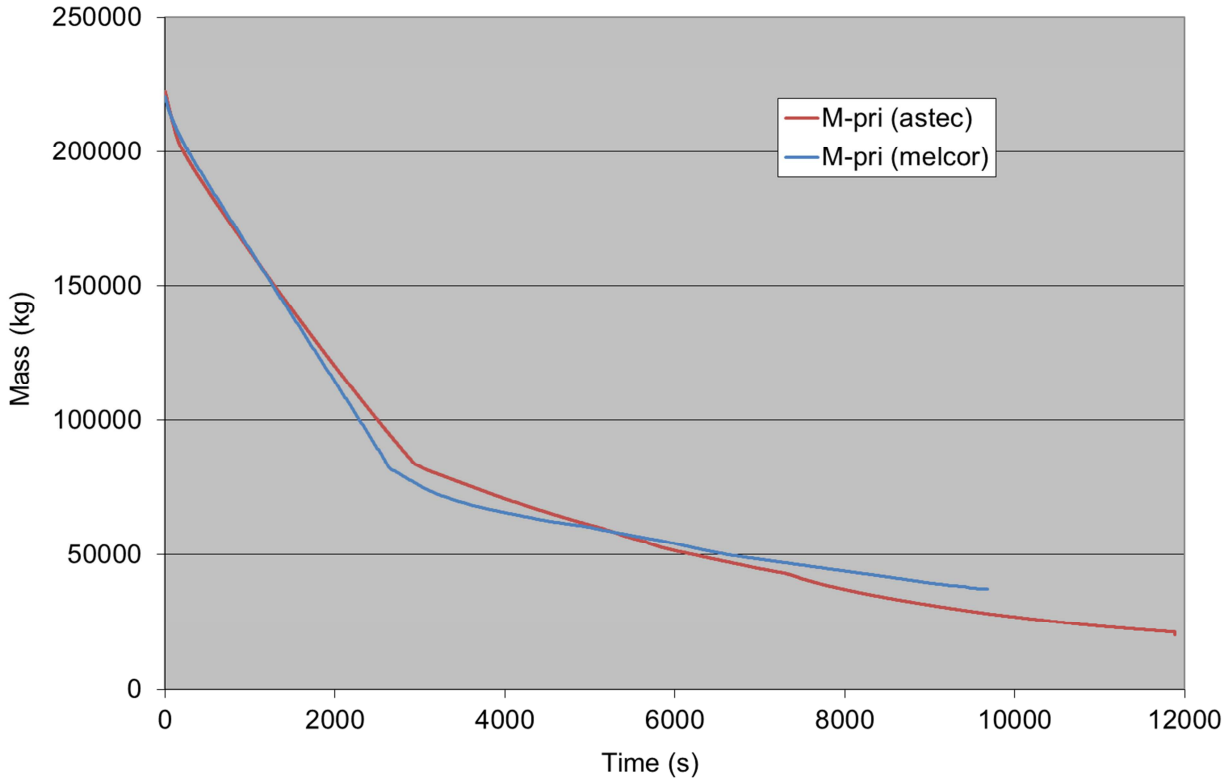

Figure 5.4**:** Total primary mass (liquid + steam)

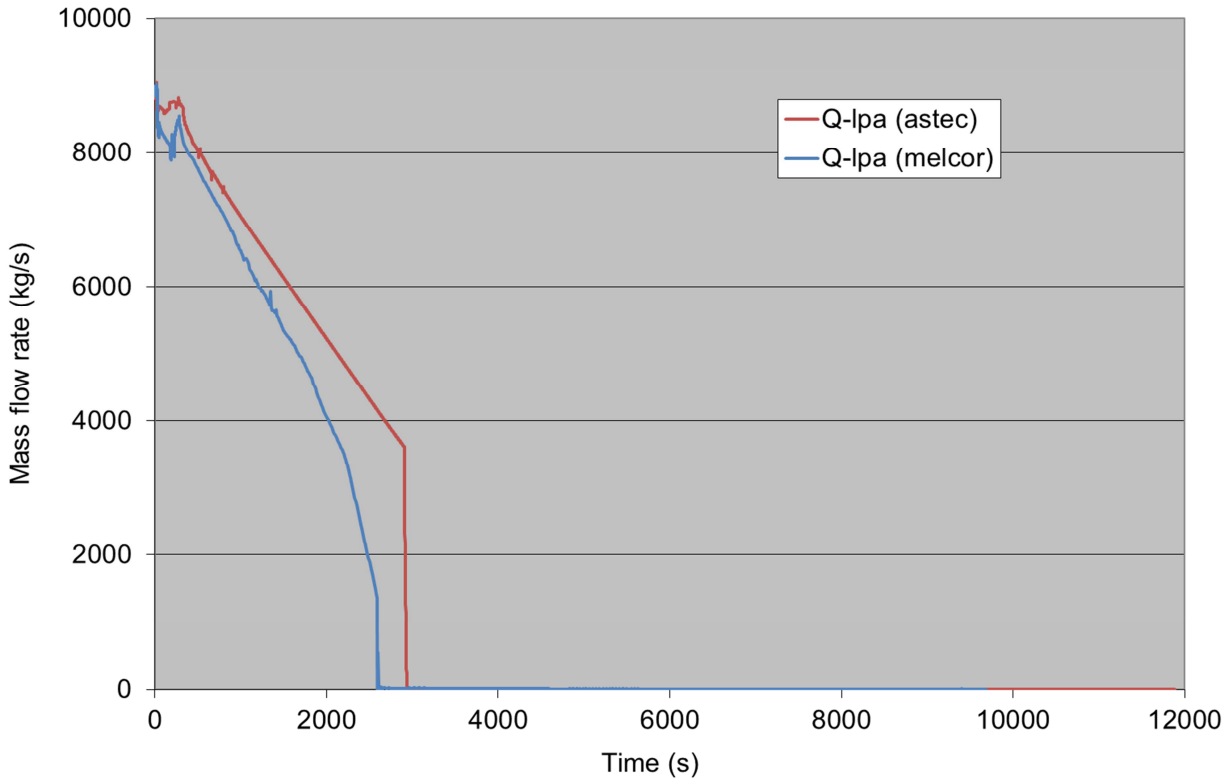

Figure 5.5**:** Loop A mass flow rate

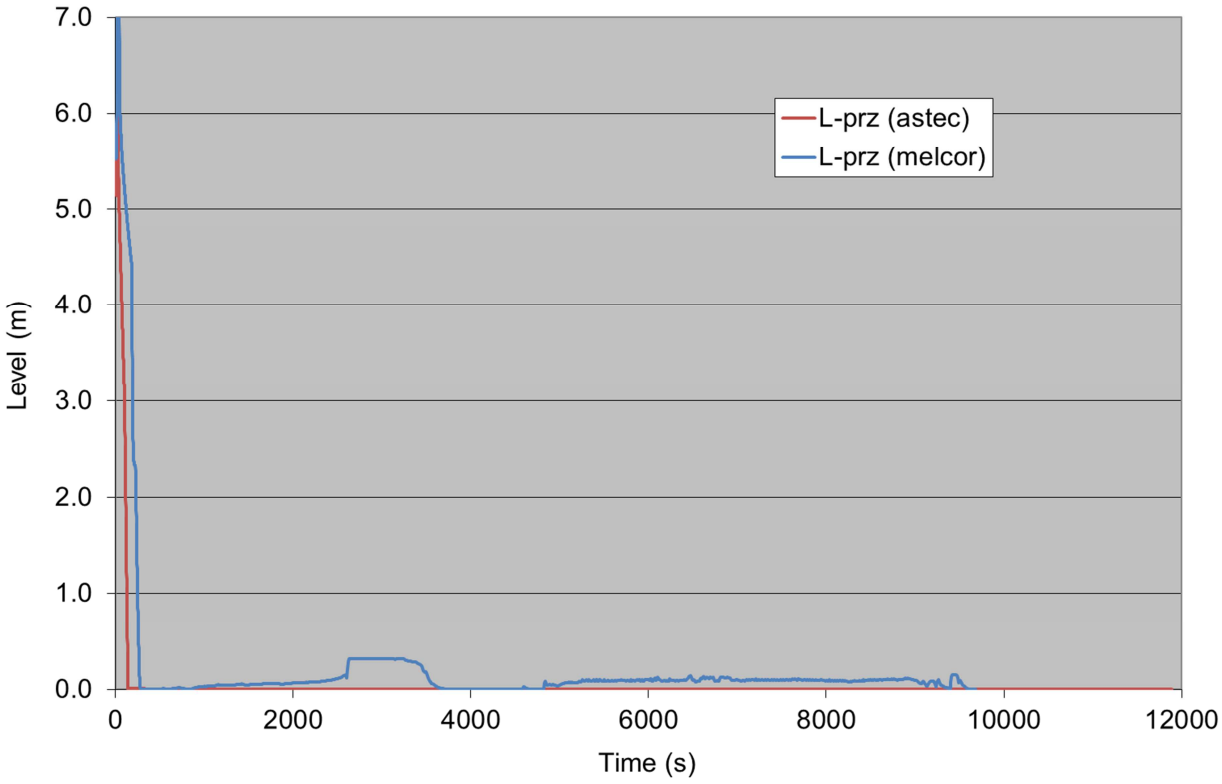

Figure 5.6**:** Pressurizer level

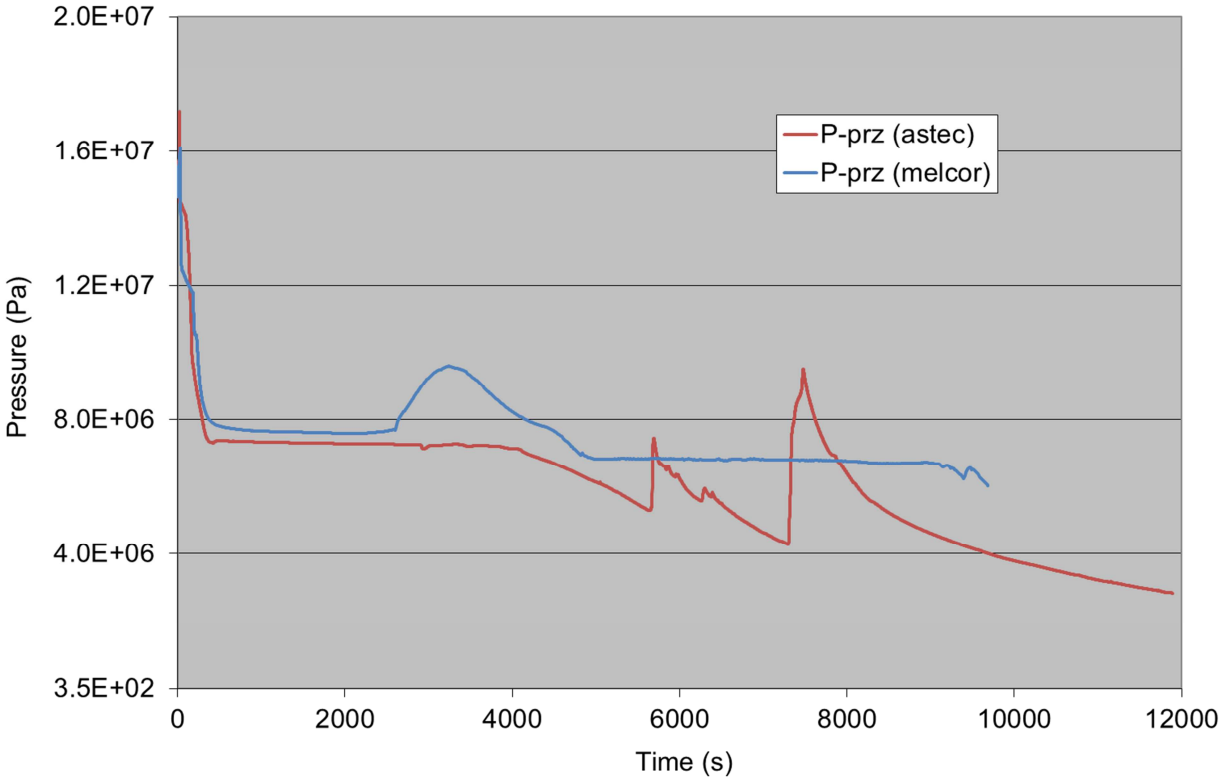

Figure 5.7**:** Pressurizer pressure

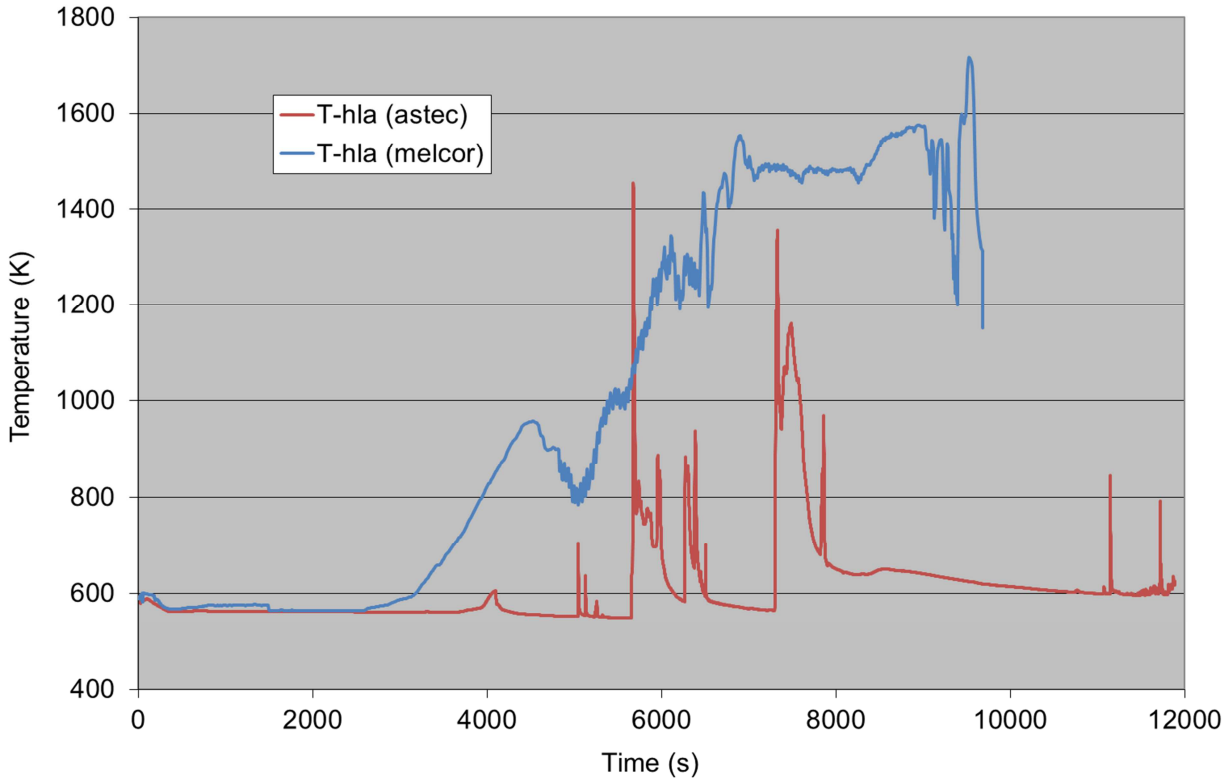

Figure 5.8**:** Hot leg A temperature

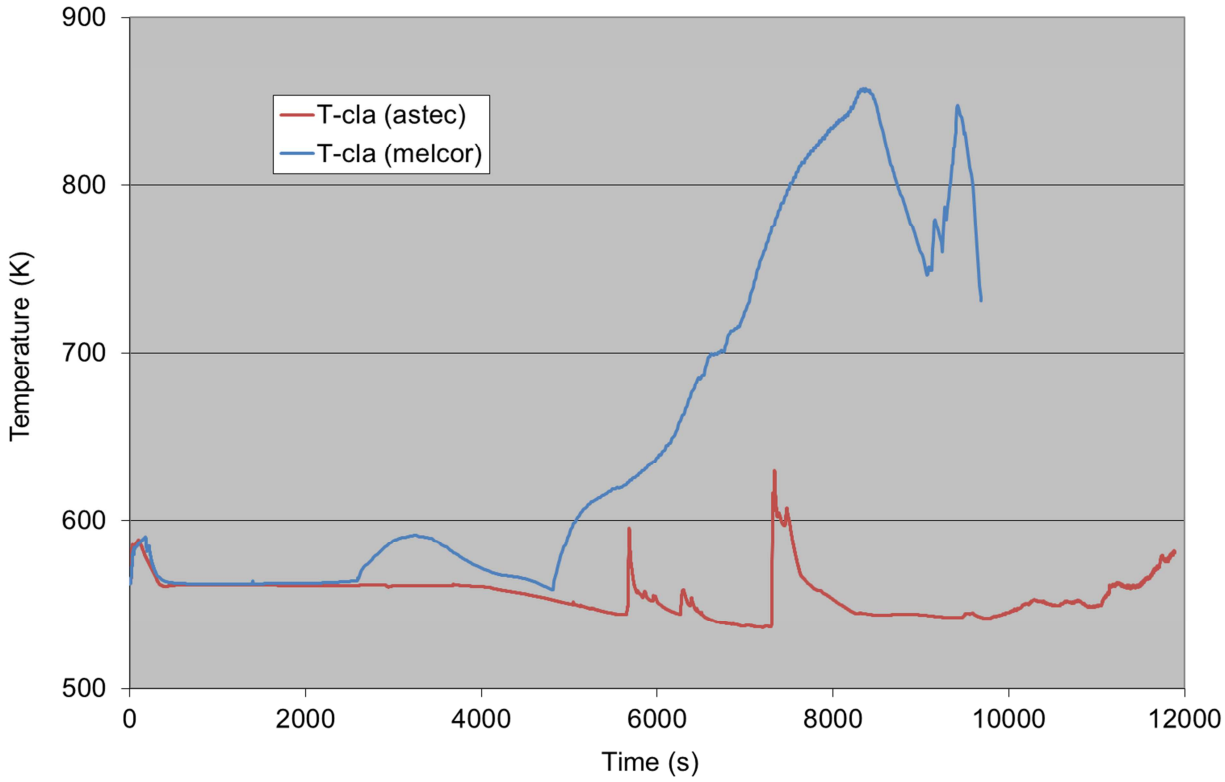

Figure 5.9**:** Cold leg A temperature

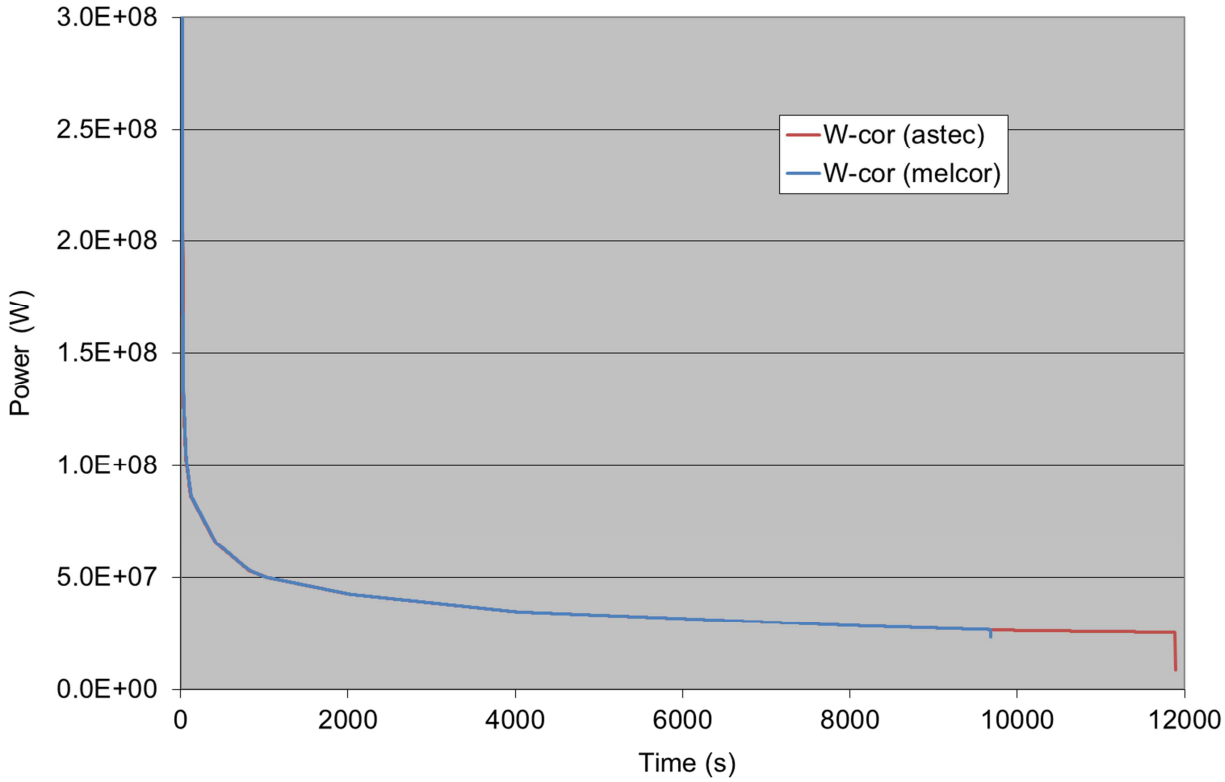

Figure 5.10**:** Core power

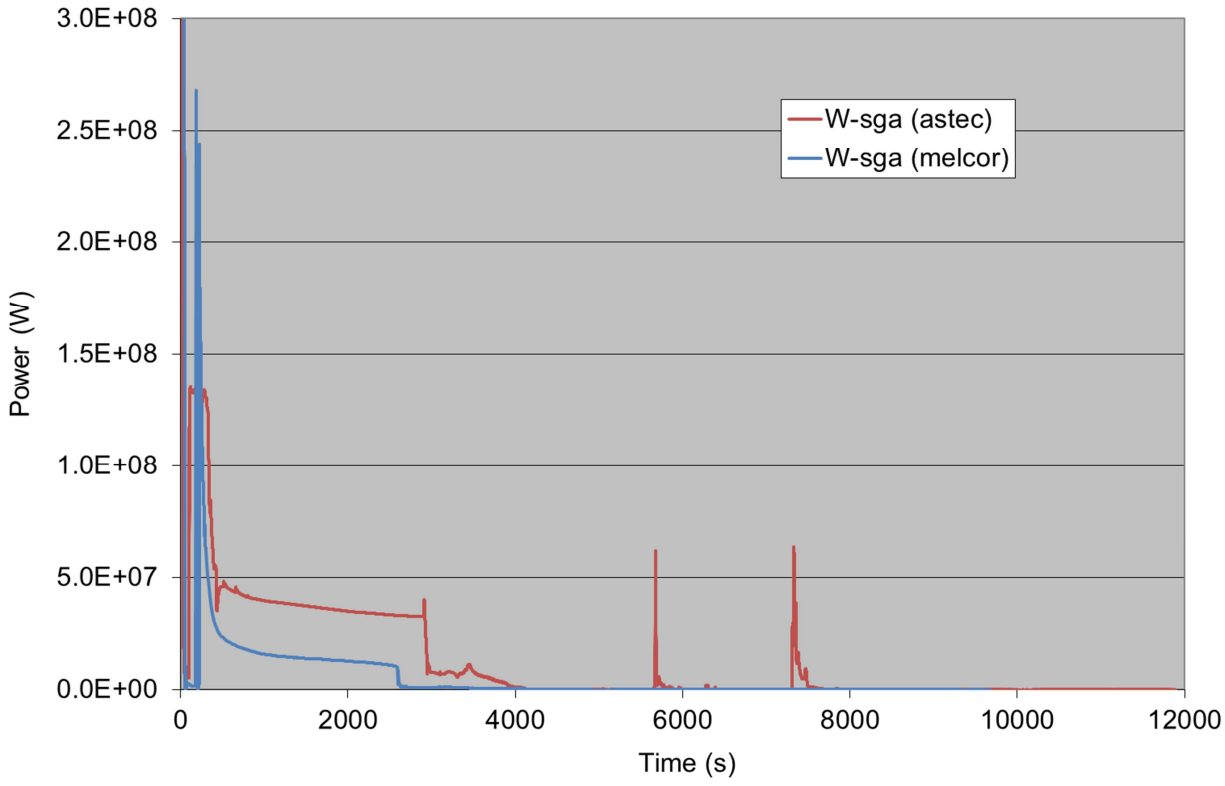

Figure 5.11**:** Power exchange with SG A

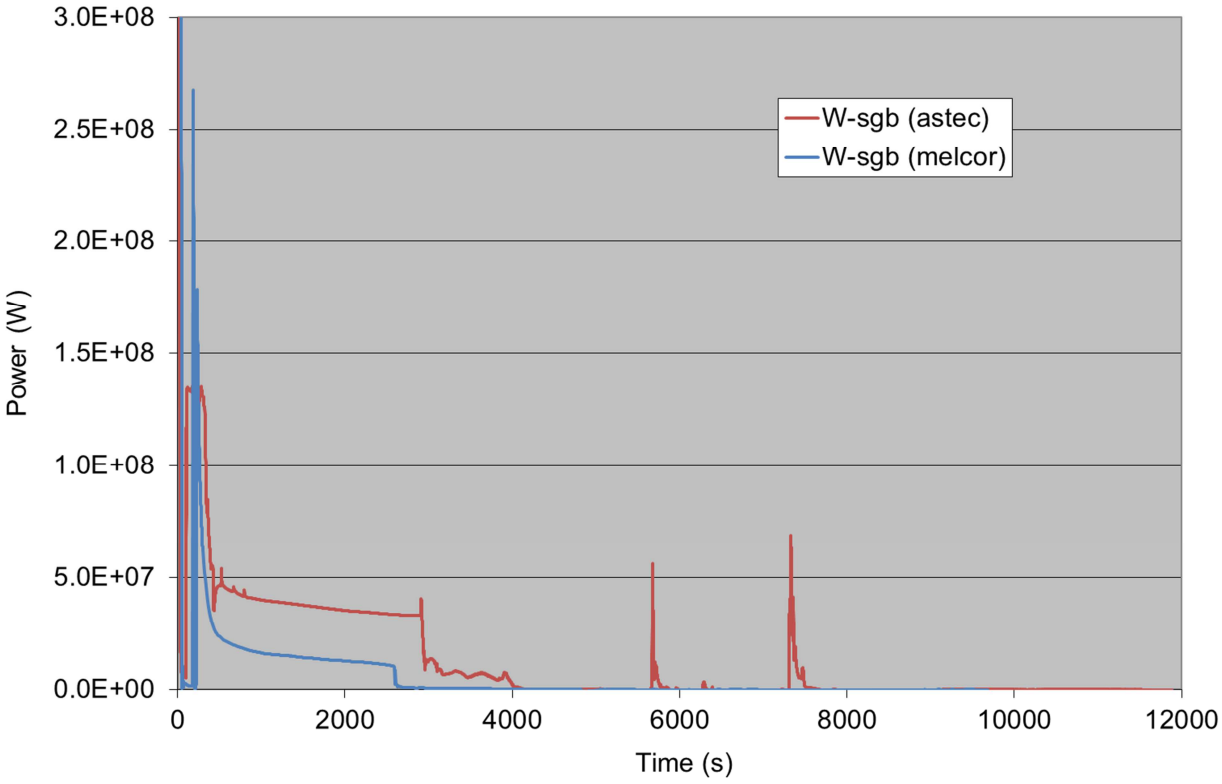

Figure 5.12**:** Power exchange with SG B

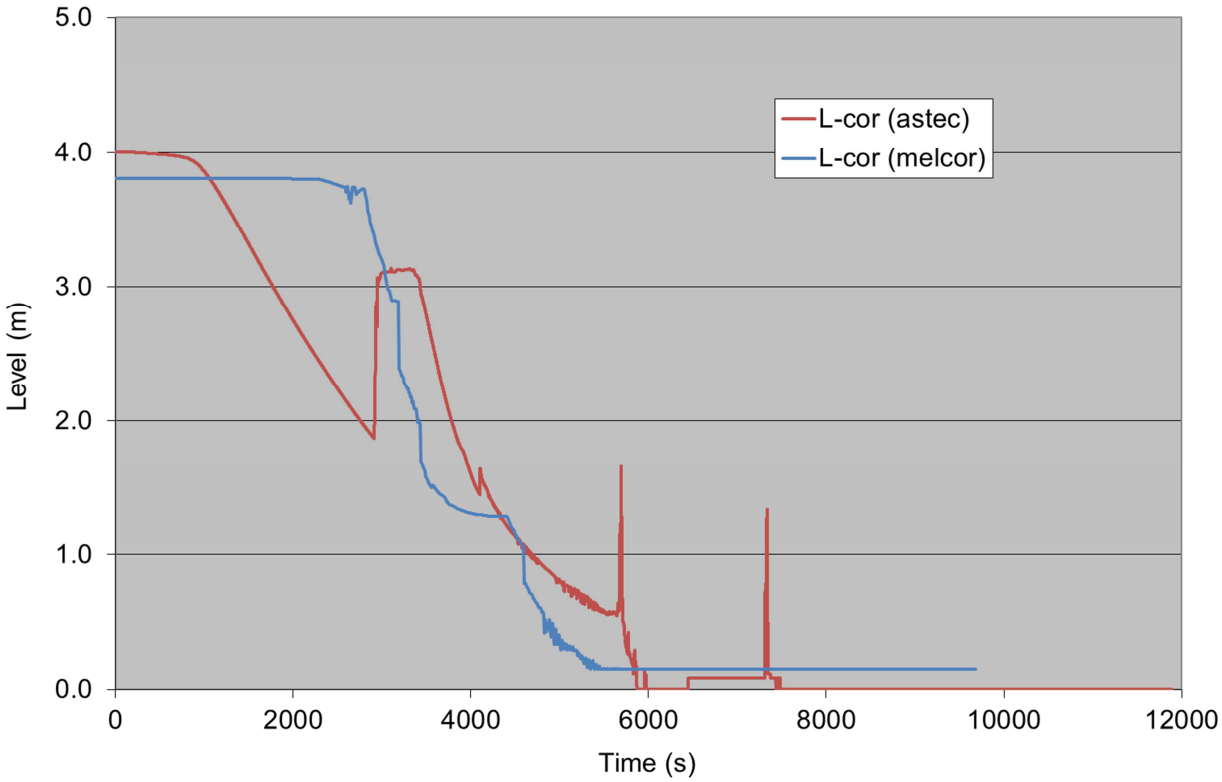

Figure 5.13**:** Core collapsed water level

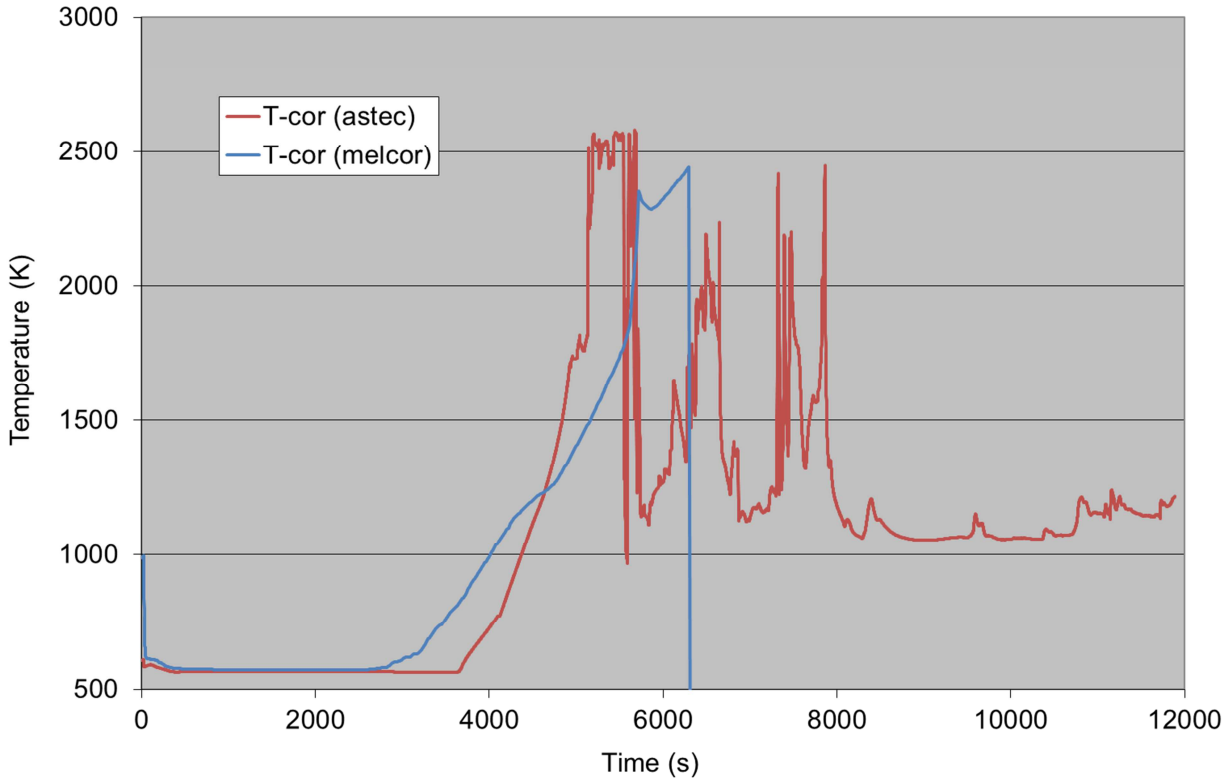

Figure 5.14**:** Fuel rod clad temperature at core top *(central ring)*

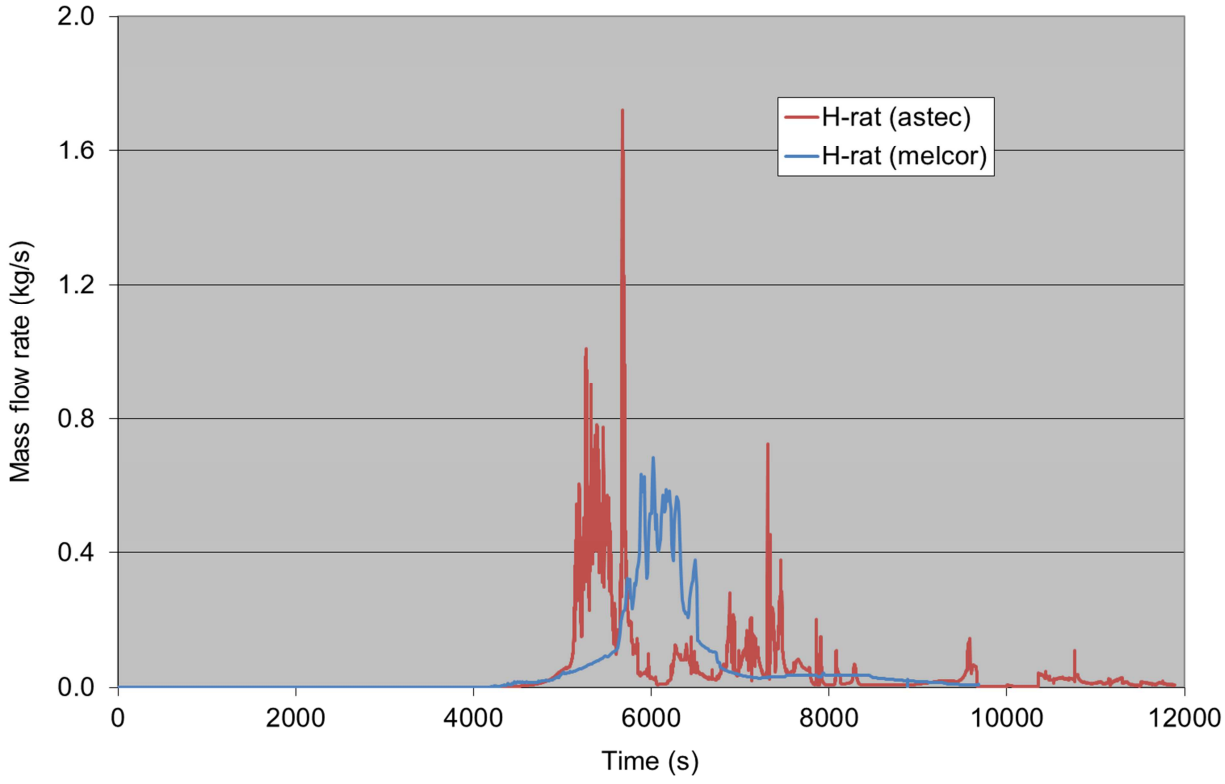

Figure 5.15**:** Instantaneous hydrogen production

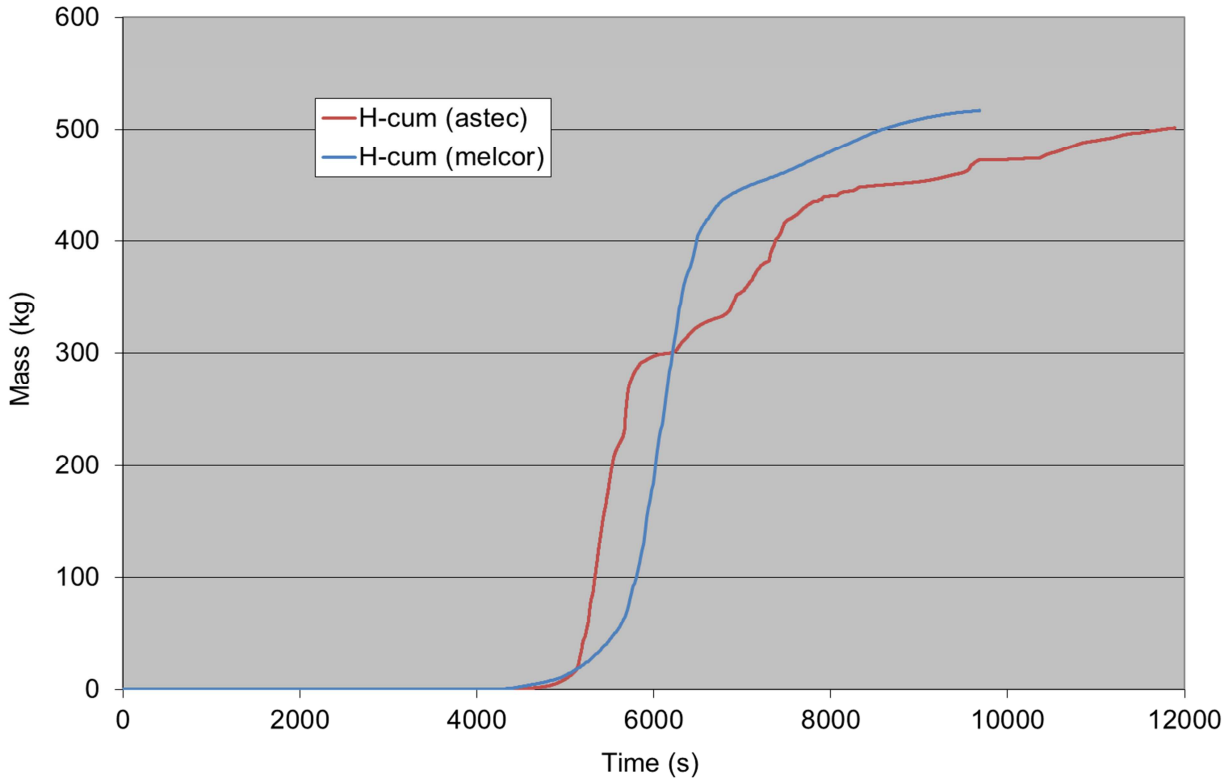

Figure 5.16**:** Cumulated hydrogen production

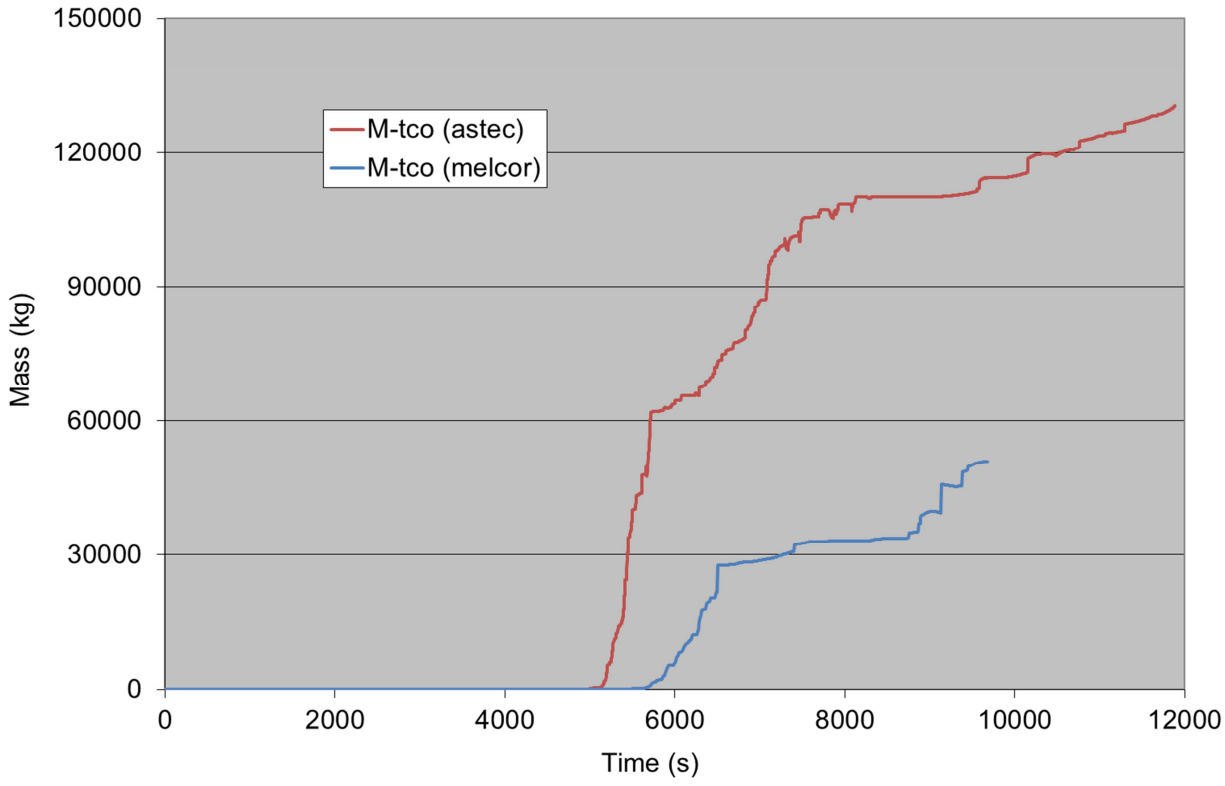

Figure 5.17**:** Total mass of degraded core materials (debris or molten, cumulated value)

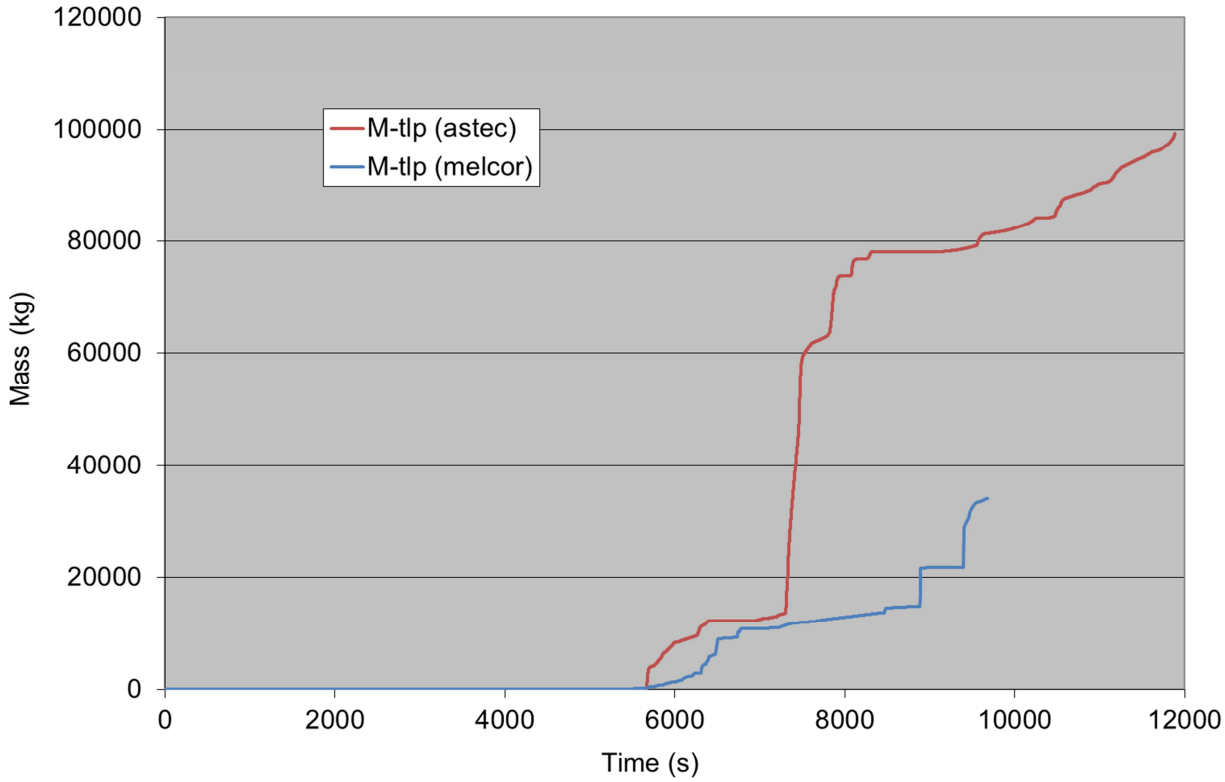

Figure 5.18: Total mass of materials in the lower plenum (cumulated value)

6. Conclusions

The calculations of SBLOCA accident sequence in the TMI-2 plant with the integral codes ASTEC and MELCOR, performed by the University of Bologna and the University of Pisa, respectively, confirm the good performances and the robustness of these numerical tools for the assessment of in-vessel core melt progression, during a severe accident in a PWR reactor, until large relocation of corium into the lower plenum with subsequent lower head failure.

Both code predicts in a qualitative way similar thermal-hydraulic conditions in the primary circuit and all core degradation phenomena which are expected to occur during the early and late degradation phases of a severe accident. However, the code result comparison has highlighted several significant discrepancies in both thermal-hydraulic behavior of the primary system during the first phase of the transient and then in the core melt progression after the onset of core uncovery and heat-up.

The main reasons for the highest discrepancies observed in the thermal-hydraulic behavior of the primary circuit are:

- The large difference in the initial water inventory of the SG secondary side which affects the very initial phase of the transient;
- The discrepancy in the break mass flow rate before primary pumps stop, which is mainly related to the model employed to evaluate the void fraction upstream the break;
- The different model adopted for the main circulation pumps and the assumptions made on the heat dissipated into the primary coolant;
- Differences in the residual heat transfer through the SGs just after primary pumps coastdown;
- The more massive or gradual corium relocation process depending on the different assumptions made for core slumping into the lower plenum.

Regarding the core melt progression, the main reasons of the highest discrepancies observed are:

- The different meshing of the upper plenum, which highly influence natural circulation inside the vessel, and might strongly impact on the core heat-up rate, the onset of core meltdown and the radial spreading of the core degradation in the colder and external rings of the core;
- The different code model options and parameters that are used to describe both early and late in-core degradation phases of the accident;
- The different options and criteria used to simulate core slumping into the lower plenum and to predict the vessel failure.

The large impact of the different code modelling options used for the late phase degradation has been confirmed by the sensitivity analysis performed with ASTEC with and without the DEBRIS model. The late phase models have a lowest impact of the cumulated

mass of hydrogen produced, since most of the hydrogen is generated during the early degradation phase.

The present analysis have highlighted the large uncertainties still existing in the assessment of the core degradation phase by current severe accident code models. Due to the limited experimental database, in particular for the late in-vessel core degradation phase, sensitivity analyses on the most uncertain core degradation parameters and different modelling options are recommended to investigate their influence on the core melt progression and the hydrogen source. 2D meshing of the upper part of the vessel seems necessary to evaluate the impact of natural circulation effects in ASTEC. This capability should be made available soon in the new version V2.1 of ASTEC which implement a new coupling procedure for the thermal-hydaulic and the core degradation modules.

CIRTEN Authors CV:

Dr. Mirco Di Giuli: degree in Chemical Engineering in 2007 at University of Bologna, Master in Design and Management in Advanced Nuclear Systems at University of Bologna in 2009, SIET Company Consultant for the core design of the ALFRED LCR prototype (in the framework of the European Research Program LEADER), at present PhD student in Nuclear and Energy Engineering and Environmental Control at University of Bologna with, as research objectives, the study of the severe accidents for SMR.

Prof. Marco Sumini: Nuclear Engineer, Associate Professor in Nuclear Reactor Physics at University of Bologna since 1987; research activities on Reactor Physics, Core Design and on Neutral and Charged Particle Transport. Experimental activities on Pulsed Power Plasma Devices.

Dr. Antonio Manfredini: degree in Nuclear Engineering in 1989 at University of Pisa, PhD in Nuclear Engineering – Safety of Nuclear Power Plants in 1992. Research activities on BDBA and Severe Accidents phenomena on nuclear power plants.

Prof. Walter Ambrosini is Associate Professor in Nuclear Plants at the University of Pisa. He graduated cum laude in Nuclear Engineering in 1985 and obtained his Dottorato di Ricerca (PhD) in Nuclear Engineering (Safety of Plants) in 1989. His research work concerns mainly the thermal-hydraulic aspects of nuclear reactor safety, while his teaching activity is focused on computational and experimental thermal-hydraulics and on numerical methods for nuclear reactors. He is presently President of both the MSc and the PhD courses in Nuclear Engineering at the University of Pisa and has been President of the Central Library of the Faculty of Engineering in past years. Prof. Ambrosini has been involved in the activities of ENEN starting with the NEPTUNO project and continuing with ENEN-II and ENEN-III, by cooperating with the former official CIRTEN representative, Prof. Bruno Panella. He presently serves the ENEN Association as its President, elected in March 2013 and reselected in March 2014.